2017

Thermal Quenching of Photoluminescence in ZnO and GaN

Nahla Albarakati
Virginia Commonwealth University

Thermal Quenching of Photoluminescence in ZnO and GaN

A Dissertation submitted in partial fulfillment of the requirements for the degree of
Doctor of Philosophy in Nanotechnology and Nanoscience
at Virginia Commonwealth University.

By:

Nahla Mubarak Albarakati

M.S. in Physics/Applied Physics

Virginia Commonwealth University

Director:

Dr. Michael Reshchikov

Professor, Department of Physics

Virginia Commonwealth University

Richmond, Virginia 23284, USA

July, 2017

Acknowledgments

All thanks and glory to Allah who make me healthy and gave me the chance to start and complete the Ph.D degree, who gave me the strength, the patience, the capability to work all day long, to gift me with insatiable desire to learn about physics complexities and to surround me by a great many people and to them I owe an enormous debt of gratitude for making the completion of this dissertation possible.

My sincere gratitude goes to my advisor Dr. Michael Reshchikov. Thank you to teach and train me in your lab. Thank you for your kindness and willing to answer all questions comprehensively. Thank you for your guidance, direction and gently nudged me to reach my goal. Thank you to teach me how to think critically and analyze data effectively. Thank you for your steadfast belief in my ability to complete the degree even when I faced many obstacles.

A particular debt of gratitude to the first person welcome me to join VCU and the most influential person in the path of my physics career, Dr. Alison Baski. I have been astounded to know a professor who meticulously cares for all students in multiple aspects to achieve scientific development. A professor inspires me how it is important to be a strong and capable woman in science. Thank you, Dr. Alison Baski, for your encouragement, wisdom, kindness and to teach us the right way in receiving the knowledge and giving it.

Gratitude and the utmost respect to my committee members, Dr. Denis Demchenko, Dr. Vitaliy Avrutin and Dr. Maryanne Collinson, who make the Ph. D degree more efficiency by make it even harder.

I would like to thank the graduate programs coordinator, Dr. John T. Hutton, who made the last moment in the VCU the happiest and non-forgettable moment. Thank you for your kindness and help.

I am thankful for my friends in the VCU Physics department: Joy, Iwona, Karen, Anita, Lauren, Ibrahima, and Joe. Together, we all have overcome many difficulties in classes and exams, collaborated on research projects, and shared life as graduate students. I would not have made it this far without your friendship.

Nobody has been more important to me in the pursuit of this work than the members of my family, especially my mother, my husband, my sisters and my kids.

To my mom who imprinted on me as example of hard work, determination and perseverance; to the one who deserve the most credit for her laudable sacrifice. A special thanks to your encouragement, constant support and faith in me. Thank you for always being there for me, for filling my heart with kind words, for praying for me and inspiring me to love to be a life-long learner then make a good impact on other.

I am grateful and cherish for my sisters, Nouf, Noor, Najat, Nouran and Nedaa, for the great support especially during the difficulties of this work and through my entire life and to help me being stronger. Thank you to fill my life with love, laughter and many memorable moments.

My indebted and heartfelt thanks to my husband, Omar, for his encouragement, and unfailing supporte me throughout all the years of study. Thank you Omar for brightened up my life with your sincer care, comfort, and grant me with hope. Thank you for your laudable sacrifice and great helpe me to overcome many obstacles. This degree would not have been possible without you. Truly, you deserve the most praise for my success. Thank you for being more than what I want.

Hazim and Rahama, My children, the hope, the smile, the sunshine and the relief who gave me more than determination and mercy, as their name mean, to overcome many study obstacles and keep going.

Last, but not least, a special gratitude and the highest regard is owed to my dad. My dad who was the power and the reason to have this chance and study abroad to finish my higher education. Ever since starting my school, his encouragement, support, and nice words with logics and faith instilled in me a love for knowledge and was the fuel to overcome obstacles with hope.

Table of Contents

Table of Figures (captions)

Abstract

Thermal Quenching of Photoluminescence in ZnO and GaN

Nahla Mubarak Albarakati

Doctor of Philosophy in Nanoscience and Nanotechnology

A Dissertation submitted in partial fulfillment of the requirements for the degree of Doctor of Philosophy in Nanotechnology and Nanoscience at Virginia Commonwealth University.

Virginia Commonwealth University

2017

Major Director:

Dr. Michael Reshchikov

Professor, Department of Physics

Investigation of the thermal quenching of photoluminescence (PL) in semiconductors provides valuable information on identity and characteristics of point defects in these materials, which helps to better understand and improve the properties of semiconductor materials and devices. Abrupt and tunable thermal quenching (ATQ) of PL is a relatively new phenomenon with an unusual behavior of PL. This mechanism was able to explain what a traditional model failed to explain. Usually, in traditional model used to explain "normal" quenching, the slope of

PL quenching in the Arrhenius plot determines the ionization energy of the defect causing the PL band. However, in abrupt quenching when the intensity of PL decreases by several orders of magnitude within a small range of temperature, the slope in the Arrhenius plot has no relation to the ionization energy of any defect. It is not known *a priori* if the thermal quenching of a particular PL band is normal or abrupt and tunable. Studying new cases of unusual thermal quenching, classifying and explaining them helps to predict new cases and understand deeper the ATQ mechanism of PL thermal quenching. Very few examples of abrupt and tunable quenching of PL in semiconductors can be found in literature. The abrupt and tunable thermal quenching, reported here for the first time for high-resistivity ZnO, provides an evidence to settle the dispute concerning the energy position of the Li_{Zn} acceptor. In high-resistivity GaN samples, the common PL bands related to defects are the yellow luminescence (YL) band and a broad band in the blue spectral region (BL2). In this work, we report for the first time the observation of abrupt and tunable thermal quenching of the YL band in GaN. The activation energies for the YL and BL2 bands calculated through the new mechanism show agreement with the reported values. From this study we predict that the ATQ phenomenon is quite common for high-resistivity semiconductors.

Common Abbreviations

ATQ: abrupt and tunable quenching

NQ: normal quenching

CC: configuration coordinate

DAP: donor-acceptor pair

eA: free-to-bound electronic transitions

GaN: gallium nitride

PL: photoluminescence

YL: Yellow luminescence

BL2: blue luminescence

ZPL: zero-phonon line

HVPE: hydride vapor phase epitaxy

MOCVD: metal organic chemical vapor deposition

IQE: internal quantum efficiency

Chapter 1: Introduction and Motivation

1.1 Photoluminescence

Point defects are often formed in semiconductors as compensation sources when impurity atoms are introduced, which known as doping, or during the growth process as a result of non-equilibrium conditions and contamination of the sources.[1] Point defects affect the electrical and optical properties of the host material and therefore affect the performance and reliability of devices. However, point defects in semiconductors are not well understood. Photoluminescence (PL) is a powerful and important technique that can be used to probe different defects in semiconductors and study them.[1, 2]

Photoluminescence (PL) is a spontaneous emission of light from material caused by absorption of light from another source.[1] The process of PL begins after the material absorbs a photon with energy above the band gap, which excites an electron to the conduction band, leaving an empty hole in the valence band. Since the hole has lower energy state, the electron returns back and recombines with the hole. The released energy split up between phonons (lattice vibrations) and photons. The photon emission is observed as PL, and the number of emitted photons that produced in unit volume per unit time known as the intensity of PL. The number of emitted phonons varies for every recombination process.[1] In the semi-classical approximation, atoms oscillate about their equilibrium positions. If the electron-hole recombination occurs when the atom is far from its equilibrium, there will be many lattice vibrations, phonons. In contrast, if the recombination occurs when the atom is closer to the equilibrium, there will be fewer lattice vibrations and less phonons emitted.[3]

1.2 Thermal quenching

One notable phenomenon observed in PL experiments is its thermal quenching (a decrease of the PL intensity with increasing temperature). After exciting electron-hole pairs with ultraviolet (UV) light, and observing the subsequent recombination as PL through various defect-related channels, PL quenching provides valuable information about the defects involved in this luminescence.[2]

Transitions of charge carriers, electrons and holes, and their recombination behavior are dependent on temperature. The temperature dependence of PL intensity is traditionally presented in the Arrhenius plot which displays the logarithm of PL intensity as a function of inverse temperature.[2] For various recombination channels, the temperature dependence of PL intensity usually consists of two parts. At low temperature, PL intensity is independent of temperature or may slowly change.[2] However, at higher temperatures, when the temperature exceeds some characteristic temperature, T_0, the PL intensity often decreases exponentially. The decrease in the PL intensity is called thermal quenching. We can distinguish two different types of thermal quenching: normal quenching, NQ, and abrupt and tunable thermal quenching, ATQ.[2]

The thermal quenching is normal quenching when the slope of the dependence of PL intensity on inverse temperature reveals the ionization energy, E_A, of the defect involved in the thermal quenching. This type of thermal quenching is observed in conductive n-type semiconductors.[4, 5] In contrast, when the intensity of PL decreases by several orders of magnitude within a small range of temperature, the PL quenching is defined as abrupt quenching.[1-3, 6] The slope of this type of thermal quenching is not related to the E_A of any defect. More interesting, in this type of quenching, the characteristic temperature, at which the abrupt quenching occurs, can be tuned by changing the excitation intensity. Thus, taking the

temperature dependence measurements of PL for different excitation intensities, P_{exc}, is a new method which was developed to determine the ionization energy, and was reliably detected only in high-resistivity semiconductors.[2, 6]

1.3 Motivation to study ZnO and GaN materials

ZnO occupies a special place among direct wide band gap semiconductor due to its availability as high-quality large bulk single crystals with direct and wide bandgap of 3.437eV at 1.6 K and 3.3 eV at 300 K.[7] Also, ZnO has large exciton binding energy of 60 meV which makes it a good candidate for exciton emission lasing devices.[5] Thus, ZnO is a promising material for wide range of optoelectronic applications such as white light-emitting devices, UV laser diodes, and photodetectors.[7] However, using ZnO in devices and achieving these technological developments has been obstructed by the lack of control over its electrical conductivity since ZnO almost always exhibits n-type conductivity.[7, 8] So, it is a major challenge to discover the ZnO properties through better understanding of its point defects and their effect on the electrical and optical properties which would substantially increase the progress in this field.

Some optoelectronic applications of ZnO overlap with another semiconductor material that has wide and direct bandgap as well. GaN with band gap of 3.50 eV at 2 K and 3.4 eV at 300 K [7] attracted unprecedented interest as material that is widely used for producing green, blue, violet, and ultraviolet (UV) emitters and detectors, high-power and high-frequency amplifiers, and other optoelectronic applications.[3] One of the most important examples is the light emitting diodes (LED) that show how efficiently the electrical power is converted into light power with high brightness. The commercial white LEDs achieve luminous efficacies of ~150 lumens/watt, the highest luminous efficacy of all white light sources, and the theoretical limit for

white LEDs is about 260-300 lm/W.[1, 9] Also, by changing the composition of Al (AlGaN) and In (InGaN) and tuning the bandgap of the compound, the LED can emit light in the entire visible range. Moreover, GaN with high heat capacity has the ability to operate at relatively high temperatures without affecting the performance of the device. However, defects in GaN reduce radiative efficiency, decrease operation lifetime and causes failure to the devices. Therefore more improvement of devices performance can be achieved by more understanding of point defects.[3]

Chapter 2: Phenomenological Theory

2.1 Point defects

Transitions of electrons and holes via point defects in semiconductors are often the dominant transitions where the majority of the recombination occurs through them. The variety of point defects in semiconductors can usually be reduced to few major types.[1-3, 6] In particular, for GaN and ZnO, the minimal set of centers involved in carrier recombination includes three types of point defects.[2] The first type is a shallow donor. An impurity in semiconductors may give off electrons and is known as a donor. For example, doping GaN with silicon where the gallium has three valence electrons and the silicon has four valence electrons, will produce Si_{Ga} donor. When an impurity has just one valence electron more than the atom replaced by it, a shallow donor is often formed.[8] Shallow donors have energy levels close to the conduction band. Shallow donors are responsible for n-type conductivity in semiconductors, and are introduced unintentionally during growth of GaN and ZnO.[1, 7, 8] The energy required for the electron to escape from a shallow donor to the bottom of conduction band is equal to the binding or the ionization energy (E_D) of that donor, Figure 1. A donor gains a positive charge (D^+) when it loses the electron and becomes an ionized donor. On another hand, donor is neutral (D^0) by having an electron.

Second type of a necessary defect is an acceptor that accepts electrons and provides excess holes to a semiconductor. The element that can be used for p-type doping to produce an acceptor must have less valence electrons than the host atom. For example, Mg in the Ga sites forms an acceptor. The negatively charged acceptor (A^-) becomes a neutral acceptor (A^0) by losing electrons. The acceptor levels are usually located not far from the valance band, and the

energy needed to thermally emit a bound hole to the top of the valence band is equal to the acceptor ionization energy (E_A), Figure 1. This type of defect (acceptor) is needed to explain defect-related PL bands in an n-type semiconductor. Since not all transitions are radiative, the third type of defects is a center that is responsible for nonradiative recombination. For some defects, recombination of electrons and holes produces multiple phonons and no photons are emitted.[1-3, 6] Non-radiative center (S) is necessary to explain the less than 100% of PL quantum efficiency. The identity of the nonradiative center is unknown, so it could be a deep donor or a deep acceptor with unknown energy level position, Figure 1. [1-3, 6]

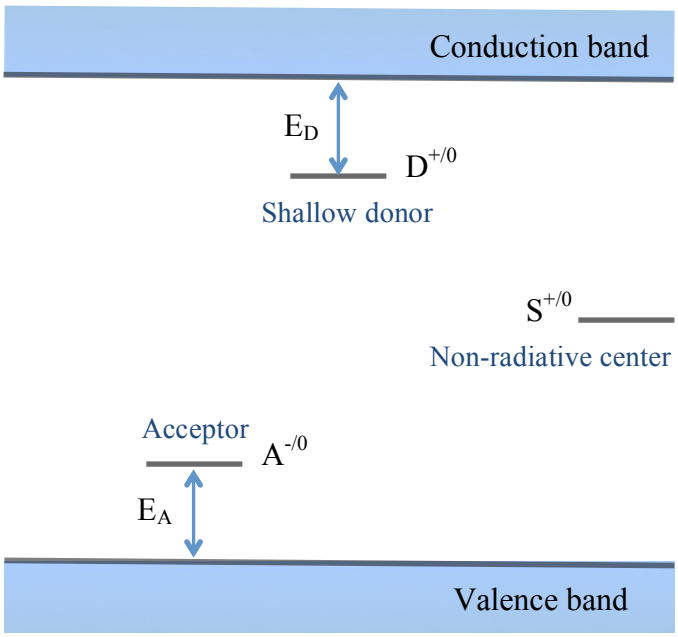

Figure 1. Energy band diagrams and schematic of positions of the three point defects levels

2.2 Rate equation model

2.2.1 Steps of transitions via defects

The electron-hole generation, with the rate G, is caused by illumination of a semiconductor with a laser emitting above band gap energy photons. [1-3, 6] The system returns back to equilibrium as a

reverse process by electron-hole recombination. The recombination via point defects occurs in two steps. Available charge carriers (electrons or holes), and available empty sites (e.g., A^- for holes and A^0 for electrons) are required for the recombination to happen. Without loss of generality, let us consider a semiconductor with one point defect, acceptor in an n-type semiconductor, where the acceptor levels are filled with electrons in dark. In the first step, a hole (as available charge carrier) in the valence band must be captured by a negatively charged acceptor (as defect having available empty site). Then, a free electron in the conduction band is captured by the neutral accepter and recombines with the hole, Figure 2. Multiplying the concentrations of available charge carriers, n for electrons and p for holes, and the concentration of available empty sites, N_A^- for acceptor defect, by a constant factor called the capture coefficient, C_{pA}, gives the transition rate equation (e.g. C_{pA} p N_A^-), Figure 2.[1, 2]

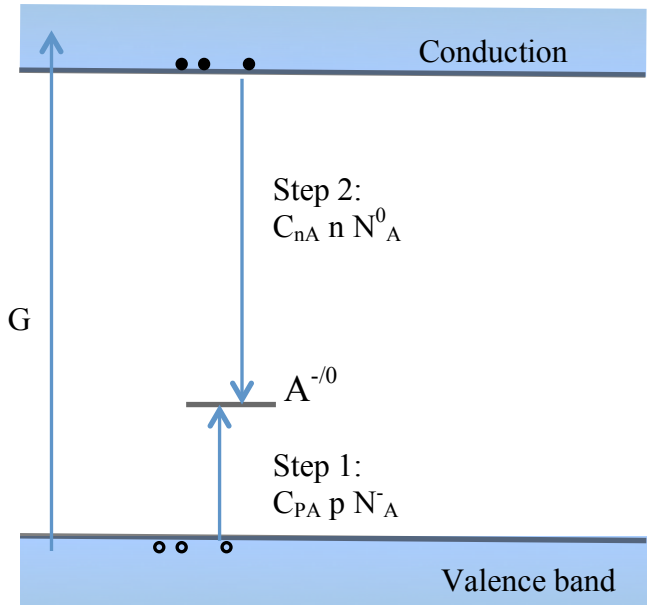

Figure 2. An energy band diagram and schematic of electron and hole transitions via one point defect, acceptor A.

2.2.2 Capture coefficient and capture cross section

Capture coefficient, C, with units cm^3s^{-1}, is a quantity that describes the capture and recombination properties for each impurity center.[10] Carriers' recombination can be radiative or nonradiative. In semiconductors, the capture coefficients for radiative recombination between electrons and holes via defects are of the order of $10^{-14} – 10^{-13}$ cm^3 s^{-1}.[7] However, the electron and hole capture coefficients for nonradiative recombination or capture may vary over a wide range $C \sim 10^{-14} – 10^{-6}$ cm^3 s^{-1}.[7] Radiative and nonradiative recombinations are in general competing and can occur simultaneously; when capture coefficient of nonradiative recombination is larger than the radiative one, nonradiative recombination is dominant.[2, 6]

A capture coefficient can be described in terms of the capture cross section, σ, which is the area where the carriers are captured. The capture coefficient, C, and the capture cross section, σ, are related to each other via the following equation:

$$C = < \nu > \sigma \tag{1}$$

$$< \nu > = \sqrt{\frac{8\,k\,T}{\pi\,m}}, \tag{2}$$

where $< \nu >$ is the mean thermal velocity of free carriers, electrons in the conduction band $< \nu_n >$ or holes in the valence band $< \nu_p >$, and m is their effective mass, m_n and m_p.[7,10]

The capture cross section is an effective area where the charge of the center plays a role. An attractive Coulomb potential makes the effective cross section area to be large. For attractive centers, capture cross-section, may significantly exceed the geometric area of the atom's size, πa^2, and become a giant trap. The neutral center is in the next order of magnitude, and the smallest one is the repulsive center, see Table 1 as example.[11]

Table 1. The general order of magnitude of the capture cross sections areas based on the center's charge.[11]

Type of trap	Example	Typical cross section
Attractive center	Electron capture by positively charged impurity, $Ge:Sb^+$	10^{-1} to 10^{2} nm^2
Neutral center	Electron capture by neutral charged impurity, $Ge: Ni^0$	10^{-3} to 10^{-1} nm^2
Repulsive center	Electron capture by negatively charged impurity, $Ge:Mn^-$	10^{-10} to 10^{-7} nm^2

2.2.3 Phenomenological model

The most basic model that can be suggested for a semiconductor to explain the behavior of PL is the one including three types of point defects.[1, 2, 6, 12] Let us consider a direct band gap n-type semiconductor containing a shallow donor D with the concentration N_D, an acceptor A with the concentration N_A and a nonradiative deep donor S with the concentration N_S. The concentrations of the D, A and S in different charge states are N_D^+, N_D^0, N_A^-, N_A^0, N_S^+, and N_S^0 respectively, and the ionization energies of the donor and acceptor are E_D and E_A, respectively.

Under continuous illumination, the photogenerated carriers (electrons and holes) are created. Steady-state concentrations of free electrons and holes are n and p, respectively. The acceptor will attract holes and the shallow donor will capture electrons. The electrons bound to the shallow donors have relatively large wave functions and large overlap with wave functions of holes bound to the acceptors. Therefore the transitions from shallow donors to different acceptors via quantum mechanical tunneling are very efficient, especially at low temperature when the concentration of free electrons is very low. This type of transition is called donor-acceptor pair (DAP) recombination. The probability of the DAP transition depends on the size of electron and hole wave functions, and on the separation between donors and acceptors.[6] With increasing temperature, the rate of the thermal emission of electrons from a shallow donor to the conduction

band becomes high. Consequently the concentration of electrons in the conduction band increases. Then the transitions from the conduction band to the acceptor, called eA transitions, become dominant over DAP transitions. At high temperature, the eA transitions contribute to PL more than DAP transitions for the same defect.

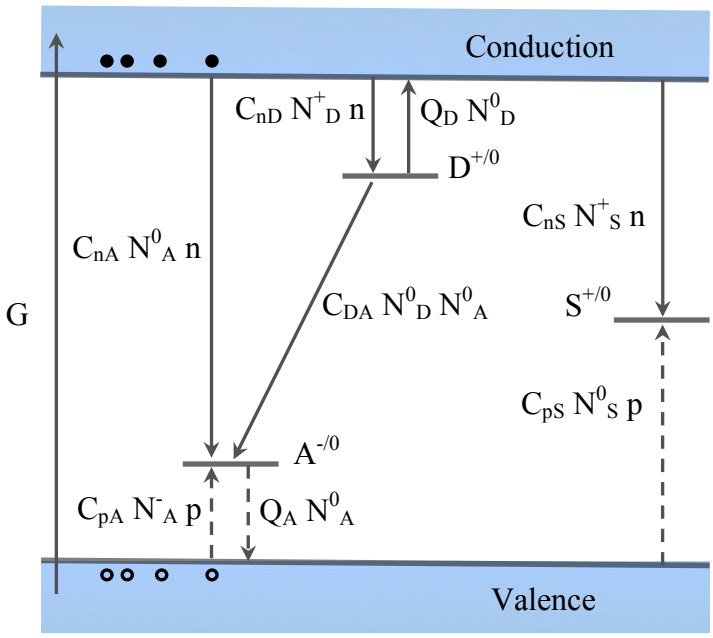

Figure 3. Energy band diagram and schematic of electron and hole transitions in a semiconductor. The electron and hole transitions are shown with solid and dashed arrows, respectively.

The main transitions that occur in such a semiconductor can be described within phenomenological model as shown in Figure 3. In particular, electrons from the conduction band are captured by acceptors, shallow donors and nonradiative centers at rates of $C_{nA}\ N_A^{\ 0}\ n$, $C_{nD}\ N_D^{+}\ n$, and $C_{nS}\ N_S^{+}\ n$, respectively, where C_{nA}, C_{nD} and C_{nS} are electron-capture coefficients for the shallow donor, acceptor, and a nonradiative center, respectively. [1, 2, 6,12] Holes from the valance band are captured by acceptors and nonradiative centers at rates of $C_{pA}\ N_A^{-}\ p$ and $C_{pS}\ N_S^{0}\ p$, respectively, where C_{pA} and C_{pS} are hole-capture coefficients for the acceptor and

nonradiative center, respectively. [1, 2, 6,12] However, the holes being captured by acceptors or S centers, are usually not captured by shallow donors because acceptors are filled with electrons in dark and are very efficient in attracting holes, and some S centers have been experimentally observed to compete in the efficiency with acceptors. Besides, transitions are usually radiative when the change in energy during the transition is very large, comparable to the band gap.

The electrons captured by shallow donors may return to the conduction band and the holes captured by acceptors may return to the valence band with increasing temperature as a result of thermal excitation at rates of $Q_D\ N_D^0$ and $Q_A\ N_A^0$, respectively. The rate of these transitions is proportional to $\exp(-E_i/kT)$, where E_i is the defect ionization energy and k is Boltzmann's constant. The emission coefficients, Q, can be found from detailed balance as

$$Q_D = \frac{C_{nD}\, N_C}{g} exp(-\frac{E_D}{kT}), \tag{3}$$

$$Q_A = \frac{C_{pA}\, N_v}{g} exp(-\frac{E_A}{kT}), \tag{4}$$

where g is the degeneracy of the donor and acceptor levels. The effective density of states in the conduction band, N_c, and in the valence band, N_v, are functions of temperature defined in the equations below as:

$$N_c = 2\ \left(\frac{m_n \mathrm{k}\ T}{2\ \pi\ \hbar^2}\right)^{3/2}, \tag{5}$$

$$N_v = 2\ \left(\frac{m_p\ \mathrm{k}\ T}{2\ \pi\ \hbar^2}\right)^{3/2}, \tag{6}$$

where T is temperature, $\hbar$ is the Planck constant, m_n is the effective mass of an electron and m_p is the effective mass of a hole. [1, 2, 6,12] Finally the transitions of electrons from shallow donor levels to acceptor levels occur at a rate of $C_{DA}\ N_D^0\ N_A^0$ where C_{DA} is the effective coefficient for the

DAP transitions.

The rate equations under steady-state conditions can be written down from the band diagram in Figure 3. The rate of changing of free electrons concentration in the conduction band is given by

$$\frac{dn}{dt} = G - C_{nA} N_A^0 n - C_{nS} N_S^+ n - C_{nD} N_D^+ n + Q_D N^0_D = 0 \quad (7)$$

The free electrons in the conduction band are generated by incident light at a rate G and by thermally excited electrons from shallow donors. The conduction band loses electrons due to their transitions to the acceptor level, the shallow donor level, and to the nonradiative center.[1,2,6,12]

The next equation describes the rate of changing of free holes concentration in the valence band and is given by

$$\frac{dp}{dt} = G - C_{pA} N_A^- p - C_{pS} N_S^0 p + Q_A N_A^0 = 0 \quad (8)$$

The balance of free holes in the valence band is derived from the photogenerated holes at a rate G plus the thermally emitted holes from acceptor along with loses of free holes when they are captured by the acceptor level and by the nonradiative center.

A third equation shows the balance of transitions at the acceptor. The sum of the rate of electrons flow from the conduction band and from shallow donor to the acceptor is equal to the flow of free holes captured by the acceptor minus the flow thermally emitted holes from the acceptor, yielding[1, 2, 6, 12]

$$C_{nA} N_A^0 n + C_{DA} N_D^0 N_A^0 = C_{pA} N_A^- p - Q_A N_A^0 \quad (9)$$

For the shallow donor, the gain and loss of electrons is described by the rate equation in which

the capture of electrons from the conduction band minus the thermal emission of electrons to the conduction band is equal to the transition of electrons from shallow donor to the accepter due to DAP mechanism, so that is given by

$$C_{nD}\, N_D^{+}\, n - Q_D\, N_D^{0} = C_{DA}\, N_D^{0}\, N_A^{0} \tag{10}$$

The last rate equation is for the nonradiative center. There is a balance in steady-state conditions between the transition rates of electrons from the conduction band and holes from the valence band, given by

$$C_{nS}\, N_S^{+}\, n = C_{pS}\, N_S^{0}\, p \tag{11}$$

Finally, charge is conserved, so that all positive charges are balanced by negative charges. Therefore, the neutrality equation will be the balance of the sum of concentrations of holes, positively charged nonradiative centers, and positively charged shallow donors with the sum of concentrations of electrons and negatively charged acceptors which is given by

$$p + N_S^{+} + N_D^{+} = n + N_A^{-} \tag{12}$$

Using these rate equations through program created with mathematical modeling software, one can theoretically analyze data, fit them and compare them with the experimental results to explain PL behavior.

2.3 Temperature dependence of photoluminescence intensity from defects

When a semiconductor is excited with a laser ($hv > E_g$), charge carriers transitions begin as explained above. The charge carriers that have been captured by some levels can be excited to the conduction or valence band either optically or thermally. The most common process is the thermal activation. The temperature at which the carriers are thermally emitted from defects

correlates with the depth of the defect levels that captured them as we can see from Eqs. (3) and (4).[13]

To find the role of temperature, let us consider an n-type semiconductor containing a shallow donor and several radiative acceptors. In an n-type semiconductor, the Fermi level is close to the conduction band. Therefore under equilibrium and low temperature, all acceptors are ionized, and there are no holes in the valence band. With illumination, electron-hole pairs are created at generation rate G (cm^{-3} s^{-1}). For simplicity, the nonradiative center is considered here to be a deep acceptor.[12] Thus the holes capture rate can be expressed in general as (C_i N_i^- p). The concentrations of holes bound to acceptors N_{Ai}^0 and nonradiative center N_S^0 can be written as N_i^0. Therefore, Eq. (8), the balance equation for the hole concentrations in valence band, can be rewritten in general form in the case of N recombination channels

$$\frac{dp}{dt} = G - \sum_{i=1}^{N} C_i \; N_i^- \; p + \sum_{i=1}^{N} Q_i \; N_i^0 = 0 \qquad (13)$$

The capture rates are usually much faster than the radiative recombination rates.[2, 6, 12] Thus, the efficiency of the recombination for each channel is proportional to the rate of capturing minority carriers which are holes in an n-type semiconductor. Therefore, the quantum efficiency of each recombination channel at low temperature, η (0), where the thermal emission of holes is negligible, is determined as the ratio of hole capture rate for one channel to the total capture rate of holes that escape from the valence band

$$\eta_i(0) = \frac{C_i \; N_i \; p}{\sum_{j=1}^{N} C_j \; N_j \; p} = \frac{C_i \; N_i}{\sum_{j=1}^{N} C_j \; N_j} \qquad (14)$$

By considering a case of low excitation intensity ($N_i^0 \ll N_i^- \approx N_i$), the concentration of

holes bound to ith defect in steady state will be the rate of holes captured by ith defect minus the holes recombination via ith channel minus the thermal release of bound holes. This is given as

$$\frac{\partial N_i^0}{\partial t} = C_i\, N_i\, p - \frac{N_i^0}{\tau_{R_i}} - Q_i\ N_i^0 = 0, \tag{15}$$

where τ_{R_i}characterizes the radiative recombination lifetime, the PL lifetime.

In order to find the concentration of holes bound to the ith acceptor N^0_i, Eqs. (13) – (15) can be re-arranged and written as

$$N_i^0 = \frac{\eta_i(0)\,(G + \sum_{j=1}^{N} Q_j\ N_j^0)}{{\tau_{R_i}}^{-1} + Q_i} \tag{16}$$

The linear system of Eq. (16) is solved to get the intensity of PL for each defect

$$I_i^{PL} = \frac{N_i^0}{\tau_{R_i}} = \frac{\eta_i}{1 + (1-\eta_i)\,\tau_{R_i} Q_i}\, G, \tag{17a}$$

Re-write Eq. (17a) in term of quantum efficiency where $\eta = I^{PL}/G$, will give

$$\eta_i(T) = \frac{\eta_i(0)}{1 + (1-\eta_i(0))\,\tau_{R_i} Q_i}, \tag{17b}$$

where

$$\eta_i(T) = \eta_i(0)\left(1 - \sum_{j\neq i}^{N} \frac{\eta_j(0)\,\tau_{R_j} Q_j}{1 + \tau_{R_j} Q_j}\right)^{-1} \tag{18}$$

In the final analysis, the temperature dependence of the internal quantum efficiency (IQE), which is the number of emitted photons as a fraction of the number of absorbed photons, $\eta = I^{PL}/G$, can be found. Substituting Eq. (3) into Eq. (17) will give an expression for the IQE of PL related to a defect.[1, 2, 6 ,14]

$$\eta\,(T) = \frac{\eta\,(0)}{1 + C\exp(-\frac{E_A}{kT})} \tag{19}$$

where $\eta(0)$ is IQE of the defect-related PL at low temperature before the quenching, and is defined as $\eta = I^{PL}/G$, (I^{PL} is the PL intensity, and G is the number of electron hole pairs created by the laser, per unit volume, per second), E_A is the ionization energy of the acceptor responsible for the thermal quenching, k is Boltzmann's constant, and C is a constant:

$$C = (1 - \eta\,(0))\,\tau_{PL} C_{pi}\,N_v/g, \tag{20}$$

where τ_{PL} is the PL lifetime, C_{pi} is the hole capture coefficient, N_v is the effective density of states in the valence band, and g is the degeneracy of the defect level.

According to Eq. (19), the temperature dependence of PL intensity consists of two parts based on the temperature range. When the temperature is low, less than a characteristic temperature $T < T_0$, PL intensity is independent of temperature. However, with increasing temperature, at $T > T_0$, another part of dependence reveals an exponential decrease in PL what is called PL quenching. The characteristic temperature T_0 at which the thermal quenching of PL begins can be found from the relation $C\exp(-E_A/kT_0) = 1$. In other words, the thermal quenching with activation energy E_A starts when $C\exp(-E_A/kT_0) \geq 1$. Such type of quenching is called the normal quenching (NQ) which is given by Eq. (19). [2, 6]

Chapter 3: Literature Review

Many studies on temperature dependence of PL were reported since earlier time.[12, 15-18] Decreasing the intensity of PL with increasing temperature is one of the most effective methods that provide valuable information about defects in semiconductors.[1-4, 12, 15-18] PL quenching studies have been recognized as a sensitive method that is widely used to explore the physical characteristics of semiconductors. Thus, it is important to understand the mechanisms involved within this quenching as will be discussed in details in this chapter. PL thermal quenching is attributed to one of three different mechanisms, Schön-Klasens, Seitz-Mott, and abrupt tunable mechanisms. [1-4, 6, 12, 15-18]

3.1 Effect of Temperature on PL

Photoluminescence from defects is usually observed as broad bands due to the strong electron-phonon coupling typical for deep-level defects.[3, 6] Increasing temperature may change the position and the shape of broad PL bands. Furthermore, the intensity of PL, I^{PL}, changes with the temperature.[2, 6, 19]

An example of two different samples exhibiting different behaviors for the PL bands with increasing temperature is shown in Figure 4. The intensity of the ultraviolet luminescence (UVL) band in p-type Mg-doped GaN decreases as the temperature increases, also its shape changes into a structure less band, Figure 4 (a).[18] In high-resistivity Zn-doped GaN, the decreasing of the blue luminescence (BL) intensity is observed by two order of magnitude over an interval that is only 10 K, however the shape and position of PL do not change for this sample in the process of the thermal quenching, Figure 4 (b).[6]

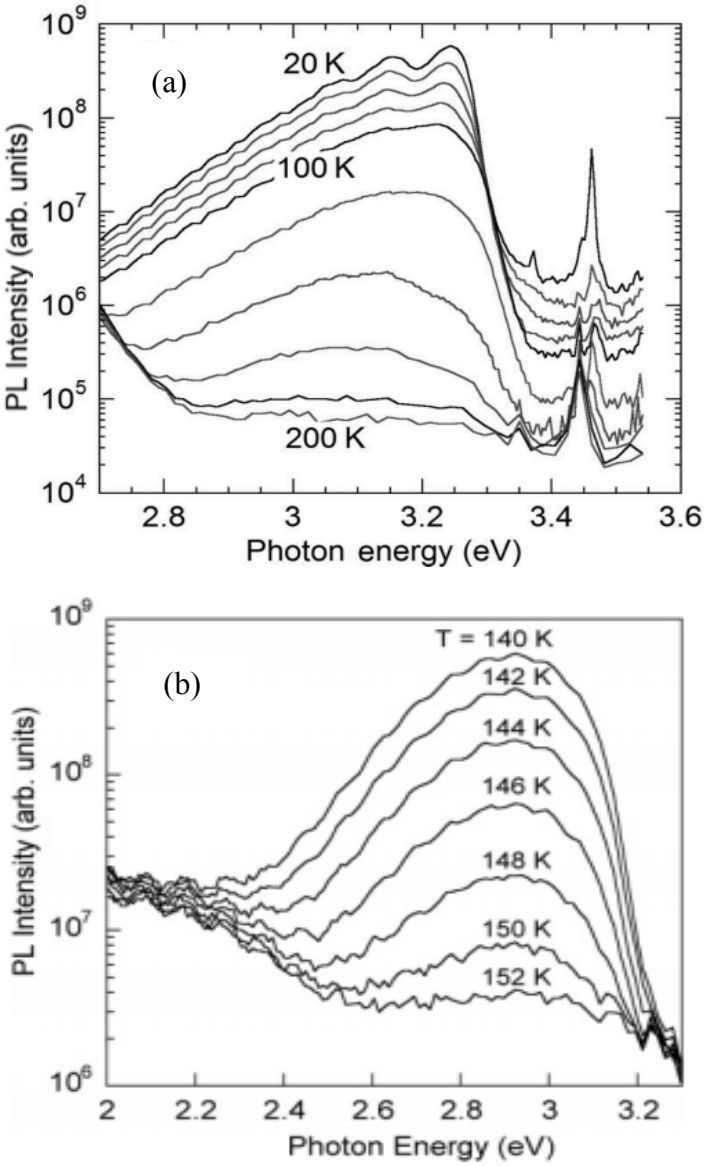

Figure 4. Evolution of PL spectra with increasing temperature in Mg-doped GaN (a), and Zn-doped GaN (b).[6, 19]

3.2 Mechanisms of thermal quenching of PL from point defects

Illumination is one of different ways to produce non-equilibrium carriers in semiconductors. The non-equilibrium carriers are created with the generation rate G and measured as the number of free electrons and holes produced per unit volume in a unit time [cm^{-3} s^{-1}]. [10] Photogenerated electrons in the conduction band are captured quickly by positively

charged shallow donors, D^+, and deep donors S^+. The photogenerated holes in the valence band are captured quickly by the negatively charged acceptors, A^- and by neutral deep donors, S^0. All these capture processes are fast, in order of 10^{-10} s, and they are nonradiative, meaning that multiple phonons are emitted instead of photons.[2] The recombination of these trapped charge carriers is the next step. Recombination of electrons and holes occurs by transition the electrons from the conduction band or shallow donors to an acceptor level and that will give the PL.

The quenching of the PL related to defects in n-type semiconductors with increasing temperature is commonly attributed to one of the following mechanisms. According to the first mechanism, the quenching of PL occurs because the holes escape from the acceptor level to the valence band with increasing temperature. The thermal emission of holes to the valance band becomes significant at some critical temperature, T_0. These escaped holes can be captured by other defect centers called the killer centers or poisons. The PL quenching takes place with activation energy equal to the ionization energy of this defect. Since this mechanism requires the presence of other types of defects to explain the PL quenching, it is called the multi-center model.[2] It was originally suggested by Schön and Klasens.[2, 15] Energy band diagram can be used to illustrate the first mechanism (Figure 5). After the electron-hole pair is created (transition 1), a free hole is captured by an acceptor and a free electron is captured by a shallow donor (transitions 2 and 3, respectively). The PL emission caused by transitions of electrons from the conduction band to the acceptor level (eA transition) and by transitions of electrons from the shallow donor to the same acceptor level (DAP transition) are indicated as transitions 4 in Figure 5. The quenching of PL begins when holes start escaping from an acceptor with increasing temperature (transition 5). These thermally emitted holes may be re-captured back by the same defect (transition 2), or recombine with electrons via other recombination channels including

nonradiative defect centers (transition 6). [2] In the case of thermal quenching of PL band with high internal quantum efficiency (IQE), there may be an increase in other PL intensities in the region of the thermal quenching of the main PL band that was quenched. The released holes in the valence band due to the thermal quenching of PL of one channel are redistributed among all other recombination channels. When they recombine radiatively, the intensity of the related PL bands increases.[2]

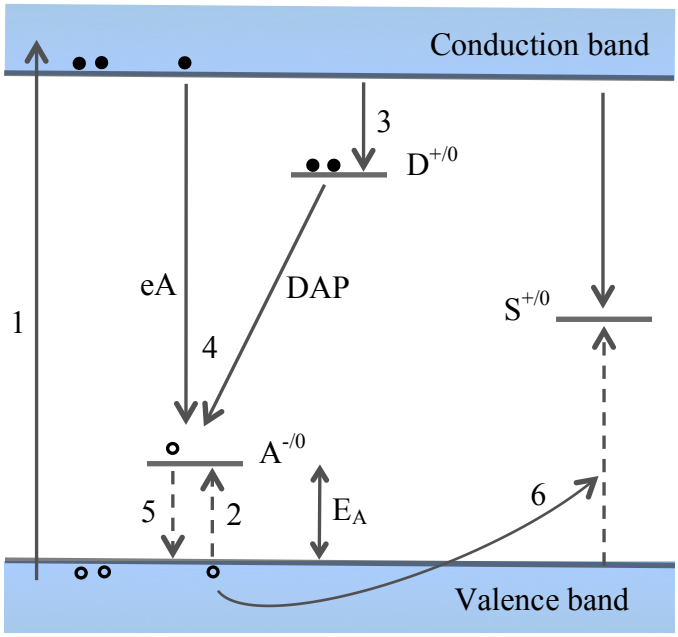

Figure 5. Energy band diagram with three type of defect in n-type semiconductor.

The Schön-Klasens mechanism was formulated in 1942 by Schön then further developed by Klasens.[2,15,16] Klasens explained the effect of temperature on changing the color of luminescence from ZnS phosphors with changing PL from different impurities. He assumed that in ZnS phosphors there are at least two types of activators (impurities causing PL): silver and copper. The centers responsible for the blue luminescence, silver, have energy level closer to the valance band, and the green luminescence centers, copper, have deeper energy level. Thus, the

color of luminescence changes from blue to green with increasing temperature due to the escaping of the holes from blue centers and transferred to the green centers. Klasens suggested that the same effect would be observed in the temperature dependence of the blue band if another defect introduces a level at larger distance from the valance band than that for the blue center. Such a defect can be nickel in ZnS. Nickel center is different from the green center where the nickels do not produce visible radiation. Increasing the amount of the nickel and keeping the same amount of silver in ZnS:Ag phosphors will decrease the intensity of the blue band as shown in Figure 6.[15]

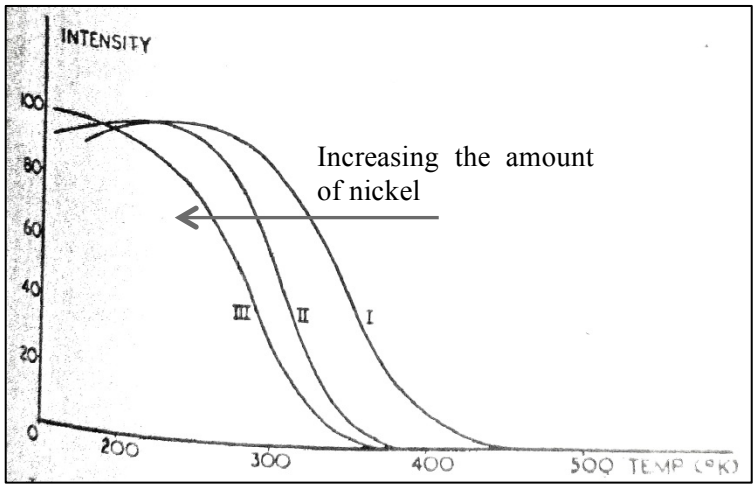

Figure 6. Influence of increasing the amount of nickel on the temperature dependence of the blue emission in ZnS.[15]

Also, the same effect will happen to the green emission in ZnS:Cu phosphors when the levels of the nickel centers are at distance greater than green center from the valence band by increasing the amount of nickel. The holes are transferred from the blue and green centers to the nickel center. Therefore, adding even a small amount of nickel kills the blue and green luminescence.[15]

Thermal quenching of PL for many defects was studied and explained.[2, 6] One example is Zn-related blue luminescence (BL) band where Zn_{Ga} is an acceptor in conductive n-type GaN.[2] The blue luminescence quenches at temperatures $T > T_0 \approx 300$ K as shown in Figure 7. The activation energy of the thermal quenching of the BL band can be obtained from measuring the slope in the Arrhenius plot. The value of the slope in the region of BL quenching is about 0.35 eV, which is in agreement with the ionization energy of the acceptor responsible to the BL band. The temperature dependence of PL intensity for three PL bands (BL, YL and NBE, which is the near band edge emission), all in one degenerate GaN:Si,Zn sample, is shown in Figure 7.[2]

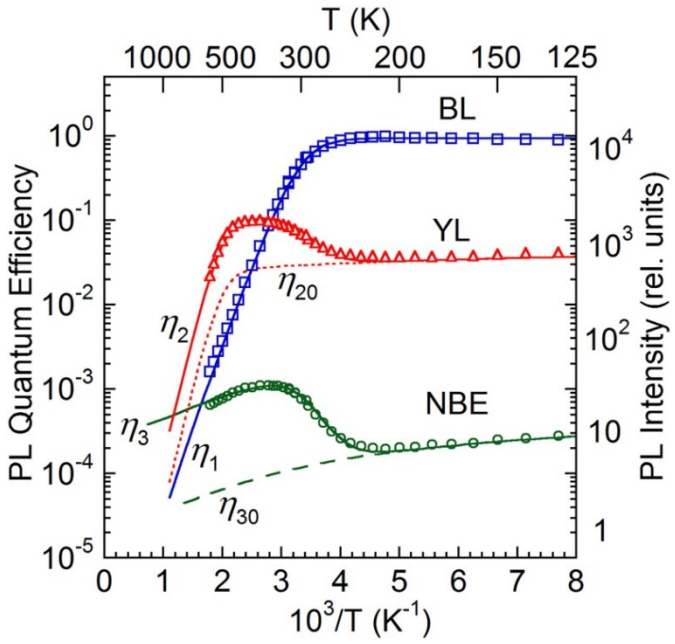

Figure 7. Temperature dependence of the absolute IQE of PL in GaN:Si,Zn.[2]

Quenching of the BL band causes significant increases in intensities of other bands, YL and NBE, due to the high IQE of the BL band in this sample (≈90%). These rises in other PL bands prove that the quenching occurs via the Schön -Klasens (multi-center) mechanism. Also, it means the Zn_{Ga} defect remains radiative at all temperatures, and the changing in the PL intensity

is due to the competition for holes between different types of defects.[2]

The second mechanism that can explain the quenching of PL related to defects was first proposed by Seitz and Mott in 1939.[2, 17] The PL quenching in this mechanism occurs due to the gradual replacement of radiative transitions with non-radiative ones for the same defect with increasing the temperature, and therefore it is called the one center model. One-dimensional configuration coordinate diagram is used to get better understanding of this mechanism (Figure 8). With increasing temperature, the defect in the excited state gets enough energy to reach the level where adiabatic potentials of its ground and excited states cross. Then, recombination of an electron with the bound hole releases energy in the form of multiple phonons and does not emit photons.[2] Seitz and Mott provided an explanation showing how a fluorescent center can return from an excited state to the ground state in two ways.[17] One way is by emitting photons (transition 4), and another way is by emitting only phonons, which causes PL quenching (transition 5). Two typical cases of thermal quenching are illustrated in Figure 8.[2]

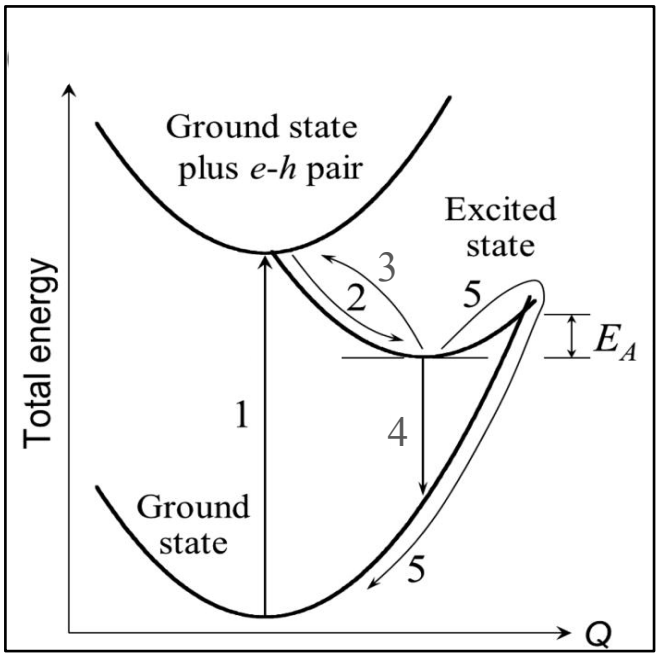

Figure 8. Schematic one-dimensional configuration coordinate diagram for an acceptor in an n-type semiconductor.[2]

Absorbed light creates electron-hole pairs and brings the system to higher energy (transition 1 in Figure 8). When the hole is captured by the accepter, the energy of the system decreases (transition 2). Moreover, the wave function of hole is localized at one bond of the acceptor, and its asymmetrical location would cause the atom to physically shift from its original sites, Figure 9.[3] Thus, transition 2 in Figure 8 shows how the system rearranges itself gradually due to the shift of atoms followed by emission of phonons.

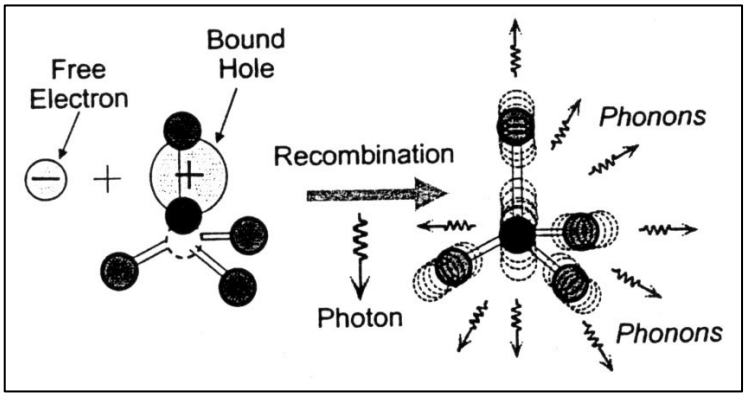

Figure 9. Schematic representation of localized hole at acceptor cause a physical shift.[3]

The system may get back to the ground state by thermal emission of the hole from the acceptor level to the valence band (transition 3), or by recombination of a free electron with a bound hole, resulting in PL (transition 4). With increasing temperature, atomic vibrations increase and the energy of the system in the excited state increases.[13] At some temperature, the energy of the system may reach the crossing of the ground and excited states. Therefore, the system can overcome the potential barrier and make a nonradiative transition to the ground state with emission of phonons (transition 5). In this case, the activation energy of the PL quenching is equal to the energy difference between the crossover point of the excited and ground states and the minimum of excited state.[2]

It is hard to distinguish if the quenching is due to Seitz-Mott or Shon-Klasens mechanisms. However, finding zero phonon line (ZPL) sometimes helps to determine the type of mechanism.[2] The position of the ZPL can be found either by observation of a sharp line in the high energy part of PL spectrum or from comparison of the PL and PL excitation (PLE) spectra. Therefore, the energy difference between the band gap and the ZPL is expected to be close to the ionization energy. In the case of the Shon-Klasens mechanism, in which the emission of holes to the valance band in n-type causes the quenching, the activation energy of the thermal quenching in Arrhenius plot is close to that value. For the Seitz-Mott mechanism, there is no relation of the ionization energy of a defect and the activation energy of the PL quenching.[2, 17]

Among many defects in GaN, the thermal quenching of the RL2 and GL2 bands in high resistivity Ga-rich GaN that grown by molecular beam epitaxy (MBE) occurs via Seitz-Mott mechanism.[3, 6] Both bands start quenching at temperature above 100 K and disappear at room temperature, Figure 10.[3]

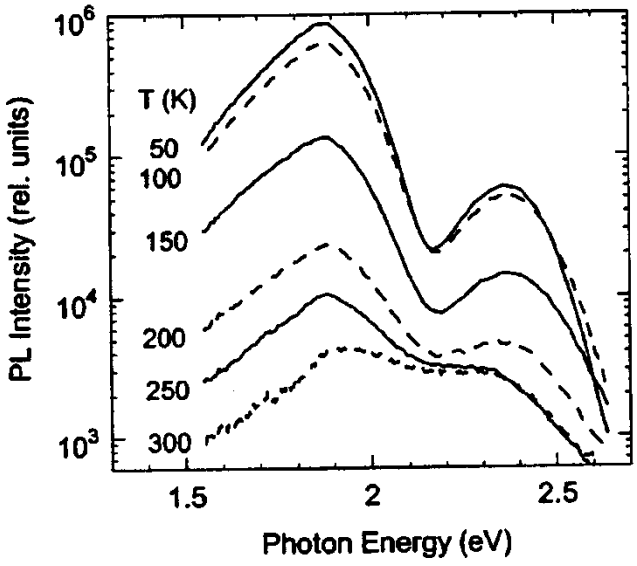

Figure 10. PL spectra of the Ga-rich GaN layer at different temperatures.[3]

The semilog plot of PL intensity of RL2 and GL2 bands versus inverse temperature is shown in Figure 11.[3]

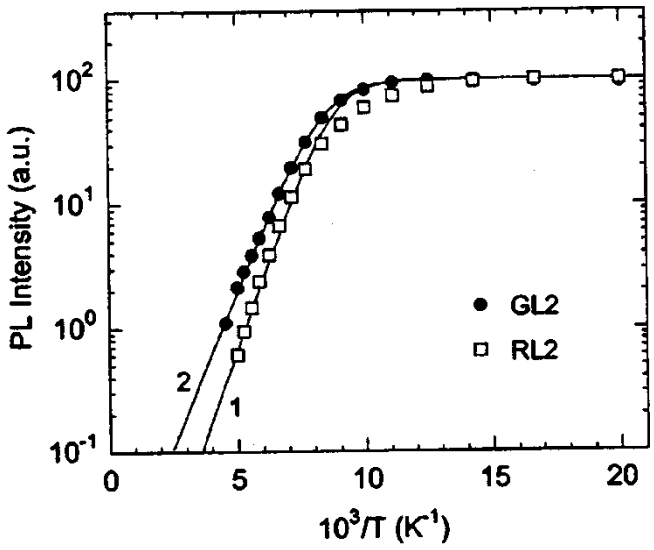

Figure 11. Temperature dependence of PL of the RL2 and GL2 band in Ga-rich GaN.[3]

The RL2 band at 1.85 eV and the GL2 band at 2.35 eV are quenching thermally with the activation energy of about 0.10-0.14 eV.[2, 3] However, from comparison of the PL and PLE spectra for these bands, the ZPL is expected between 2.1 and 2.7 eV for the RL2 band, and between 2.7 and 3.4 eV for the GL2 band. Thus, the activation energy of the quenching in Figure 11 gives an ionization energy that is very small to the one obtained through the ZPL.

Furthermore, the PLE spectrum for the RL2 band can be resolved into two Gaussian-like bands (curve 3 with a maximum at 3.10 eV and curve 4 with a maximum at 3.38 eV in Figure 12).[3] Gaussian shape of the PL and PLE bands reveals that the defect has a strong electron-phonon coupling, and the recombination of carriers at this defect results in emission of large number of phonons.

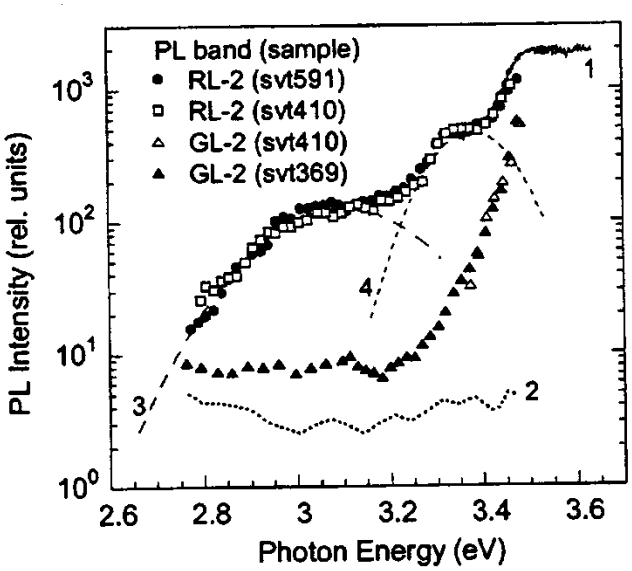

Figure 12. PLE spectra at 15 K for the RL2 and GL2 bands in Ga-rich GaN. Curve 1 shows a part of the PLE spectrum for the RL2 band and curve 2 is the PLE spectrum represents the noise signal.[3]

Moreover, the analysis of peak position of the RL2 and GL2 bands after a pulsed excitation displays no noticeable shift in their position, and both bands decay exponentially.[3, 6] This behavior is completely different from the non-exponential PL decay due to the escape of holes from an acceptor to the valence band in n-type. This indicates that the RL2 and GL2 bands cannot be attributed to DAP type recombination at low temperature. To sum up, it is possible that the PL quenching for the RL2 and GL2 bands occur by Seitz-Mott mechanism.[2, 3]

In both models, the multi-center (Schön -Klasens mechanism) and one center (Seitz-Mott mechanism), the temperature dependence of the PL efficiency can be described with Eq. (19).[2]

$$\eta\,(T) = \frac{\eta\,(0)}{1 + C\exp(-\frac{E_A}{kT})}, \tag{19}$$

3.3. Abrupt and tunable thermal quenching of PL

Abrupt and tunable thermal quenching of PL is a relatively new phenomenon with an unusual behavior of PL that can be observed in the Arrhenius plot. This feature can be found in high resistivity semiconductors, n-type and p-type, where the thermal quenching of PL occurs in a much narrower temperature range; i.e., the quenching is abrupt.[1-3, 6] In this case, the simple formulas derived for conductive n-type semiconductors fail and may produce unreasonable and unphysical parameters.[6]

Moreover, a characteristic feature of the abrupt quenching is that it is tunable by the laser power. The tunable quenching of PL has been reported early in the 1940's in studies of phosphors. Klasens, Vergunas and Gavrilov observed a drop in PL intensity from defects in ZnS at characteristic temperature $T = T^*$, and the temperature at which the PL intensity suddenly dropped is shifted significantly to higher temperatures with increasing the excitation intensity.[1-3, 6, 12, 15-18]

An example of the abrupt and tunable thermal quenching for PL band related to Zn-doped GaN is shown in Figure 13. The temperature dependence of blue luminescence (BL) band shows a sharp drop in the intensity at $T = T^*$, and the temperature where the abrupt quenching begins, increases from 130 to 216 K with increasing the excitation intensity from 3×10^{-7} to 0.3 W/cm^2.[9]

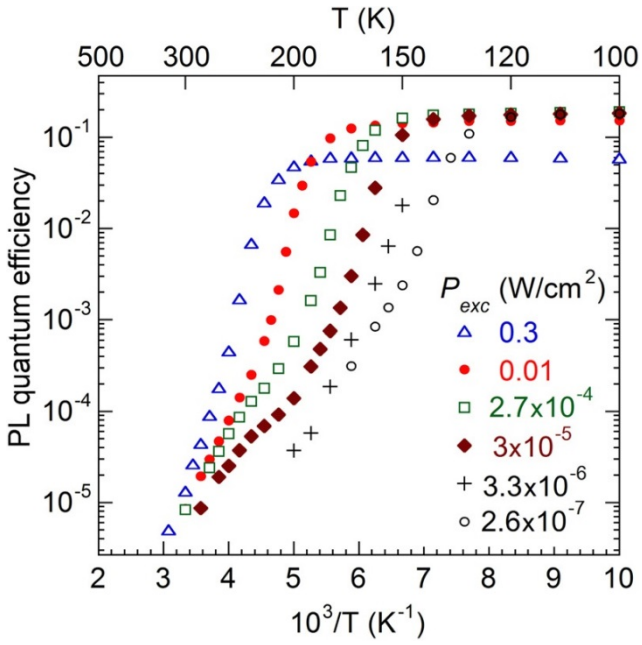

Figure 13. Temperature dependence of quantum efficiency of the BL band in Zn-doped GaN at several excitation intensities.[2]

3.3.1 Explanation of Abrupt Thermal Quenching

The abrupt and tunable quenching of PL is caused by a sudden redirection of the recombination flow from a defect related to a radiative recombination channel to a nonradiative recombination channel.[2, 6] This happens when the concentration of holes thermally emitted from the radiative defect to the valence band becomes comparable to the concentration of photogenerated holes at some characteristic temperature, T_0. In the model explaining abrupt and tunable quenching, at least three types of defect centers must be involved, Acceptor, shallow donor and nonradiative deep donor.

Under illumination and up to a temperature close to the characteristic temperature, at $T < T_0$, the carriers are generated in the semiconductor only due to illumination. Photogenerated electrons are quickly captured by nonradiative deep donors, S, and photogenerated holes are quickly captured by acceptors, A. With continuous illumination, nonradiative deep donors

become filled with electrons and acceptors become filled with holes, thus population inversion is observed at $T < T_0$.

With increasing temperature, electrons are thermally emitted from shallow donors to the conduction band. The radiative recombination, PL, of electrons from the shallow donors or from the conduction band with holes at the acceptors is dominant because the nonradiative centers are saturated with electrons. Meanwhile, the acceptors usually slowly capture electrons due to the long PL lifetime, which leads to accumulation of electrons in the conduction band, and then n-type photoconductivity is observed.

At higher temperatures above the characteristic temperature, $T > T_0$, thermal emission of holes from the acceptor level to the valence band becomes significant. The additional holes in the valance band recombine with electrons trapped at the nonradiative centers which helps to open the bottleneck of these channels. Gradually, normal population is observed at $T > T_0$ (nonradiative deep donors are almost filled with holes and acceptors with electrons), and photoconductivity switches from n-type to p-type.

For this process to happen, the nonradiative centers S should have large capture cross-section for both electrons and holes. Also, the nonradiative centers S have sufficiently deep levels, so that charge carriers (electrons or holes) cannot escape from them at reasonable temperatures. In such a situation, most of recombination occur via the S channels and cause a dramatic decrease in the amount of electrons in the conduction band, which leads to a sudden drop in the PL quantum efficiency at the characteristic temperature T_0. This process may be slow in time but abrupt upon small change of temperature.[2, 6]

Thermally emitted holes change the balance in the system, and the system undergoes from one type of behavior to another at the characteristic temperature, T_0. Just below T_0, the

nonradiative centers S are filled with electrons, and the acceptors accumulate holes. For example, in case of Zn-related PL in high-resistivity GaN, the quantum efficiency of nonradiative channel is about 80%, and the other 20% recombine through the radiative channels, mostly produced the BL band. Above T_0, the nonradiative centers S become empty from electrons, and the acceptors become saturated with electrons. The dramatic change in concentrations at the characteristic temperature T_0 results in abrupt quenching of the acceptor-related PL intensity, and the quantum efficiency of the S channel becomes almost 100%. [6]

The shape and position of PL bands do not change in case of the abrupt quenching. Increasing the excitation power density (P_{exc}) shifts the abrupt quenching to higher temperatures. Figure 14 demonstrates the tunable quenching where there are several curves of PL quantum efficiency for high-resistivity Zn-doped GaN, one for each excitation intensity.[6]

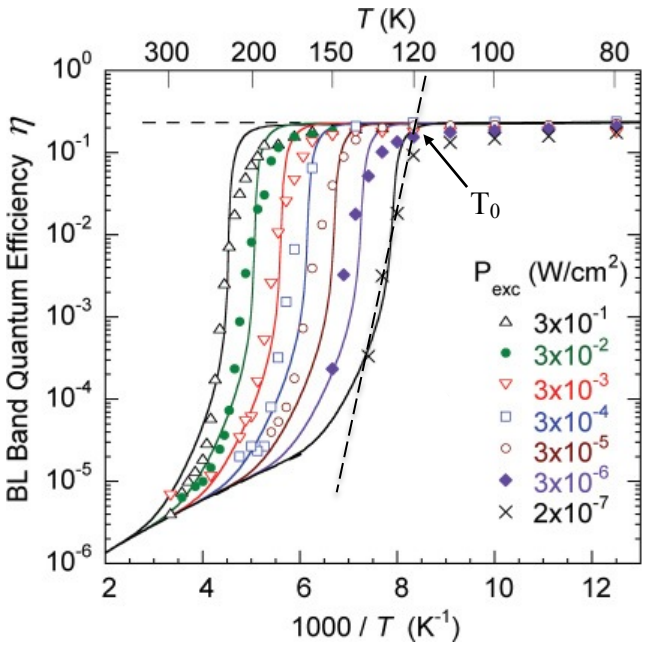

Figure 14. Temperature dependence of quantum efficiency of the BL band in Zn-doped GaN.[4]

The characteristic temperature, T_0, at which the thermal quenching takes place, is a crossover temperature where the system physically changes from one type of behavior to another.[2, 6] Finding the characteristic temperature requires performing a precise fit by using numerical solutions of the rate equations that yield the solid curve as shown in Figure 14. However, it is easier from the same graph, the Arrhenius plot, to find the temperature of the quenching by extrapolating the low-temperature part, that is almost horizontal, and the high-temperature part with the largest slope to the point where they cross, which can be defined as the characteristic temperature T_0 (Figure 14). The difference between the values of T_0 in the both methods is small and independent of the excitation intensity. However, the plot of both of these temperatures as a function of the excitation intensity gives straight lines with the same slope.[6] For convenience, the excitation intensity is expressed as electron-hole generation rate, G, through the expression of simplest model of light absorption, $G = \alpha P_{exc}/\hbar\omega$, where $\alpha = 10^5$ cm^{-1} for GaN and $\hbar\omega = 3.81$ eV for a HeCd laser.[1]

The dependencies of T_0^{-1} on G for several high-resistivity GaN:Zn samples demonstrating the abrupt and tunable thermal quenching of the BL band are shown in Figure 15. The slopes of the dependences are about the same for all the samples, and they determine the ionization energy of the acceptor that emits holes to the valence band and causes the sudden drop in BL intensity. The ionization energy reveals through the abeupt and tunable modet (ATQ), E_A= 350 meV, is consistent with the binding energy of Zn_{Ga}.[6]

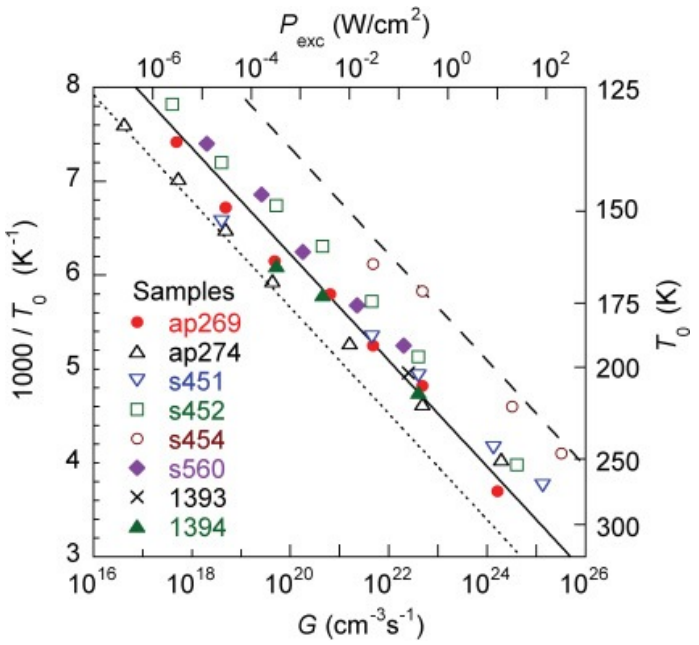

Figure 15. Dependence of the characteristic temperature on excitation intensity for high resistivity GaN:Zn samples.[4]

In 1965, Maeda observed tunable thermal quenching of PL in an insulating sample of GaP, in which the characteristic temperature increased with the excitation intensity.[18] However, the activation energy of the PL thermal quenching based on Maeda's calculation from his experimental data in the Arrhenius plot reveals the slop of 0.118 eV. Figure 16 shows the dependence of the characteristic temperature of PL abrupt quenching on the excitation intensity for GaP derived from the experimental data of Maeda. The figure displays two sets of characteristic temperatures (T_1 and T_2) because the quenching of PL contains three regions for Maeda's data in the Arrhenius plot. However, each region with different activation energy and the break points between them are defined as T_1 and T_2. The dependence gives straight lines with slopes of 0.08-0.09 eV for an acceptor that is responsible of PL quenching. This value is close to the one was calculated by Maeda for the slope of thermal quenching.[2, 6]

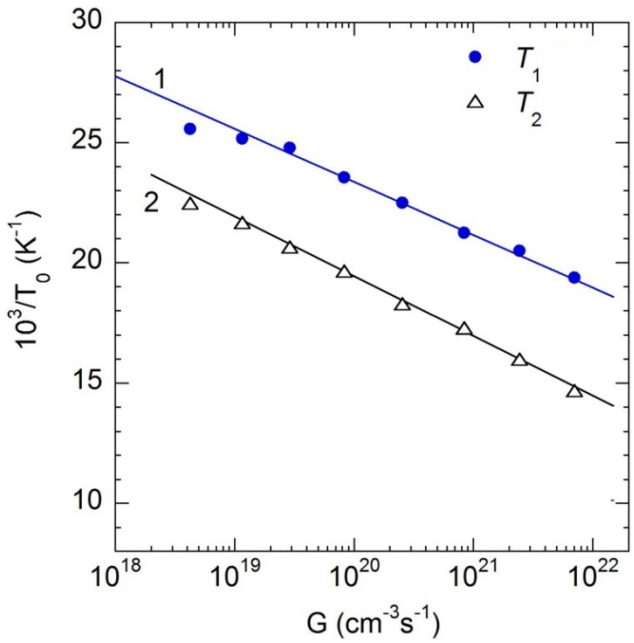

Figure 16. Dependence of the characteristic temperature on excitation intensity for insulating GaP sample.[2]

3.3.2 Normal and abrupt quenching

It is useful to compare two different types of PL quenching (normal and abrupt) to see how great the new effect may be. PL quenching in high resistivity Zn-doped and conductive n-type undoped GaN samples is shown in Figure 17. The high concentration of Zn causes a high resistivity in Zn-doped GaN which is the reason for the abruptness of the BL band quenching. The BL band can also be observed in undoped GaN due to uncontrolled contamination with Zn during the growth. However, the concentration of Zn in undoped GaN is very low because it could not be detected by secondary ion mass-spectrometry (SIMS) which makes a conductive n-type sample.

With increasing temperature, the Zn-related BL band as a dominant PL band in Zn-doped GaN presents a sharp drop in the PL intensity at a characteristic temperature T_0. While, increasing temperature for undoped GaN shows less dramatic decrease in the PL intensity for the

YL band. The BL band in same type of sample, undoped GaN, shows similar quenching behavior like YL band. However, the YL band is attributed to an acceptor deeper than the one involved in the BL band, which is quenched at higher temperatures with larger slope in the semilog plot.[6]

The BL bands in undoped and Zn-doped GaN are attributed to the same transitions involving the Zn_{Ga} acceptor. By using the traditional model used for normal quenching for n-type undoped GaN, and using the abrupt tunable model for high resistivity Zn-doped GaN, both reveal ionization energy of 300–400 meV which is consistent with the binding energy of Zn_{Ga}.[2, 6]

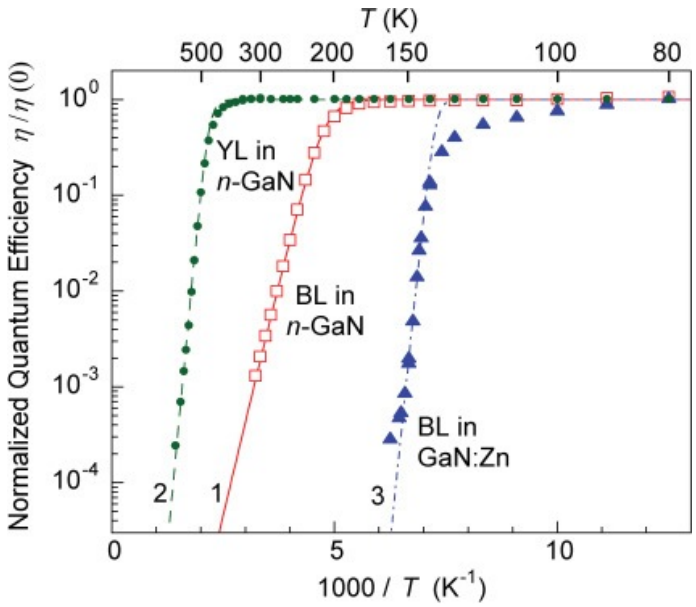

Figure 17. Temperature dependence of the BL band quantum efficiency in undoped GaN and doped GaN. The temperature dependence of the YL band quantum efficiency in another undoped GaN sample shown for comparison.[6]

The thermal quenching is normal quenching (Schön-Klasens, multi center mechanism), when the slope of the temperature dependence of the PL intensity, the slope in the region of PL quenching, reveals the ionization energy, E_A, of the defect involved in the thermal quenching. According to equation 19, the E_A can be found through this equation

$$I^{PL} = c \exp\left(\frac{E_A}{kT}\right) \tag{21}$$

The characteristic temperature at which the quenching begins, T_0, for normal quenching is independent of excitation intensity, Figure 18 (a) shows a dependence, which has, in fact, been observed in experiments for n-type GaN.[2, 6]

In contrast, the PL quenching is defined as abrupt quenching when the intensity of PL decreases by several orders of magnitude within a small range of temperature. So, it is not reasonable to describe it with normal quenching because the abruptness of this slope in the Arrhenius plot has no relation to the ionization energy, E_A, of any defect. In this type of quenching, ATQ, the characteristic temperature strongly depends on excitation intensity that can be tuned by changing the excitation intensity, Figure 18 (b).

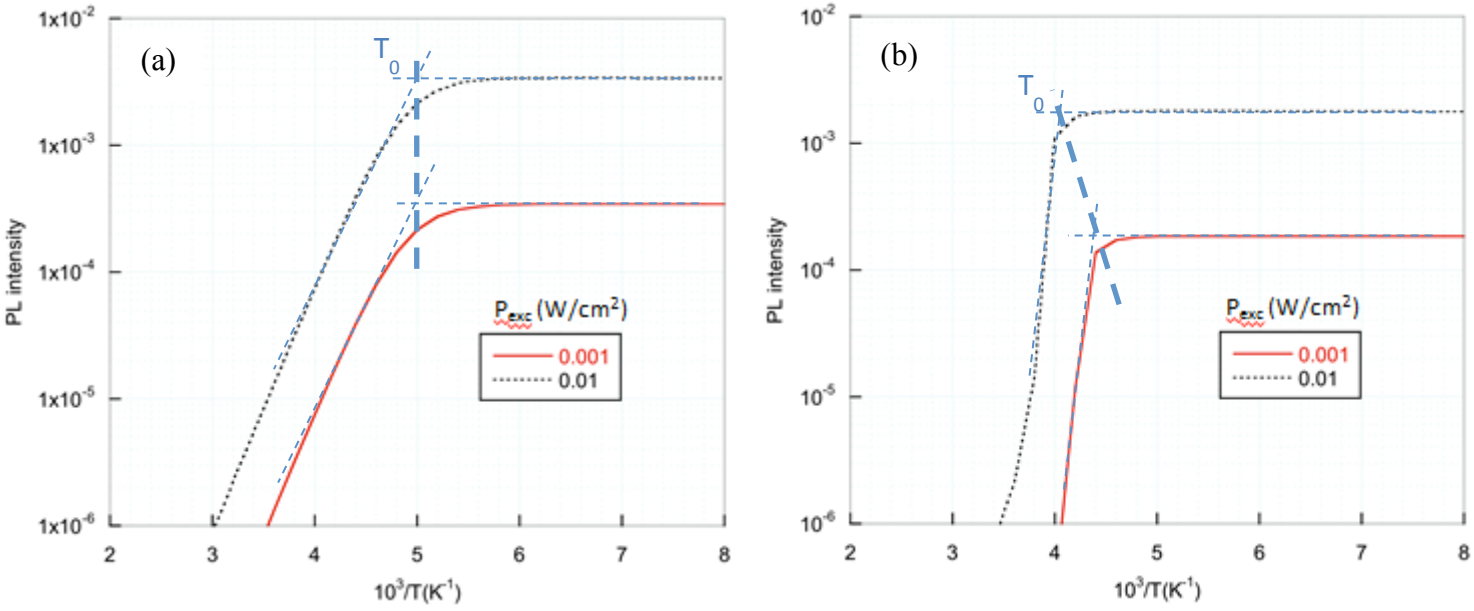

Figure 18. The difference between the two types of thermal quenching: normal quenching (a), and abrupt and tunable thermal quenching (b).

Taking the PL measurements for different excitation intensities, P_{exc}, is a new method which was developed to determine the ionization energy for the abrupt quenching. With

increasing P_{exc}, the characteristic temperature, T_0, of ATQ shifts significantly to higher temperature and thus is tunable with excitation intensity. The ionization energy of the defect can be calculated from the dependence of the inverse of characteristic temperature of quenching on the excitation intensity. The excitation light intensity P_{exc} (W/cm^2) generates electron-hole pairs in a semiconductor with the rate G (cm^{-3} s^{-1}). Assuming that electron-hole pairs are generated with uniform density only in an active region near the surface, which has a width equal to the inverse of the optical absorption coefficient α. Thus, for convenience, the excitation intensity is expressed as electron-hole generation rate G. In the simplest model of light absorption,

$$G = \alpha P_{exc}/\hbar\omega, \tag{22}$$

where $\alpha = 10^5 cm^{-1}$ for GaN and $\hbar\omega = 3.81$ eV for a HeCd laser, which is used in our work.[1]

Plotting the inverse characteristic temperature, $1/T_0$, as a function of logarithm of electron-hole generation rate, G, should give a linear dependence. The dependence of $T_0(G)$ can be fit with the following equation to determine the ionization energy: [2, 6]

$$T_0 = \frac{E_A / k}{\ln\left(B / G\right)} \tag{23}$$

where B is a sample-dependent constant and given as

$$B = C_{pA}\left(\eta_0^{-1} - 1\right)\left(N_A - N_D\right)\frac{N_v}{g} \tag{24}$$

For the case of normal quenching, the $T_0(G)$ dependence is: [2, 6]

$$T_0 = \frac{E_A / k}{\ln\left(C_{pA}\tau N_v / g\right)} \tag{25}$$

Figure 19 shows the dependences of the characteristic temperature of PL thermal quenching on the electron-hole generation rate, with reasonable parameters given in the caption. In case of

normal quenching, T_0 is independent of G, according to Eq. 25, Fig. 19a, and in case of ATQ the dependence of T_0^{-1} on ln (G) gives a slope inversely proportional to E_A, according to Eq. 23, (Fig 22b).

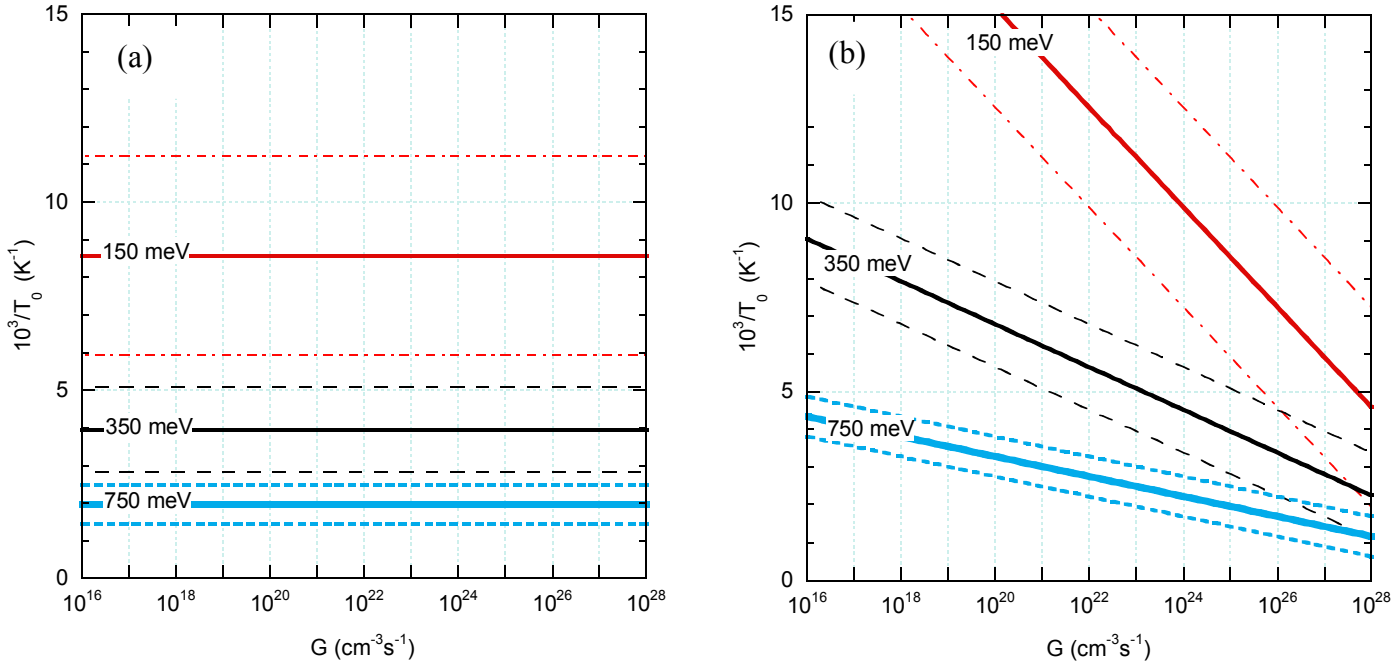

Figure 19. The dependence of the characteristic temperature of thermal quenching of PL on the electron-hole generation rate. (a) Normal quenching. (b) Tunable quenching. Solid lines are calculated using Eqs. (23) and (24) with the following parameters: $C_{pA} = 10^{-7}$ cm^3/s, $g = 2$, $\eta_0 = 0.01$, $N_v = 2.5\times10^{19}\ (T/300)^{3/2}$ cm^{-3}, $N_A - N_D = 10^{18}$ cm^{-3}, $\tau = 10^{-5}$ s. These parameters correspond to $B = 10^{32}$ cm^3/s. The values of E_A are indicated on the graphs. The dashed, dash-dotted and dotted lines in (b) indicate the range where B varies from 10^{30} cm^{-3}s^{-1} (lower line) to 10^{34} cm^{-3}s^{-1} (upper line). The same in (a) indicate the range where $C_{pA}\tau$ varies from 10^{-14} cm^3 (lower line) to 10^{-10} cm^3 (upper line).

Recently, the abrupt and tunable thermal quenching of defect related PL was observed in the following high-resistivity samples: Zn-doped, Mg-doped GaN and undoped GaN.[19, 20] To the best of our knowledge, ATQ was not observed in other semiconductors. According to existing experimental results and theoretical calculations in our lab, the abrupt and tunable thermal quenching is predicted to occur in high-resistivity semiconductors. This interesting phenomenon can be regarded as a third mechanism of PL quenching for high-resistivity materials; the other

two mechanisms of thermal quenching, namely Seitz-Mott mechanism (a conversion of a defect from radiative to nonradiative) and the Schön-Klasens mechanism (normal quenching). Therefore, one of the goals of this work was to study new cases of ATQ thermal quenching, classify and explain them, and predict new cases by finding how common this unusual thermal quenching is for high-resistivity semiconductors.

3.3.3 Other Methods to determine the ionization energy of defects in semiconductors

To characterize the defects in semiconductors, numerous researches have been conducted over the years to realize a technique that is rapid, sensitive and rather easy to analyze. Alongside the PL technique, other approaches, such as capacitance techniques, have the ability to provide information on defects and determine the ionization energy of them.[21] Deep-Level Transient Spectroscopy (DLTS) is one of these techniques. It is a high frequency (MHz range) capacitance transient thermal scanning technique that helps in observing various defects (known as charge carrier traps) in semiconductors and determining their ionization energies.[22] With this method, it is possible to bring to view the defects spectra in crystals as negative and positive peaks on a level baseline as functions of temperature. Thus, activation energies, concentration of defects, as well as hole- and electron-capture cross sections can be determined by using DLTS technique.[22] The measurement system employed in DLTS comprises one or two pulse generators to bring about rapid changes in the bias of the diode, sensitive equipment to measure capacitance with satisfactory transient responses, a variable temperature cryostat and two-gated signal integrator and an X-Y recorder. Peak signs, negative or positive, of every peak on flat baselines plotted as functions of temperature indicate if it is a result of a minority-carrier or majority-carrier trap (defect). [22, 23] Furthermore, peak heights vary proportionally with their respective defect

concentrations. The essential feature of this technique is its ability to set an emission rate window in a way that the measurement equipment responds only on seeing a transient with a rate within this said window.[22]

DLTS has advantages in the sense that the range of observable defect depths as well as ultimate sensitivity is way greater than other techniques. Besides, it is not limited to majority-carrier traps.[24] Also, the basic DLTS scheme applies to capacitance transients as well as current transients.[21]

Steady-state photocapacitance (SSPC) is another popular capacitance-based techniques that can detect point defects with low concentrations.[21] However, it is not really useful as a technique for survey as the data has to be taken point by point and a rather cumbersome analysis of optical cross sections is needed to achieve accurate defects parameters. Additionally, this technique is limited to defects that are deeper than approximately 0.3 eV.[22]

Among capacitance-based techniques, Admittance Spectroscopy method is commonly used to characterize majority-carrier trapping defects. It is at its best for shallow defects and exhibits decreasing sensitivity for deeper defects.[5] This technique presents resolved peaks that correspond to each defect and is independent of the thermal scan or direction.[24, 25]

Another method is thermally stimulated capacitance (TSCAP) and was previously the best capacitance survey method. In fact, DLTS may be viewed as an improvement of TSCAP. TSCAP possesses the following advantages: much greater sensitivity; way more convenient to utilize and interpret; and much greater range of observable defects depths.[26]

Another technique is Photoinduced Current Transient Spectroscopy (PICTS). PICTS measurements are carried out in a temperature range of 100 – 400K, with a temperature

difference of 1K. At each variation, an electron beam pulse excites a sample. After the excitation pulse ends, the photocurrent transient comes. Then the measurements are taking by using a current amplifier, converted to digital form and stored.[27] The photocurrent transient values recorded at time duration t_1 and t_2 and the difference is plotted against temperature.[28] Hole or electron traps existing in the samples bring about a peak in the PICTS spectrum. For example, centers located below the Fermi level capture holes and the holes emissions to the valence band are observable in photoinduced current transient spectroscopy spectra. [29]

Deep Level Optical Spectroscopy (DLOS) is also another technique. The activation energies of the defects detected by DLOS are determined by the onsets of the steady state photocapacitance (SSPC) spectrum, whereas concentrations for individual defects are calculated from the corresponding step heights.[30] DLOS reveals that very deep states in mid-bandgap and near valence band regime do not show a strong dependence on V/III ratio.[31]

Most of traps in GaN are nonradiative defects.[21] Electron traps cannot be detected by PL, because these are donors with energy levels in the upper half of the band gap. Photogenerated holes are captured by these deep donors less likely than by negatively charged acceptors in n-type GaN. Besides, transitions of electrons from the conduction band to these donors correspond to photons with low energy and therefore most probably nonradiative. Hole traps can be detected by a modification of DLTS, called the Optical DLTS (ODLTS), where a light pulses are used to manipulate with depletion region of a Schottky diode or a p-n junction.[32] From numerous hole traps detected with ODLTS in the lower half of the band gap (with activation energies from 0.25 to 1.2 eV),[33, 34] only two traps apparently correspond to defects observed by PL in GaN.[21] The H1 trap with the ionization energy of 0.85 eV is the same defect as the one responsible for the YL band. It is also likely that the H5 trap is responsible for the red luminescence band.[21]

Chapter 4: Experimental Details

4.1 Photoluminescence (PL) set-up

The necessary components of a PL set-up, shown in Figure 20, are a laser, a cryostat, a monochromator, and a photomultiplier tube, PMT (detector). Moreover, other components are needed such as filters and focusing lenses. Steady-state PL is excited with a continuous-wave Helium Cadmium (HeCd) laser with 30 mW of power and photon energy 3.81 eV. The HeCd laser is a gas laser in which high voltage is discharged through a gas to produce coherent and continuous light. It is a metal ion laser that uses helium in coupling with cadmium which vaporizes at a relatively low temperature to produces a high quality beam at 325 nm, UV light. Also, this laser light does not cause damage for the samples. Therefore, it is a good choice for use in PL experiments.[35]

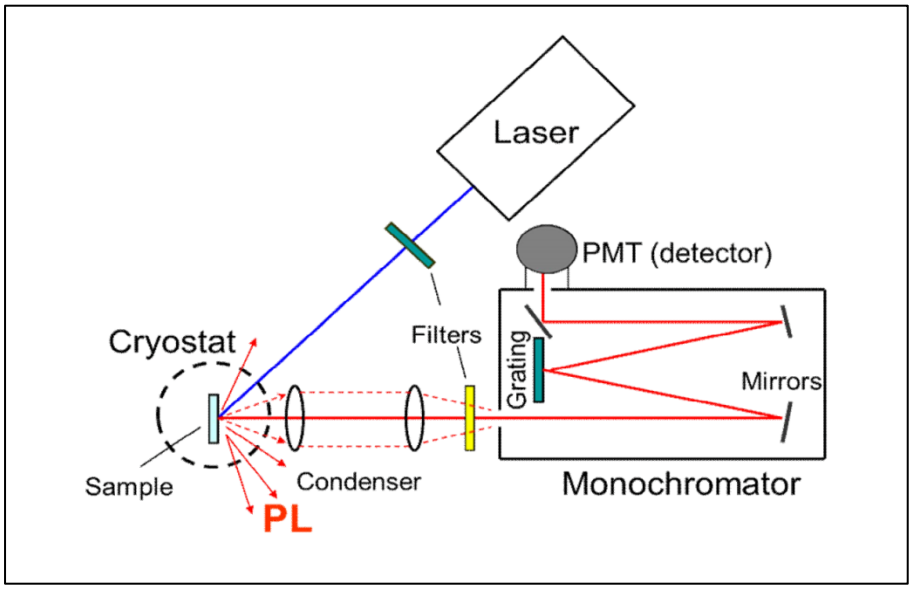

Figure 20. Experimental setup for PL measurements.[35]

The laser beam is incident to the sample through various neutral-density filters to attenuate the excitation intensity. The excitation power density (P_{exc}) is varied from 2×10^{-7} to 0.3 W/cm^2 using an unfocused beam with a diameter of 4 mm, and can be obtained a P_{exc} up to 200 W/cm^2 using focused beam with diameter of 0.1-0.2 mm. Changing the power density allows to alter the PL spectra. The attenuated laser beam continues toward a sample that is mounted on a holder in a closed-cycle optical cryostat.

Since the temperature greatly affects the PL spectra, the cryostat is needed to vary the range of the temperature during the experiment. A cryostat (from cryo meaning cold and stat meaning stable) is a vacuum chamber that is used to maintain the temperature of samples. Two different cryostats were used through the studying our samples. A closed-cycle optical cryostat and a high-temperature cryostat both from Janis Research Co. are used to study PL in the ranges of 13 – 330 K and 160 – 650 K, respectively. [6, 35]

The PL is emitted in all directions, so only small portion of PL is collected with a lens and then directed to the monochromator to analyze the PL spectrum. The set of two lenses is called the condenser. The first lens collects PL and causes the light to travel through the condenser in a parallel beam, and the second lens focuses the light beam into the slit on the monochromator. Before the luminescence entering the monochromator, there is another set of filters. The PL passes through them, and a certain wavelength range is blocked. Namely, the scattered light at 325 nm PL can be eliminated from entering into the monochromator. A 560 nm long pass (yellow filter) was used for the range of 560 – 820 nm to suppress strong emission from the UV or blue region of PL.

The monochromator is an optical device, which can converts broadband light into monochromatic light by dispersing it. The name comes from the Greek roots of "mono" which

means single, "chromo" which means color and the Latin suffix of "ator" which denotes an agent. Inside the monochromator, the wavelengths are dispersed by the use of a diffraction grating, Figure 21. The beam that enters into the slit of the monochromator is collimated by a concave mirror. The collimated light is then refracted by a diffraction grating and reflected by another mirror that refocuses the light toward the exit slit. The separated wavelengths that exit are selected by the rotation of the grating, so that different wavelengths can be studied at various times. In our experiment, a 1200 rules/mm grating in a 0.3 m monochromator model Triax 300 from Jobin Yvon Horiba is used.

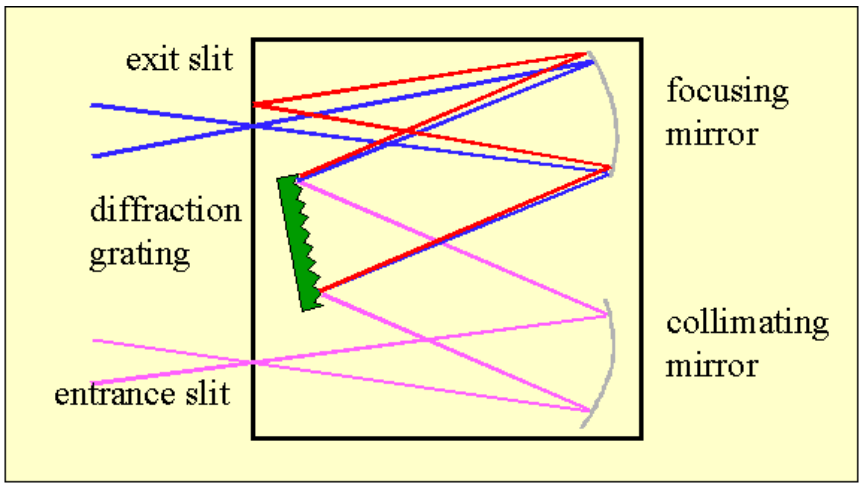

Figure 21. Diagram of typical monochromator, (http://web.nmsu.edu/)

Outside of the monochromator, the passed light is detected by a photomultiplier tube (PMT). The PMT is a very sensitive light detector that converts photons into electrical signal. The PMT multiplies the current to allow individual photons to be detected when the flux of light is very low. A PMT consists of a photocathode, a series of dynodes and an anode in a high-evacuated glass enclosure, Figure 22. The photon of sufficient energy that is coming from the monochromator strikes the photocathode material. The photocathode behind the entry window is

covered with a thin layer of a multialkali to produce electrons as a consequence of the photoelectric effect. The focusing electrode directs the photoelectrons toward the electron multiplier by the process of secondary emission, and accelerated towards the anode by a series of additional electrodes called dynodes. An electronic device called a photon counter analyzes the electrical signal from the PMT. Then, the data is transferred to the computer system and graphed with a program called SynerJy through the electrical connection.

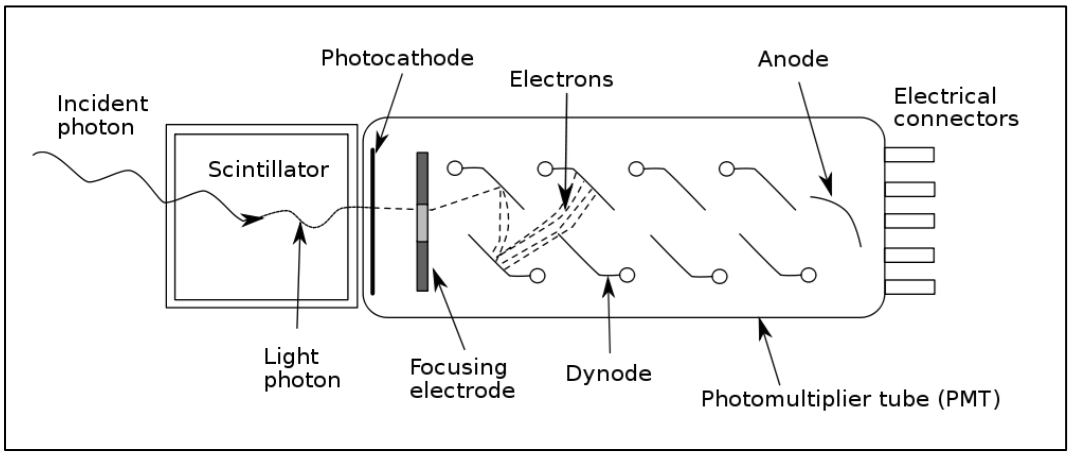

Figure 22. Schematic of a photomultiplier tube (PMT), (**http://en.wikipedia.org/wiki/** Photomultiplier tube).

In this research, the high-resistivity samples have been studied over a wide range of temperatures and excitation intensities. These include ZnO, GaN:C and GaN:Fe. The ZnO samples (M6, M27 and M28) used in this work are undoped bulk ZnO and grown by the hydrothermal method by the MTI Corporation (Richmond,CA). The hydrothermal method is known to produce high-resistivity ZnO samples due to the compensation of shallow donors by the Li_{Zn} acceptors originating from the mineralizer which is typically LiOH and KOH. [7, 8]

The high-resistivity GaN samples investigated in this work are undoped and Fe-doped GaN. Undoped (un-intentionally carbon doped) GaN was grown by metal-organic chemical vapor deposition (MOCVD) in the group of Prof. Morkoç at VCU, sample CVD 4229. The high concentration of carbon was produced in undoped GaN due to the way of the growth. Therefore, a deep acceptor states were induced which compensate the residual donor concentration, resulting in high-resistivity GaN:C sample.

Fe-doped GaN samples were grown by two different growth methods; Hydride vapor phase epitaxy (HVPE), (samples AE3273, AE3260 and AE3276) and by MOCVD, sample LG. The HVPE GaN samples were grown at Kyma Technologies, Inc., and the LG sample was grown at Lumilog Company.

4.2 Calculating the quantum efficiency of PL bands for the studied samples

To estimate the quantum efficiency, η, we compared the integrated intensity of the PL bands in the studied samples with PL intensity obtained from calibrated samples.[35, 36] The calibration is necessary to obtain a reasonable estimate of the absolute internal quantum efficiency of PL. The calibrated samples are other samples that show unusual high radiative efficiency. The absolute internal quantum efficiency, IQE, of PL of several calibrated samples was determined reliably with several independent methods.[1-3, 6]

One method is from the temperature dependence of the PL in degenerate n-type GaN co-doped with Si and Zn.[3, 6] The PL spectra of this sample include two defect-related bands: the blue luminescence (BL) and the yellow luminescence (YL) band, and near-band-edge (NBE). With increasing temperature, the BL band is quenched. Simultaneously, the NBE and YL bands rise as shown in Figure 23.[6]

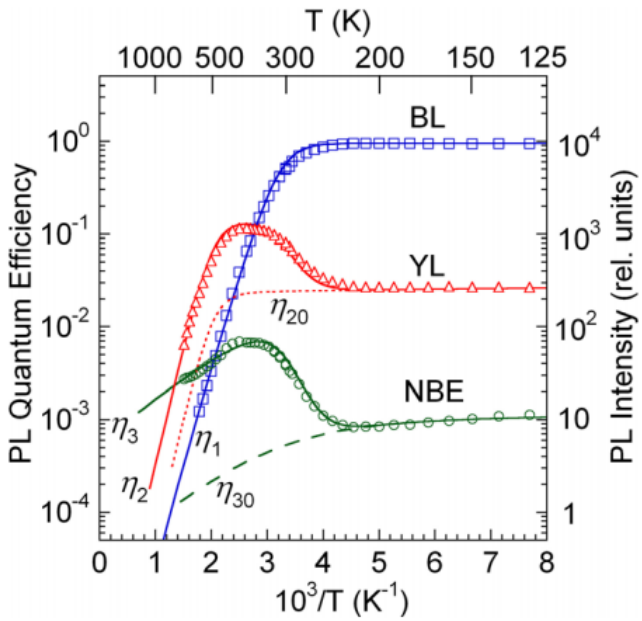

Figure 23. Temperature dependence of the absolute IQE of PL in GaN:Si,Zn (sample 1141) at P_{exc}= 0:0015 W/cm^2. Points are experimental data. Solid blue curve shows g1 calculated by using Eq. 19.[6]

According to the phenomenological model, a quenching of a recombination channel with high internal quantum efficiency, IQE, results in a high increase in the efficiency of all the other PL bands. As we can see in Figure 23 that a rise of the YL and NBE band intensities by about one order of magnitude in the same temperature region of BL band thermal quenching.[3] The IQE was determined from the quantitative analysis of the dependence of the PL intensity on the temperature. The expression of the absolute IQE of the PL band has been derived in Chapter 2. Substituting Eq. (17b) denoted with index i for BL band into Eq. (18) denoted with index j for the exciton and YL bands, we will arrive at [2]

$$\frac{\eta_j(T)}{\eta_{j0}(T)} = \frac{1-\eta_i(T)}{1-\eta_i(0)} \tag{26}$$

The temperature dependence of $\left(\frac{\eta_j(T)}{\eta_{j0}(T)}\right)$ is known from the experiment and $\eta_i(T) = 0$ for the BL band after thermal quenching. Then, the dependences can be fitted with Eq. (26) with the only fitting parameter which is $\eta_i(0)$. The absolute IQE of the PL in GaN:Si,Zn was calculated and shows more than 90%, with the largest contribution coming from the blue luminescence (BL) band. For the YL band, $\eta_i(0)$ = 0.91 while for the NBE band is $\eta_i(0)$= 0.94.[35, 36] Such sample can be used for the calibration of the internal quantum efficiency. However, if the absolute internal quantum efficiency for the calibration sample can be determined, then the internal quantum efficiency of different PL bands for other samples can be estimated by comparing the integrated PL intensities, provided that all the samples are measured under identical conditions.[2,35, 36] This method is better to use when there are clearly isolated bands and they are not obstructed by other bands.

Additionally, the relative quantum efficiency can be found if the PL bands are overlapped and obscure each other. Measuring the peak intensity and multiplying it by the full width at half maximum (FWHM) of the band is proportional to the integrated intensity. In particular, for the broad defect-related bands that have Gaussian shape, this product is equal to 0.94 from the integrated Gaussian curve. At low temperature, the width is independent of temperature, up to about 100 K. As the temperature increases to 200-300K, the width of the PL band increases by about 20-50% of the initial width. [3] The temperature dependence of the band width can be measured in samples where this band is not obscured by other bands. Then, the temperature dependence for this band can be accounted for to estimate the "integrated intensity" when only the peak intensity can be measured. To convert the relative QE obtained with this method into the absolute QE, we need to find the absolute QE at least at one temperature by performing the deconvolution of overlapped PL bands and measuring integrated PL. Since one method maybe more reliable in a given temperature region than the other, it may be useful to find QE with both methods (by integrating the PL band intensity at every temperature point and by finding a product of PL intensity on its width at each temperature).

4.3 Calculating the temperature dependence of the BL2 band intensity for MOCVD grown GaN:C and GaN:Fe samples

Usually the peak maximum of PL band reveals the PL intensity. The peak maximum of BL2 band is known to be between 3.0 - 3.05 eV which is close to Zn-related BL band with maximum at 2.8 -2.9 eV.[6, 14, 37, 38] Thus, the intensity of BL2 band for the studied samples, GaN:C and GaN:Fe, was measured a little farther from its peak maximum to avoid BL band contribution. In GaN:C sample, the BL2 intensity was taken at 3.25 eV since there was no major

change in the shape of the band with increasing temperature. Thereafter, we subtracted the value of the background, the last measurement (highest temperature) of the BL2 intensity at 3.25 eV, from all the measurements to reduce any other contribution from different bands. This process was used for all temperature range and for different excitation intensities, P_{exc}.

The same method was applied to analysis of another sample, GaN:Fe. However, the best measurements of BL2 intensity were taken at 3.1 eV which is little closer to the maximum because the ultraviolet luminescence (UVL) band with the main peak at about 3.27 eV contributed nuch at higher photon energies at relatively low temperatures, as shown in Figure 24.

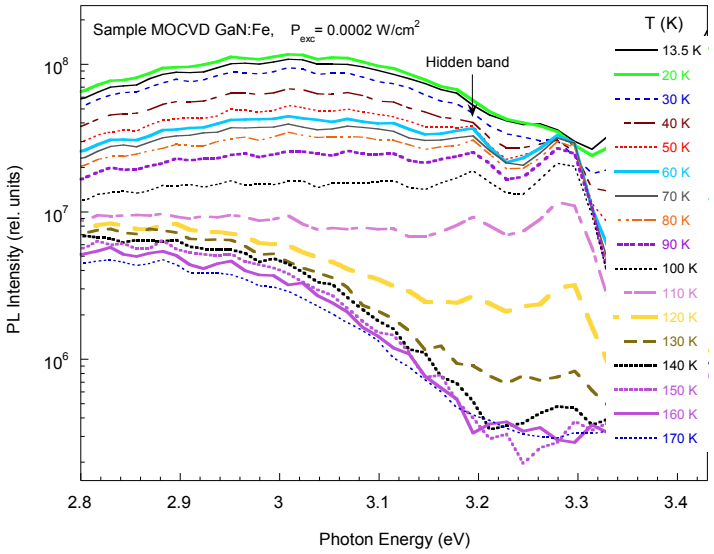

Figure. 24 Zoomed-in region for the temperature dependence of PL spectra for sample GaN:Fe

Figure 25 shows the PL spectra at different temperatures for the BL2 band in case where the intensity measurements were taken at the maximum, Fig. 25(a), and in another case where the intensities were taken at 3.1 eV, Fig. 25(b), for the same sample, GaN:Fe. We can see that the BL band contributed much in the first case (Fig. 25(a) at temperatures exceeding ~120 K. Namely, when the BL2 intensity was taken at the maximum, there was some saturation revealed as tails and we assumed that this happened because of contribution of other bands. Also, there

was small change in the drop of quenching comparing to the one taken at 3.1 eV where the change in the drop of the quenching is several orders of magnitude. The latter is useful to trace the slope and find the characteristic temperature, T_0, more reliable.

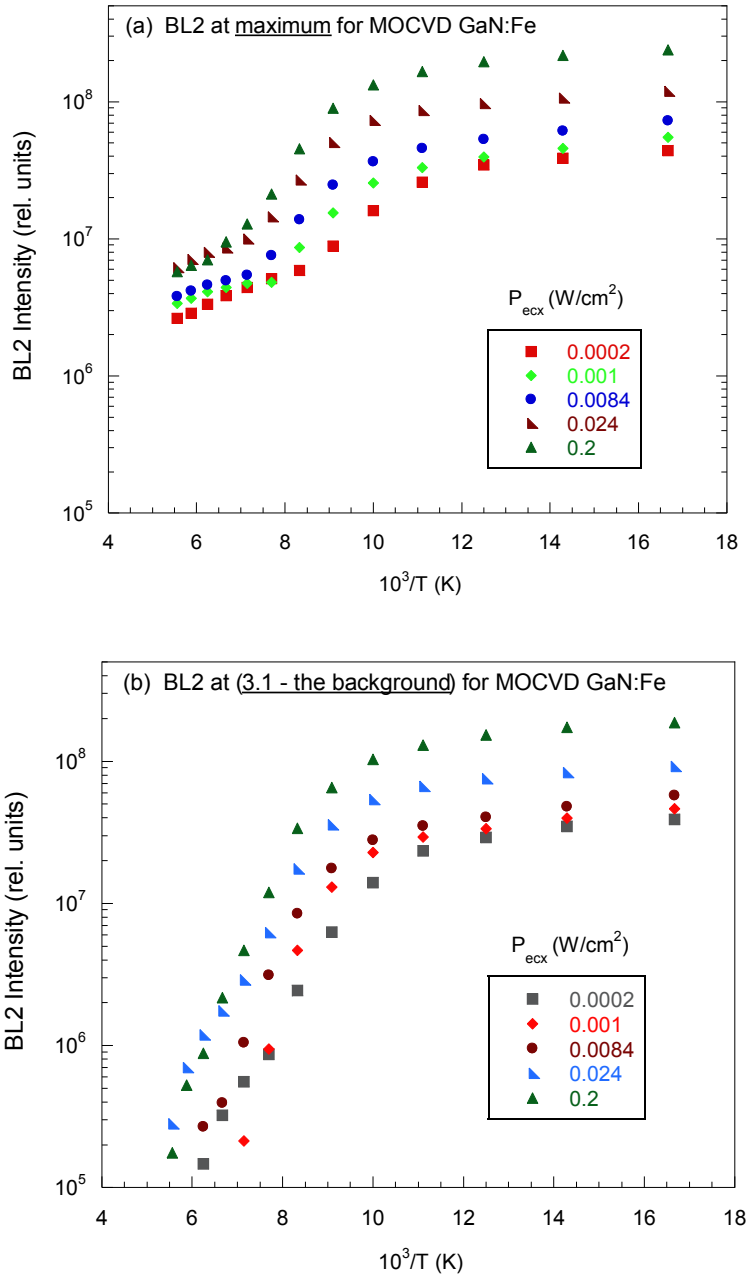

Figure. 25 Temperature dependence of BL2 for sample GaN:Fe at different excitation intensity, P_{exc}. (a) BL2 intensities were taken at maximum and (b) BL2 intensities were taken at (3.1 eV - the background).

4.4 Resolving the overlapped bands in HVPE grown GaN:Fe samples

The BL2 band in all the three samples, AE3273, AE3260 and AE3276, overlaps with other PL bands related to defects, BL, GL2 and YL bands.[3] Resolving overlapped bands and finding the contribution of each band are needed to calculate the quantum efficiency. So, the shapes of the all bands can be modeled with the following equation (26) derived from a one-dimensional configuration coordinate model. [39]

$$I^{PL}(\hbar\omega) = I^{PL}_{max}\ exp\left[-2S\left(\sqrt{\frac{E_0-\hbar\omega}{E_0-\hbar\omega_{max}}}\right)^2 - 1\right] \quad (26)$$

where S is the Huang-Rhys factor that represents the mean number of emitted phonons, $\hbar\omega$ is the photon energy, $\hbar\omega_{max}$ is the energy of the PL band maximum, $\hbar\Omega$ is the energy of the dominant phonon mode and E_0 is the zero-phonon line (ZPL) energy. The parameters that were used in the fit are obtained from previously reported parameters in literature where they were determined for these PL bands observed without overlap.[4, 39, 40]

The intensities of the band maxima, as the only fitting parameters, were varied during modeling with reasonable values for each band until the summation of all four bands coincide with the experimental spectrum. Figure 26 shows an example for one of the three samples (AE3273) that demonstrates the way of calculating the intensities for all bands at temperature T = 13.5 K and excitation intensity, P_{exc} = 26.5 mW/cm^2.

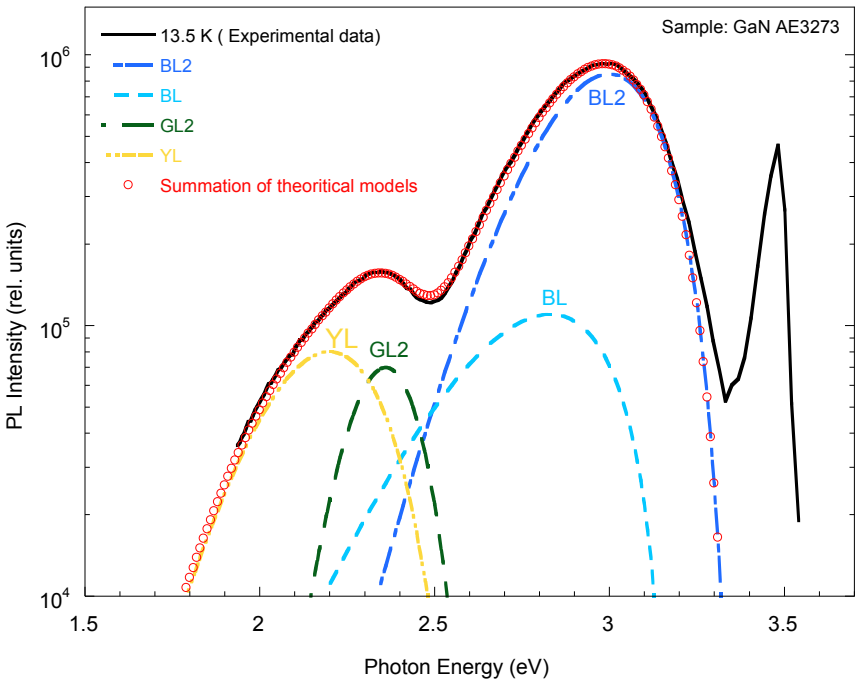

Figure. 26 The simulated shapes of the BL2, BL, GL and YL bands by using Eq. (25) in comparison with the PL spectrum from GaN (AE3273), at T=13K and P_{exc}=26.5 mW/cm^2.

In Figure 26, the sum of the simulated PL bands, shown with red open circles, matches the black solid line that shows the experimental data. This method was used for all three samples and repeated for all dependences in the whole temperature range with a step of 10 K, and for the different excitation intensities that varied between 0.128 to 26.5 mW/cm^2.

Chapter 5: Theoretical simulation of PL

To achieve a significant progress in analyzing and understanding the temperature behavior of PL in high-resistivity semiconductors, theoretical and experimental studies were conducted in my research work. The phenomenological model with three types of major point defects is used through Mathematica program to explain the general trends of PL temperature dependence in many cases, and to predict observation of NQ and ATQ.

5.1 Modeling the temperature dependence of PL

The Mathematica program can be used as computational software for lengthy numerical calculations and graphical representation of those calculations. Modeling the rate equations with Mathematica program becomes a useful analytical tool to investigate the properties involved in the temperature dependence of PL. This model helps to explain how common the abrupt and tunable thermal quenching of PL is in high-resistivity semiconductors. The parameters entered into the program should be reasonable and consistent with the information that we obtain from other sources.[2, 37, 40] By varying the parameters of the model we can find which of the parameters affect mostly different PL behaviors, and, in particular, cause the abrupt and tunable quenching of PL.

Several point defects may contribute to the radiative and non-radiative recombination mechanisms. However, using a three-defect model reduces the complexity of the Mathematica modeling program and at the same time corresponds to the most common cases of PL in GaN or ZnO. These defects are an acceptor, a shallow donor and an unknown nonradiative center. The starting values of the parameters used in the model for the OL band in ZnO are the following.

The acceptor and shallow donor concentrations are $N_A = 3\times10^{15}$ cm^{-3} and $N_D = 1.3\times10^{15}$ cm^{-3}, respectively, with ionization energy expected to be $E_A = 0.5$ eV for the acceptor and $E_D = 0.05$ eV for the shallow donor. The typical values of the electron and hole capture coefficients C_{nA} and C_{pA} of the acceptor have been found from previous studies as 2×10^{-12} cm^3/s and 1×10^{-6} cm^3/s, respectively. The electron capture coefficient for the shallow donor (nonradiative capture) was estimated as $C_{nD} = 1\times10^{-9}$ cm^3/s, and the effective coefficient for the DAP recombination (radiative transition) is about $C_{DA} = 1\times10^{-13}$ cm^3/s. We assume that the non-radiative center is a simple deep donor (a deep non-radiative acceptor will also be included later). However, the concentration and the capture coefficients parameters are unknown for the non-radiative center S, so we can choose reasonable initial parameters, $N_s = 1.9\times10^{15}$ cm^{-3}, $C_{nS} = 1\times10^{-10}$ cm^3/s, and $C_{pS} = 3\times10^{-6}$ cm^3/s. The relative concentrations N_A, N_D and N_S are chosen such that semiconductor is high-resistivity at room temperature, what is confirmed for studied ZnO by Hall effect measurements. Based on the parameters mentioned above, the PL simulation will be discussed for a high-resistivity, n-type semiconductor where $N_D+N_S > N_A > N_D$.

The temperature dependencies of the PL quantum efficiency for high-resistivity semiconductors, where the parameters of the model are changed one by one, will be shown below. First of all, using the program shows how the abrupt and tunable behavior is apparent in high resistivity but not in n-type conductive semiconductor with varying the excitation intensity, Figure 27. The value of shallow donor concentrations that was used in the modeling is increased only for n-type, $N_D = 1.3\times10^{16}$ cm^{-3} to reproduce relatively high concentration of free electrons. Other parameters did not change.

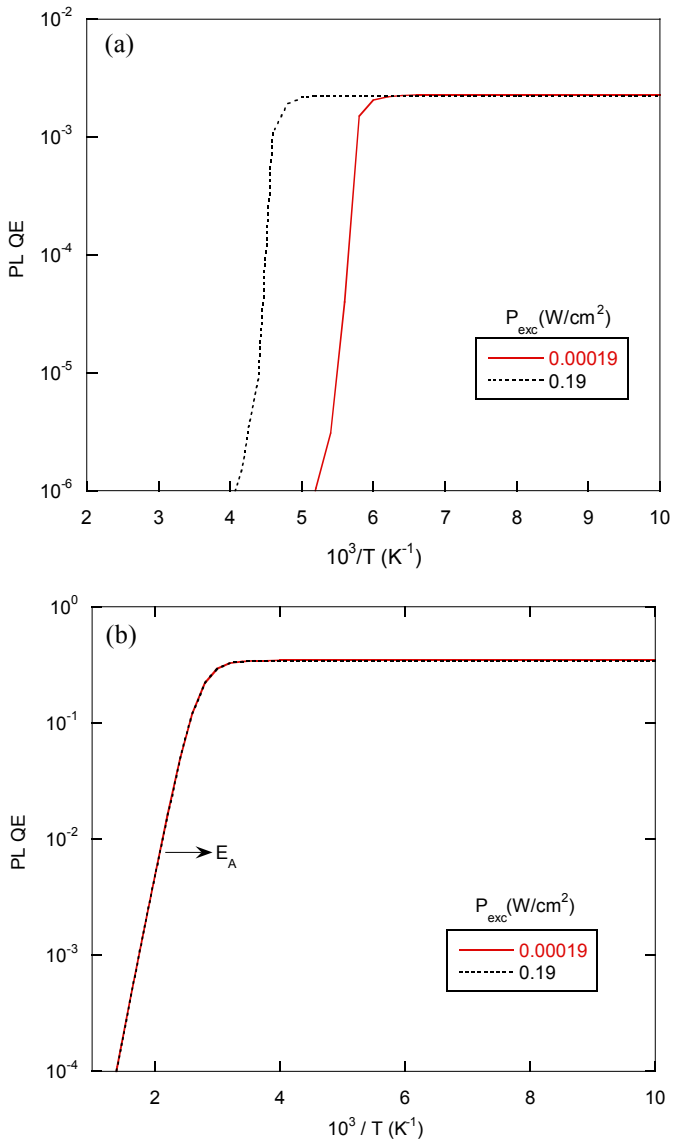

Figure 27. Temperature dependence of PL QE with varying G. (a) High-resistivity. (b) n-type conductive semiconductor.

Figure 27(a) shows the drop of PL intensity at a characteristic temperature. The region of the thermal quenching shifts to higher temperature with increasing the excitation intensity. In contrast, Figure 27(b) shows the thermal quenching of PL in conductive n-type semiconductor which is normal quenching and T_0 is independent on the excitation intensity.

Figure 28 shows the temperature dependencies of PL QE where the electron capture coefficient for the S center is varied between 10^{-12} and 10^{-5} cm^3/s. We can see that the abrupt thermal quenching of PL becomes significant if C_{ns} is large enough, when $C_{ns} \geq 1\times10^{-8}$ cm^3 s^{-1}. Otherwise, the quenching is not abrupt and the activation energy for that is equal to the ionization energy of the acceptor that setted up in the program, $E_A \approx 0.5$ eV.

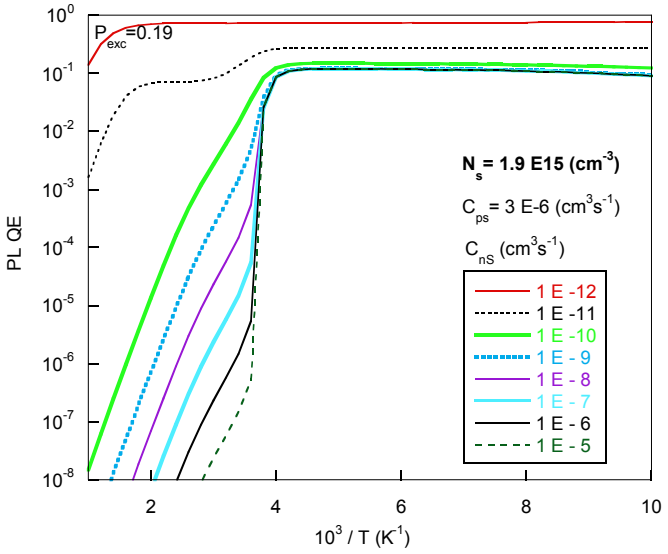

Figure 28. Temperature dependence of PL QE with varying electron capture coefficient for (S-donor) at higher excitation intensity. Other parameters did not change.

With changing excitation intensity, as shown in Figure 29, a significant shift is observed for the characteristic temperature, T_0, of quenching comparing to the one at high excitation intensity in Fig. 28, which means the quenching is tunable. Also for low excitation intensity as shown in Figure 29, the abrupt thermal quenching of PL becomes significant if C_{ns} is large enough, $C_{ns} \geq 1\times10^{-8}$ cm^3 s^{-1}.

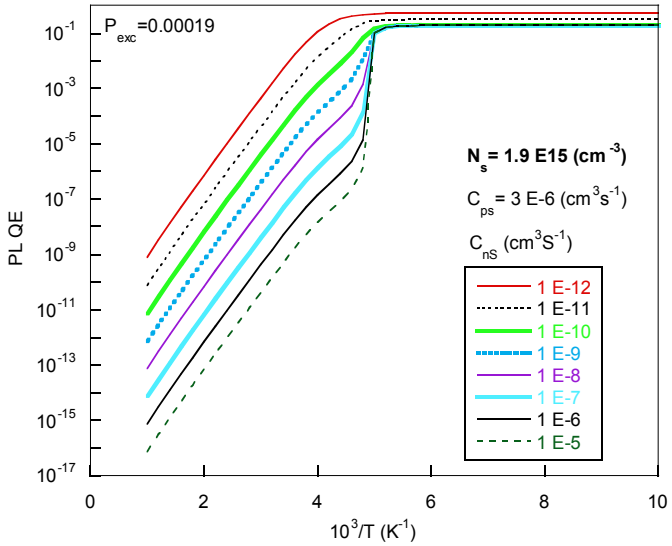

Figure 29. Temperature dependence of PL QE with varying electron capture coefficient for S center (a nonradiative donor) at low excitation intensity. Other parameters did not change.

Since the concentration of nonradiative centers are not the same in different samples, Figure 30 shows that by increasing the concentration of the non-radiative center, S, one order of magnitude, N_S from 1.9×10^{15} to 1.9×10^{16} cm^{-3}, the value of C_{ns} needs to be increased by factor of ten to observe a significant abruptness in PL quenching.

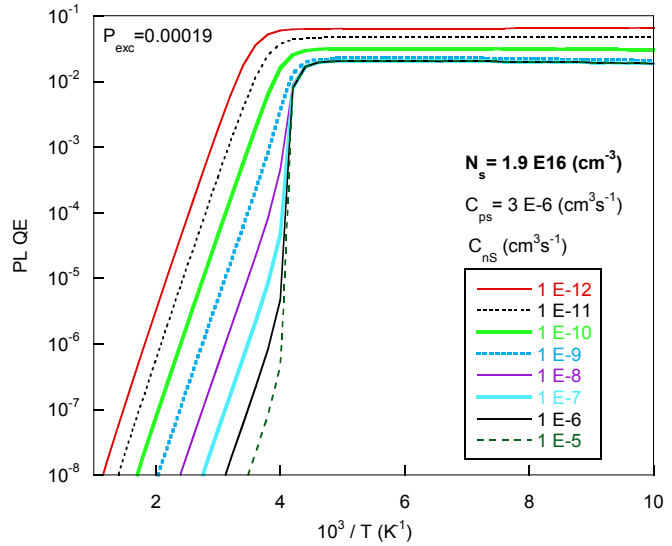

Figure 30. Temperature dependence of PL QE with varying C_{nS} after increasing the concentration of the non-radiative center, S, by one order of magnitude. Other parameters did not change.

Moreover, the abrupt thermal quenching of PL is observed if C_{ps} is large, but not too larger (up to about 1×10^{-4} cm^3 s^{-1} for $C_{ns} = 10^{-7}$ cm^3 s^{-1}i), as shown in Figure 31, where the C_{ns} is fixed at 10^{-7} cm^3/s and C_{ps} is varied between 10^{-10} and 10^{-1} cm^3/s, the concentration of the non-radiative center is changed back to 1.9×10^{15} cm^{-3}.

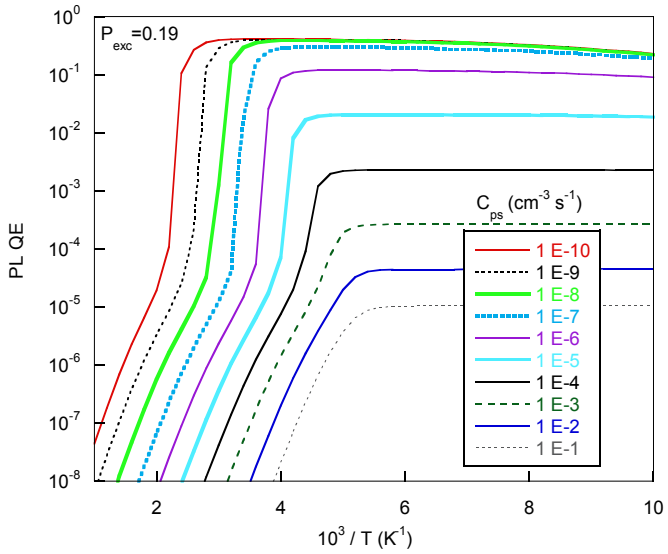

Figure 31. Temperature dependence of PL QE with varying C_{pS}. C_{ns} is fixed at 10^{-7} and other parameters did not change.

The fast capture of electrons and holes at non-radiative centers is the feature that causes an abrupt drop in the PL intensity. When the non-radiative center is saturated with photogenerated electrons, this recombination channel is blocked. At the same time, the concentration of electrons in the conduction band increases and the acceptor become partly filled with holes due to their long life time. So, population inversion is observed at low temperature, at $T< T_0$. With increasing temperature, at $T >T_0$, the thermally emitted holes from acceptor to the valance band open the blocked nonradiative channel. This sudden redirection of the flow of carriers from radiative channels to the non-radiative channel causes an abrupt quenching, with result that equilibrium population is restored. Thus, abrupt thermal quenching of PL occurs in high-resistivity semiconductors if C_{ns} and C_{ps} are large enough.

In contrast, variation of parameters C_{nD} and C_{DA} does not affect T_0 and the magnitude of the PL drop as shown in Figure 32. Nevertheless, an increase in C_{DA}, results in an increase in PL QE at low temperature, at $T < T_0$, Figure 32 (b). The activation energy of the PL quenching, (Figure 32(a-b)) is close to the ionization energy for the acceptor, $E_A \approx 0.49$ eV.

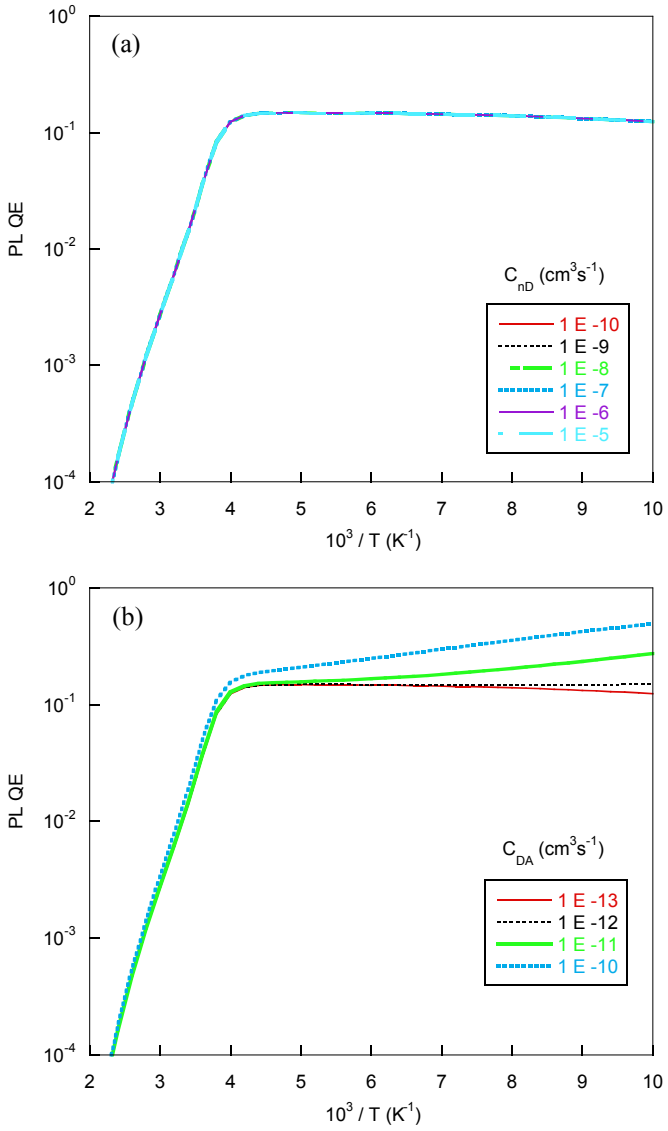

Figure 32. Temperature dependence of PL QE with varying C_{nD} (a), and C_{DA} (b). Other parameters did not change.

Figure 33 shows the temperature dependencies for PL QE where the hole capture coefficients for the acceptor and for the S center are varied between 10^{-7} and 10^{-4} cm^3/s. We can see that, the competition for capture of holes between A-center and S-center determines the dominant recombination channel, radiative or non-radiative. Also, the higher the C_{pA}/C_{ps} ratio, the higher is PL QE at $T < T_0$. Additionally, T_0 is decreasing with increasing C_{pA} and C_{ps}.

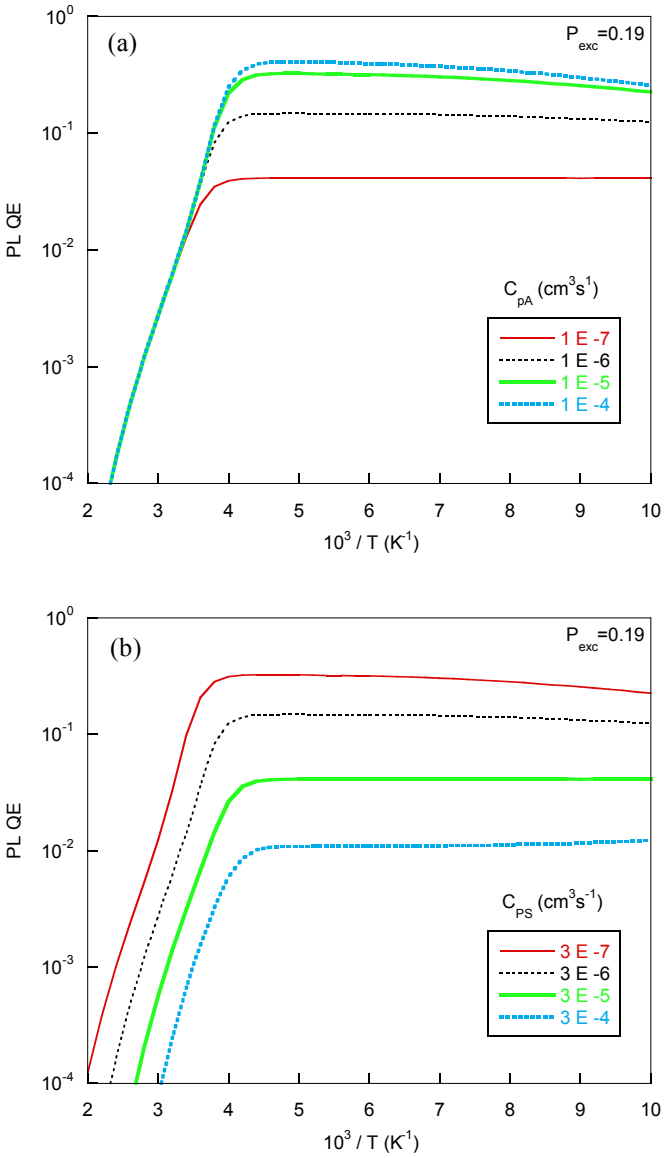

Figure 33. Temperature dependence of PL QE with varying C_{pA} (a), and C_{pS} (b). Other parameters did not change.

Chapter 6: Temperature dependence of PL in ZnO samples

The ZnO samples (M6, M27 and M28) used in this work are undoped bulk ZnO and grown by the hydrothermal method at the MTI Corporation (Richmond, CA). The hydrothermal method is known to produce high-resistivity ZnO samples due to the compensation of shallow donors by the Li_{Zn} acceptors originating from the mineralizer which is typically LiOH and KOH.[7, 8, 41-44]

A typical PL spectrum of undoped ZnO contains sharp excitonic lines in the UV region of the PL spectrum, with one or more broad bands in the visible part.[13] The most recognizable PL band related to defects in the studied samples is the orange luminescence band (OL). This band is distinguishable by its Gaussian shape at low temperature, full width at half maximum (FWHM) of about 0.51 eV and peak position with maximum at 2.0 eV at T= 13 K.

In several works, [7, 8, 19, 45] the defect responsible for the OL band was identified as a Lithium atom in the Zinc site, Li_{Zn}, which is an acceptor. The exact value of the ionization energy of the Li acceptor is not accurately determined and there is some disagreement in the literature. This work includes the first observation of abrupt and tunable thermal quenching of OL in ZnO. Thus, the energy level of the Li_{Zn} acceptor can be found reliably.

The temperature dependence of ZnO samples, including the OL and the exciton bands, were studied at different excitation intensities. The excitation intensity, P_{exc}, was varied between 1.9×10^{-4} and 0.9 W/cm^2 using calibrated neutral density filters. Figure 34 shows the PL spectra with increasing temperature, in the range of 120 – 310 K, for one of the ZnO samples (M6) where $P_{exc}=9.7\times10^{-4}$ W/cm^2.

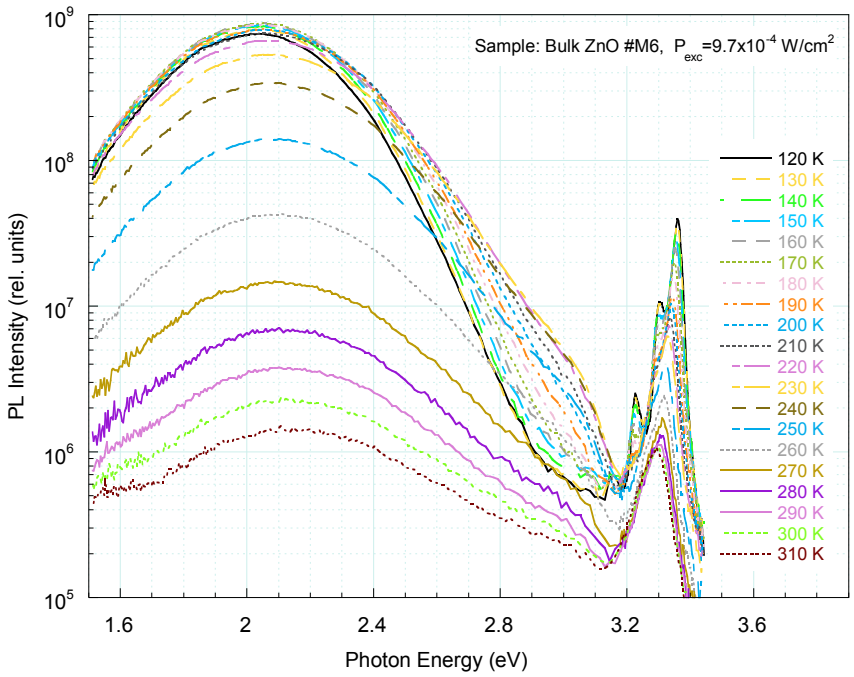

Figure 34. PL spectra from undoped ZnO (sample M6) with increasing temperature with step of 10K.

6.1 Calculating the temperature dependence of quantum efficiency of the orange luminescence (OL) and the exciton bands

The quantum efficiency of the PL, η, is given by the expression, $\eta = I^{PL}/G$, where I^{PL} is the integrated PL intensity and G is the concentration of electron hole pairs created by the laser per second, and known as the generation rate. The quantum efficiency of the OL band and exciton luminescence band is obtained from the spectra by two approaches, see chapter 4 for more details. Since one method maybe more reliable in a given temperature region than the other, the relative QE obtained by the second approach was multiplied by an arbitrary factor to coincide with the absolute QE obtained by the first approach to produce an accurate data. Finally, the quantum efficiency of the OL and exciton luminescence bands is plotted as a function of inverse temperature at different excitation intensities, Figure 35 and 36, respectively.

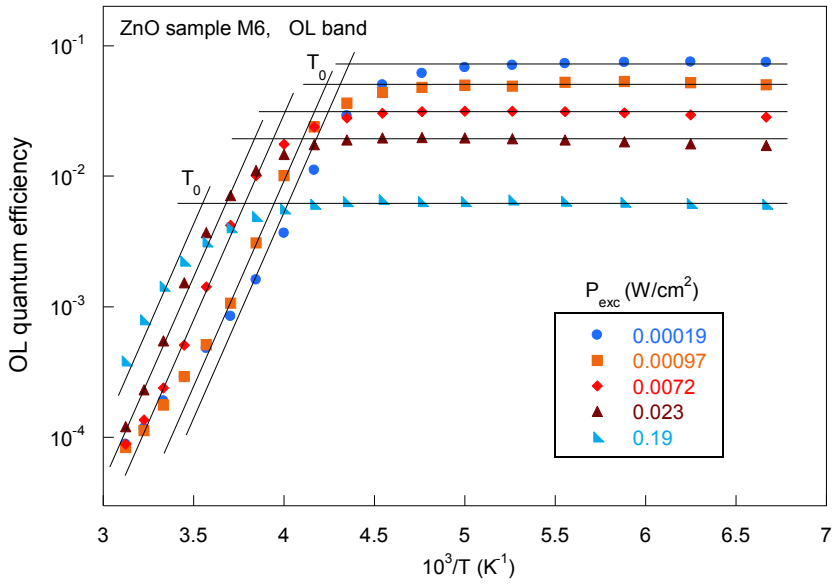

Figure 35. Temperature dependence of the quantum efficiency of the OL band in high resistivity ZnO (sample M6) for different excitation intensities, P_{exc}.

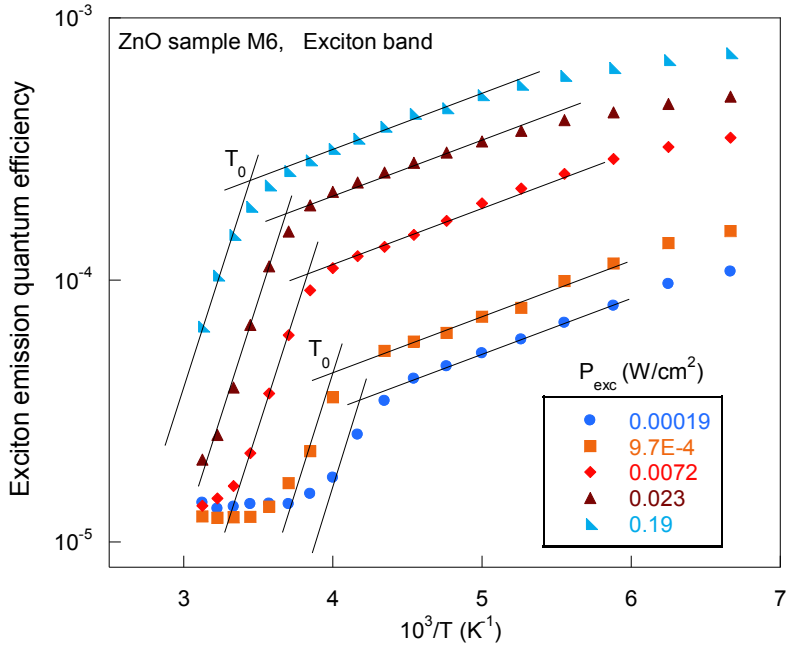

Figure 36. Temperature dependence of the quantum efficiency of the exciton band in high resistivity ZnO (sample M6) for different excitation intensities, P_{exc}.

6.2 Dependence of the characteristic temperature on the excitation intensity

The characteristic temperature T_0, at which the quenching begins, can be determined by extrapolating the low-temperature part and the high-temperature part to the point where they cross in an Arrhenius plot. It can be seen from Figure 35 that the characteristic temperature T_0 shifts significantly to higher temperatures with increasing excitation intensity; this is to say that the abrupt quenching is tunable for the OL band. According to the theory of the abrupt and tunable model, all radiative channels (which involve free electrons) are abruptly quenched at $T \approx T_0$, because the concentration of electrons in the conduction band suddenly drops at $T \approx T_0$. Therefore, the abrupt and tunable thermal quenching of the exciton band as shown in Figure 36 verifies the assumption that the quenching of the OL band is abrupt and tunable.

Usually in traditional model used for normal quenching, the slope of PL quenching in the Arrhenius plot determines the ionization energy of the defect causing the PL band. However, in high-resistivity ZnO samples the abrupt and tunable thermal quenching is observed and the slope of the dependence has no relation to the acceptor ionization energy. In this case, the ionization energy can be found by plotting the inverse of characteristic temperature, $1/T_0$, as a function of electron-hole generation rate, G, which gives a straight line dependence. This dependence can be fit with equation (23), and the slope of this straight line gives the ionization energy of the defect. Figure 37 shows the dependence of the characteristic temperature T_0 on excitation intensity of the OL and exciton bands for the three ZnO samples (M6, M27 and M28) with their fitting lines.

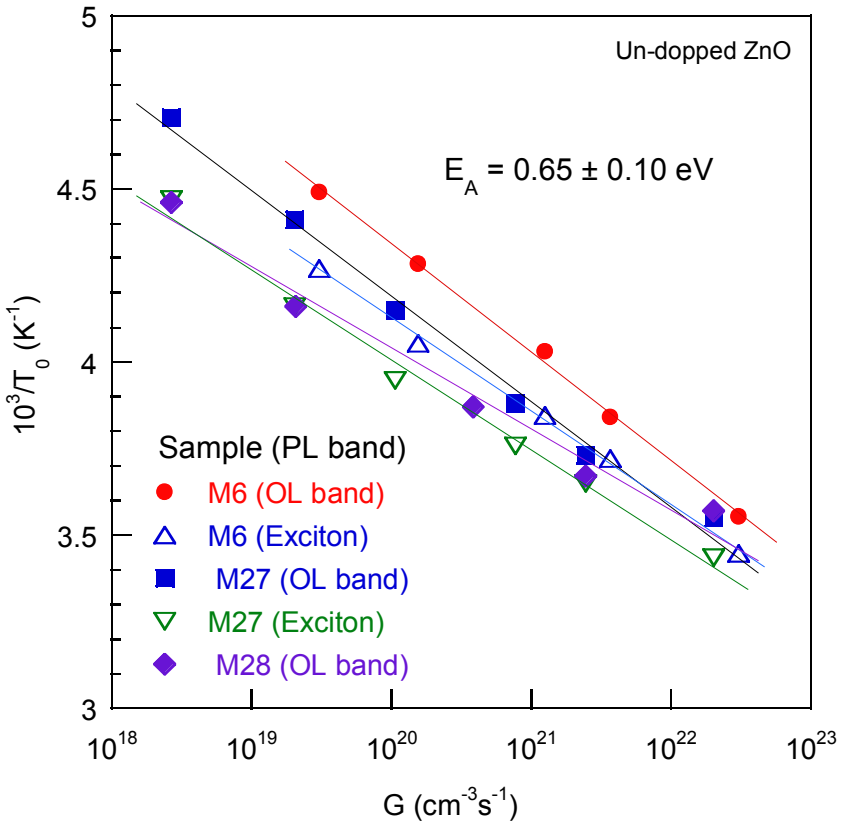

Figure 37. The dependence of the characteristic temperature on the electron-hole generation rate for the OL and exciton bands in three ZnO samples.

From the fit of five dependences for the OL and exciton bands in ZnO samples, the position of the acceptor level can be obtained with an average activation energy of E_A= 0.65±0.10 eV and the coefficient B is in the range between 10^{32} and 10^{35} cm^{-3} s^{-1}.

The fact that all radiative recombination channels (OL and exciton), for all three ZnO samples, (M6, M27 and M28), demonstrate the ATQ behavior and reveal almost the same activation energy in the T_0 (G) plot, is another evidence that the quenching occurs by abrupt and tunable quenching mechanism and therefore the energy of the acceptor level can be accurately determined.

Chapter 7: Temperature dependence of PL in GaN samples

High-resistivity GaN samples have been studied over a wide range of temperatures and excitation intensities. The samples investigated in this work are GaN:C (un-intentionally carbon doped) and GaN:Fe. GaN:C was grown by metal-organic chemical vapor deposition (MOCVD), sample CVD 4229. GaN:Fe samples were grown by two different growth methods; Hydride vapor phase epitaxy (HVPE), (samples AE3273, AE3260 and AE3276) and by MOCVD, sample LG.

7.1 Temperature dependence of PL for MOCVD grown GaN samples

The spectral dependence of PL intensity in the temperature range of 13.5–200 K for MOCVD grown un-doped GaN and Fe-doped GaN are shown in Figures 38 and 39, respectively.

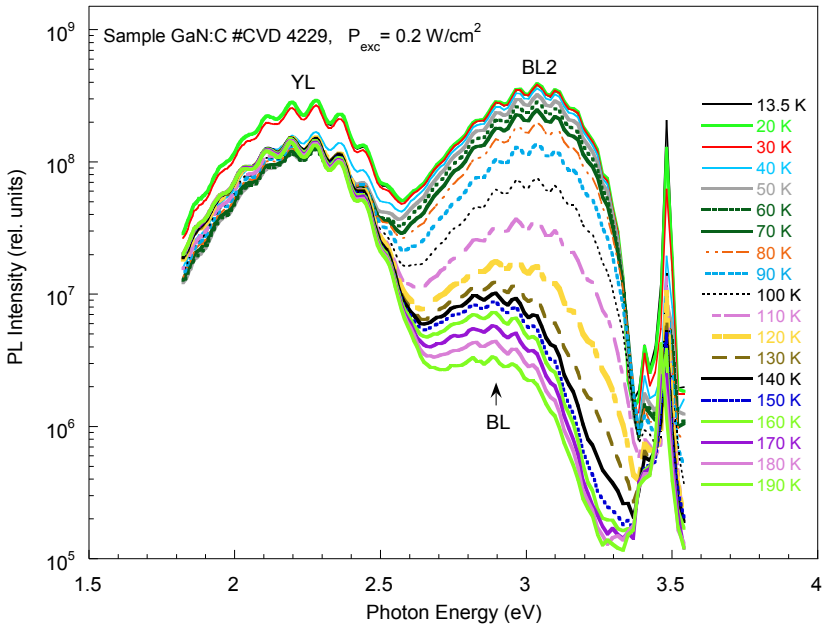

Figure 38. The PL spectra from GaN:C sample (CVD 4229) for temperatures up to 190 K.

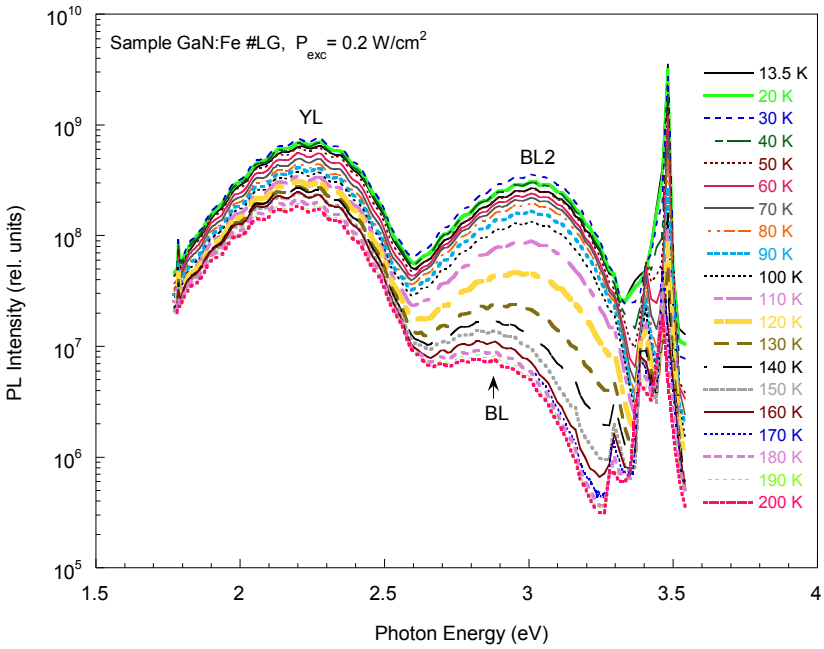

Figure 39. The PL spectra for the GaN:Fe sample (LG) for temperatures up to 200 K.

The defect-related PL bands dominating in the studied samples are the yellow luminescence (YL) band, a broad band in the blue spectral region (BL2) and exciton band with a peak at about 3.48 eV. The temperature dependence of the quantum efficiency of the YL, BL2 and exciton band at high excitation intensity, 0.2 W/cm^2, for each sample, GaN:C and GaN:Fe are shown in Figures 40 and 41, respectively. The intensity of YL band remains almost unchanged with increasing temperature up to the room temperature. Then at higher temperature around 500 K, the intensity of YL suddenly dropped. In another hand, the intensity of BL2 begins to quench at relatively low temperature, between 95-125 K. quenching BL2 band at low temperature reveals another band under it, BL band.

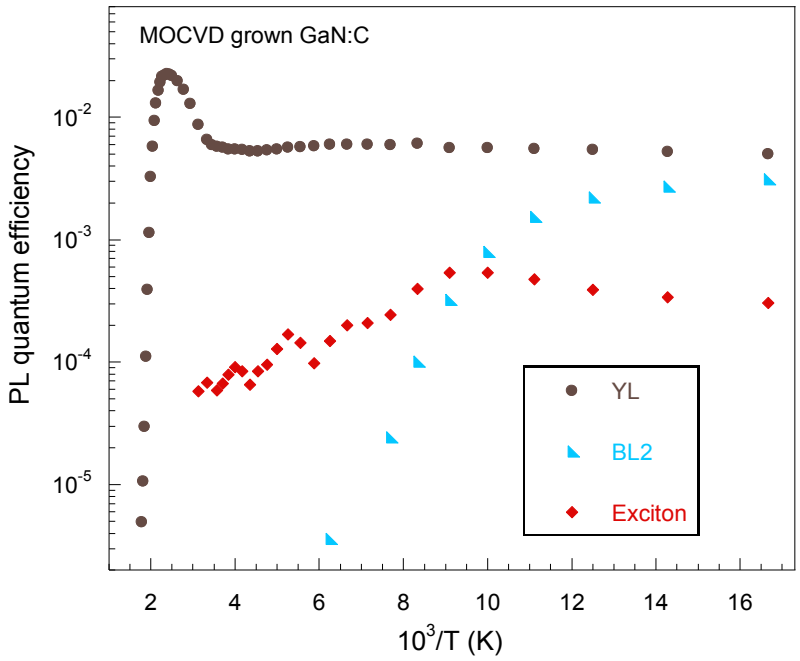

Figure 40. The temperature dependence of the quantum efficiency of the YL, BL2 and exciton bands at 0.2 W/cm^2 for GaN:C.

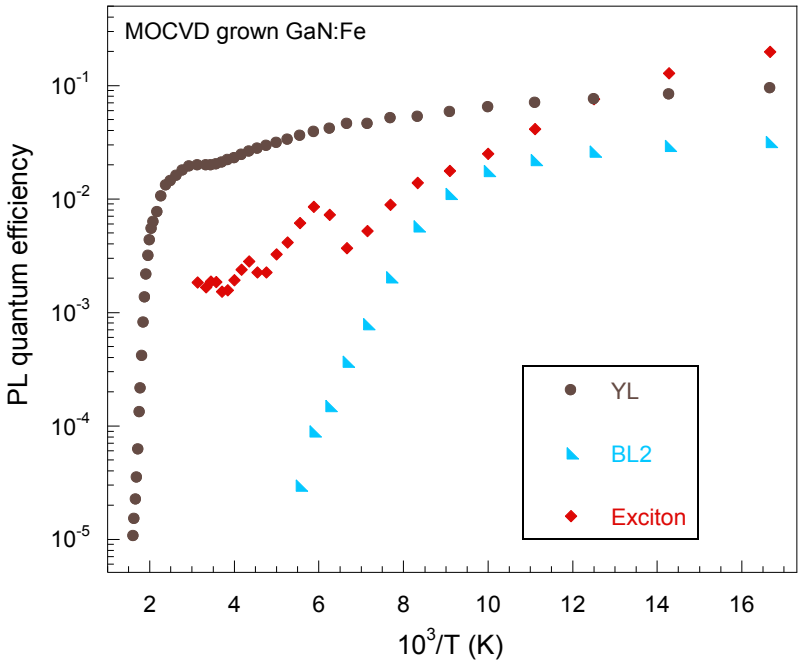

Figure 41. The temperature dependence of the quantum efficiency of the YL, BL2 and exciton bands at 0.2 W/cm^2 for GaN:Fe.

7.1.1 Evolution of PL spectra under continuous UV exposure for MOCVD grown GaN

An important feature of the BL2 band is that it bleaches under continuous above-bandgap illumination, indicating a metastable behavior.[37, 38] An example, sample GaN:C, is shown in Figure 42, and a zoomed-in region is shown in Figure 43. We can see that with gradual decreasing in the BL2 intensity, the YL band intensity increases simultaneously.

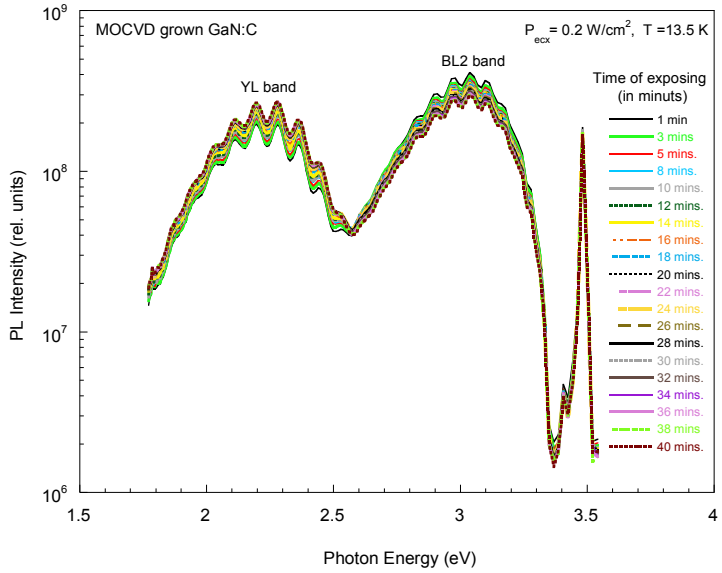

Figure 42. The bleaching of BL2 under prolonged UV exposure for GaN:C at T= 13.5 K and P_{exc}=0.2W/cm^2.

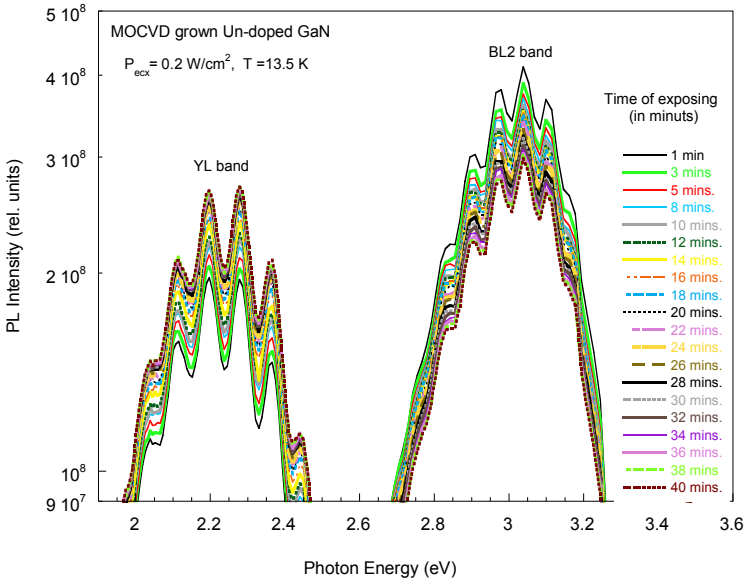

Figure 43. A zoomed-in region of the PL intensity for the major bands under continuous UV exposure.

The BL2 band transforms into the YL band under prolonged UV exposure, as the sum of the YL band and BL2 band remains almost constant, Figure 44. This suggests that the source responsible for BL2 band converts into the source of YL band. Since the YL band is attributed to either the C_N defect or the C_NO_N complex, [20, 21, 29] and abundance of hydrogen maybe produced in GaN samples grown by MOCVD method. It was suggested that the BL2 band is related to a hydrogen-carbon defect, either C_NO_N-H_i or C_N-H_i. [37, 38, 46, 47] Thus, the bleaching of BL2 occurs due to the possibilities that the C_NO_N-H_i and C_N-H_i complexes dissociate under prolonged ultraviolet (UV) exposure by releasing hydrogen atoms.

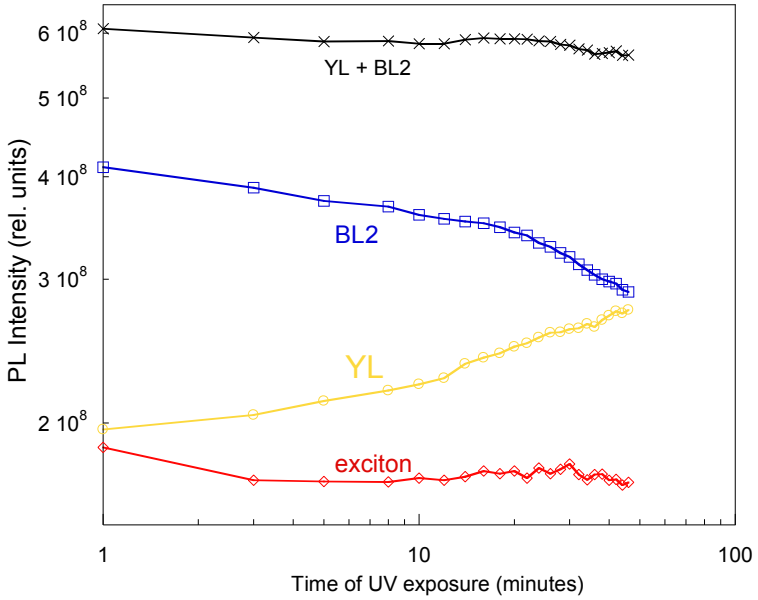

Figure 44. The behavior of PL intensity for main bands in un-doped GaN under continuous exposure with He Cd laser with P_{exc} =0.2 W/cm^2 at T=13.5 K.

7.1.2 Blue luminescence band (BL2) in MOCVD grown GaN samples

In high-resistivity GaN samples, a broad band in the blue spectral region with a maximum at 3.0 - 3.05 eV is observed and is labeled as the BL2 band. It is different from the BL band that is peaking at 2.9 eV in conductive n-type or Zn-doped GaN. Moreover, BL2 band is identified by its characteristic fine-structure at the high-energy side with the zero-phonon line (ZPL) at 3.33-3.34 eV. Based on the position of the ZPL, the transition level responsible for the BL2 band was suggested to be located at 0.15 eV above the valence band.[37, 38] The BL2 band is observed in the studied sample GaN:C, Figure 45.

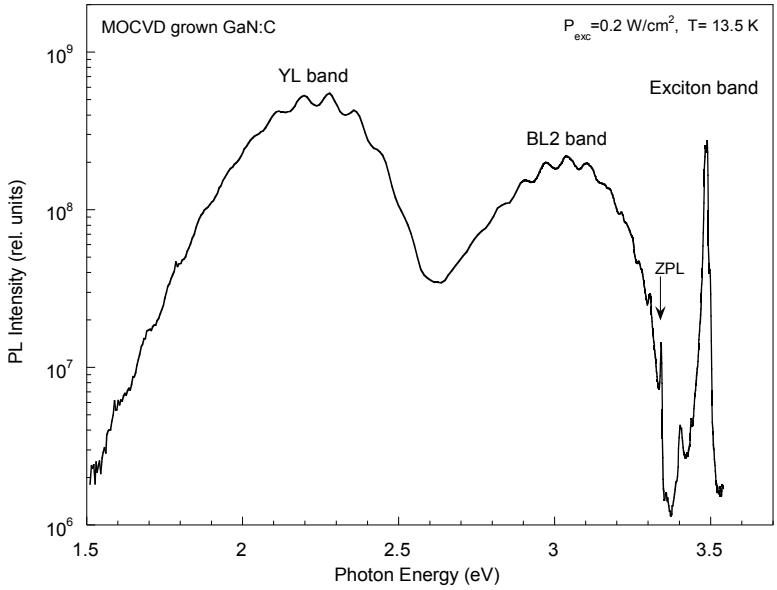

Figure 45. Low-temperature (T= 13.5 K) PL spectrum at P_{exc}= 0.2 W/cm^2 of GaN:C. The BL2 band has a maximum at 3.04 eV and ZPL at 3.34 eV.

A. Thermal quenching of the BL2 band for GaN:C and GaN:Fe grown by MOCVD

The temperature dependence of the quantum efficiency of the BL2 band for GaN:C and GaN:Fe samples have been studied at different excitation intensities as shown in Figures 46 and 47, respectively. The PL measurements were taken for the temperature range of 13.5 – 320 K,

and for excitation intensity, P_{exc}, which was varied between 0.2 to 5.2 $\times 10^{-5}$ W/cm^2 for GaN:C and between 0.2 to 1×10^{-3} W/cm^2 for GaN:Fe by using neutral density filters.

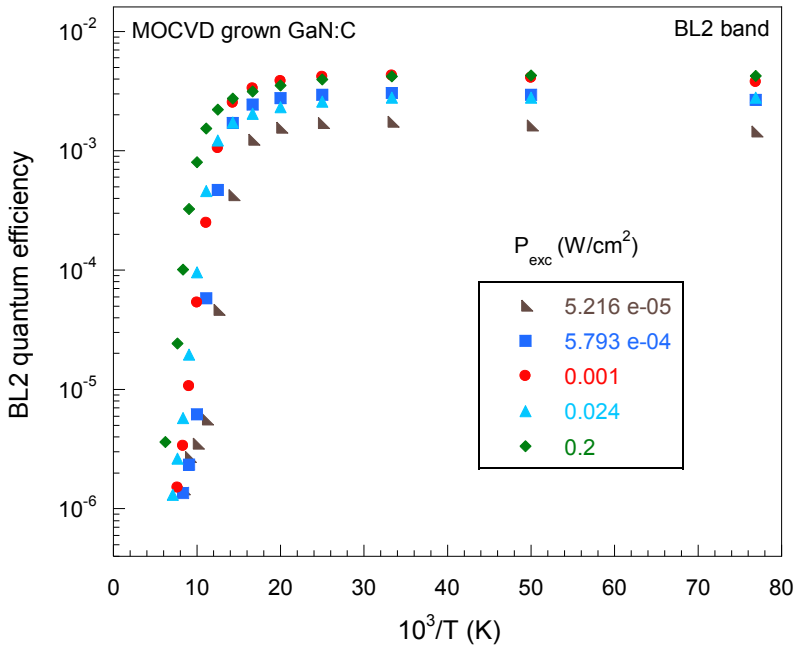

Figure 46. Temperature dependence of the quantum efficiency of the BL2 band for GaN:C.

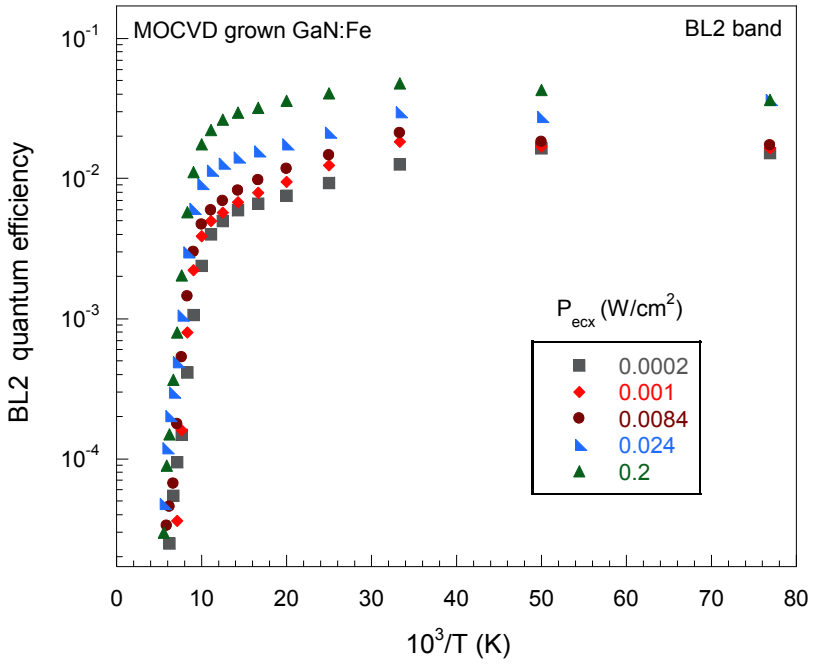

Figure 47. Temperature dependence of the quantum efficiency of the BL2 band for GaN:Fe.

We can see that in Figures 46 and 47, the BL2 intensity is nearly constant in the temperature range of about 13.5-90 K. Then, with increasing the temperature to around 100 K, the intensity of BL2 band decreases (PL quenching). A zoomed-in region for each sample, GaN:C in Fig. 48 and GaN:Fe in Fig. 49, shows a close-up view for the thermal quenching.

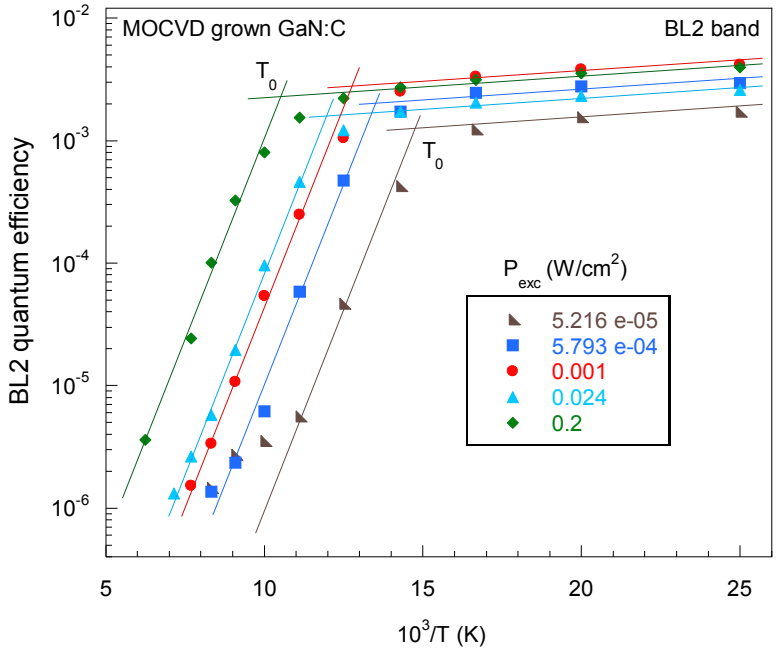

Figure 48. A zoomed-in region of the temperature dependence of the quantum efficiency of the BL2 band for GaN:C.

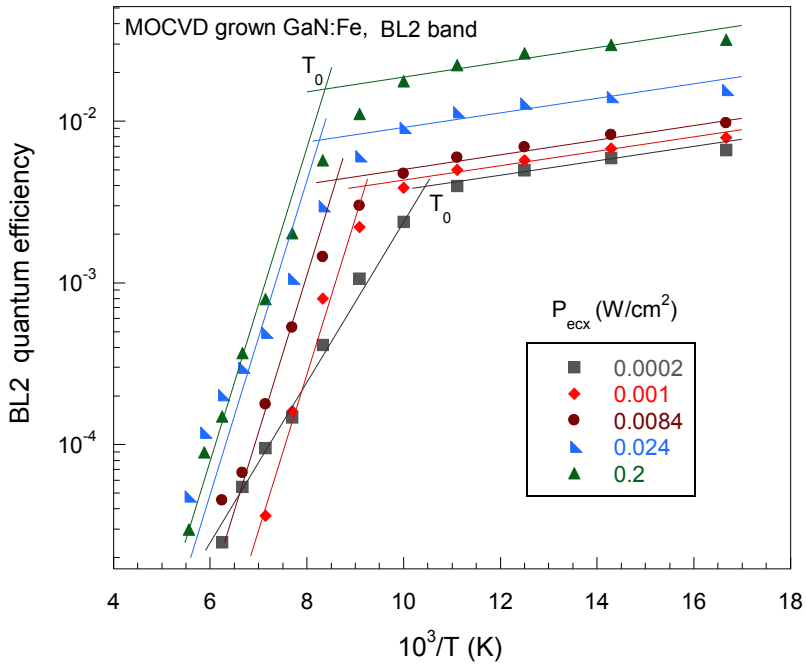

Figure 49. A zoomed-in region of temperature dependence of the quantum efficiency of the BL2 band for GaN:Fe.

B. Dependence of the characteristic temperature on excitation intensity for BL2 band

The characteristic temperature, T_0, the temperature at which the exponential or abrupt quenching of PL band begins, can be found by extrapolating the slopes of the low and high temperature dependences and finding the intersection in an Arrhenius plot. If the characteristic temperature, T_0, is independent of excitation intensity, the thermal quenching may reveal the ionization energy, E_A, of the defect responsible for the PL band. It is given by the slope of the dependence in the Arrhenius plot. On the other hand, if T_0 shifts with excitation intensity to higher temperature, the thermal quenching is likely to occur as abrupt and tunable quenching [6]. In this case, the slope of the quenching in the Arrhenius plot has no relationship to E_A. Then, the ionization energy, E_A, can be found from Eq. (23) by plotting the inverse of characteristic temperature as a function of excitation intensity, and it is given as the slope of the dependence.

It can be seen from Figures 48 and 49, for high-resistivity samples, GaN:C and GaN:Fe, that the characteristic temperature of quenching, T_0, increases and shifts to higher temperatures with increasing excitation intensity; i.e., the BL2 quenching is tunable by the excitation intensity. Therefore, the abrupt and tunable thermal quenching is observed, and the dependence of inverse of T_0 on the excitation intensity can reveal the ionization energy, E_A. The excitation intensity is expressed as electron-hole generation rate, G, through the expression of simplest model of light absorption, which is used in this work, $G = \alpha P_{exc}/\hbar\omega$, where $\alpha = 10^5$ cm^{-1} for GaN and $\hbar\omega = 3.81$ eV for a HeCd laser.

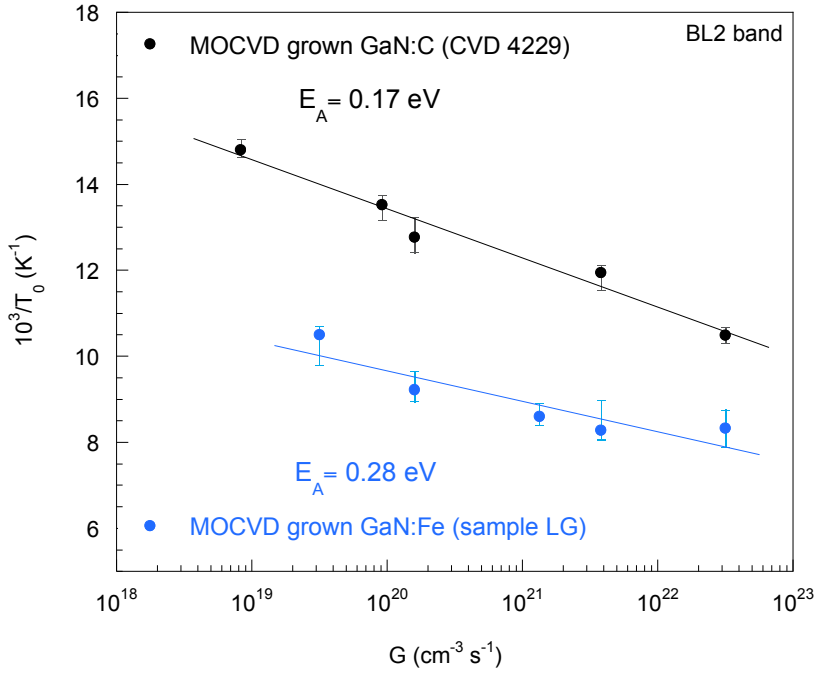

Figure 50. Dependence of the characteristic quenching temperature T_0 on generation rate, G, for the BL2 band in MOCVD-grown GaN:C and GaN:Fe samples.

Figure 50 shows the dependence of the inverse of characteristic temperature as a function of electron-hole generation rate, G, for the BL2 band in GaN:C and GaN:Fe. The activation energy, E_A, can be calculated by fitting the dependence of the BL2 band in Fig. 50 with Eq. (23),

$$\frac{10^3}{T_0} = \frac{10^3 k \ln(B/G)}{E_A} \tag{23}$$

where (10^3k/ E_A) is the slope of the dependence.

The ionization energy of the acceptor causing the BL2 band is determined: $E_A = 0.17_{-0.02}\, eV$ for GaN:C and $E_A = 0.28^{+0.03}_{-0.06}\, eV$ for GaN:Fe. The errors originate from the uncertainty in finding the characteristic temperature, T_0. Taking various slopes of quenching in addition to the one that was found as best fit slope, Figures 48 and 49, gives other possible values of T_0. Within the range of the error bars in Fig. 50, the steepness of the slope of the dependence was changed between the largest and smallest slope to estimate the errors of the ionization energy.

The values of E_A found here are obtained by using the model of abrupt and tunable thermal quenching. These values are close to the one reported before, E_A= 0.15 eV, and was determined from the slope of the temperature dependence of the PL intensity in the Arrhenius plot.[37, 38]

The calculated ionization energy for GaN:Fe is a little higher, $E_A = 0.28^{+0.03}_{-0.06}\, eV$, and this is most likely because there is no significant shift of T_0 to higher temperatures with increasing excitation intensity as shown in Fig. 50 . More measurements of PL intensity with different laser excitation intensities could resolve this uncertainty.

Furthermore, the coefficient B which is a sample-dependent constant, is determined and gives reasonable values, B= 4.3×10^{31} $cm^{-3}s^{-1}$ in GaN:C, and B= 9.8×10^{32} $cm^{-3}s^{-1}$ in GaN:Fe. The range of coefficient B was calculated by using equation (24),

$$B = C_{pA}\left(\eta_0^{-1} - 1\right)\left(N_A - N_D\right)\frac{N_v}{g} \tag{24}$$

The reasonable parameters are the following. For the maximum value of B: $\eta_0 = 0.001$, $C_{pA} = 10^{-6}$ cm^3/s, $N_A - N_D = 10^{18}$ cm^{-3}. For the minimum value of B: $\eta_0 = 0.1$, $C_{pA} = 10^{-8}$ cm^3/s, $N_A - N_D = 10^{14}$ cm^{-3}, and $g = 2$, $N_v = 2.5\times10^{19}$ $(T/300)^{3/2}$ cm^{-3} for both cases. These parameters correspond to B in the range between 10^{26} and10^{34} cm^{-3}/s.

7.1.3 Yellow luminescence band (YL) for MOCVD grown GaN samples

Yellow Luminescence is the most studied defect-related band that is observed in GaN. The YL is a broad band with a maximum in the range of 2.1–2.3 eV. The defects responsible for the YL band have been the topic of many discussions. However, it is likely that more than one source exist in GaN that may cause YL. Most recently, the YL band has been assigned to the electronic transitions via either the isolated defects carbon C_N or the C_N-O_N complex.[6, 37, 38, 46]

A. Thermal quenching of the YL band in GaN:C and GaN:Fe, both grown by MOCVD

With increasing temperature, at least up to the room temperature, YL remains nearly unchanged as we can see that in PL spectra in Figures 38 and 39. Thus, a high-temperature cryostat from 300 to 600 K is used to study the thermal quenching of the YL band. The quantum efficiency of the YL band as a function of inverse temperature at different excitation intensities for GaN:C and GaN:Fe are shown in Figures 51 and 52, respectively. At high temperature, the YL intensity drops abruptly, e.g. at 490 K for P_{exc} = 0.2 W/cm^2 in Fig. 51. The slope of the dependence, E_A= 2.4 eV, has no relation to the binding energy of the defect causing the YL band. Interestingly, the temperature (T_0) at which the PL quenching begins, increases with increasing the excitation intensity which means the abrupt quenching is tunable by the laser power. Thus, the ionization energy can be found by using the model of the abrupt and tunable quenching. In this work, we report for the first time the observation of abrupt and tunable thermal quenching of the YL band in GaN.

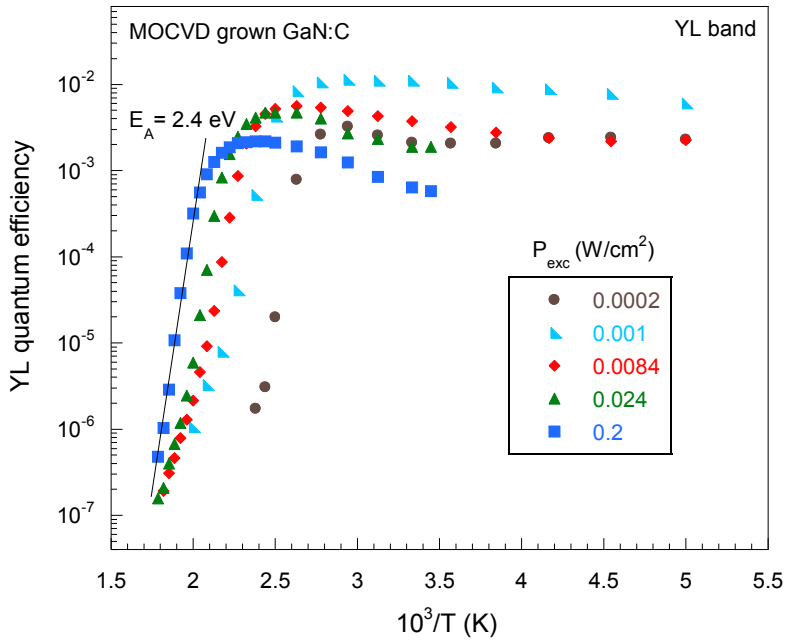

Figure 51. The temperature dependence of the quantum efficiency of the YL band at different excitation intensities for GaN:C

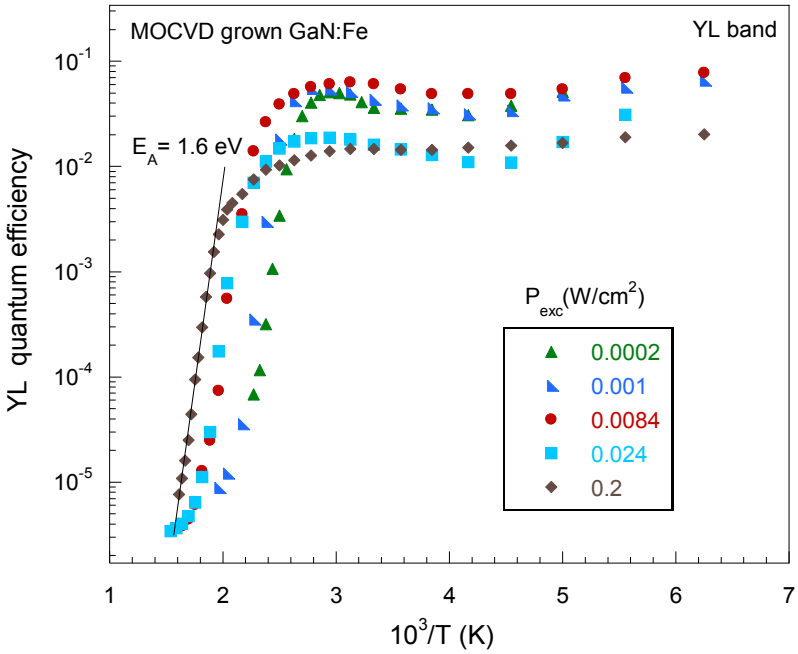

Figure 52. The temperature dependence of the quantum efficiency of the YL band at different excitation intensities for GaN:Fe

A zoomed-in region of the temperature dependence of the quantum efficiency of the YL band at different excitation intensities for samples, GaN:C and GaN:Fe, is shown in Figures 53 and 54, respectively.

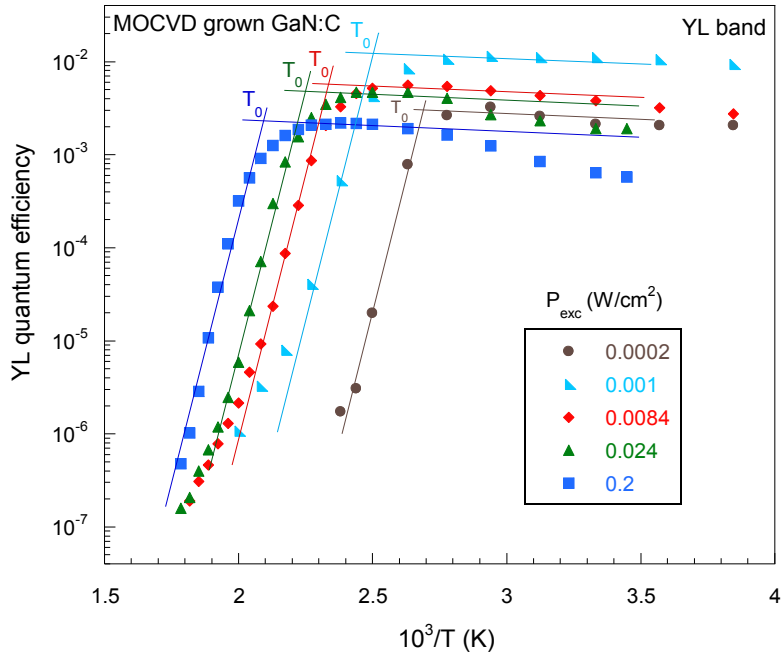

Figure 53. A zoomed-in region of the temperature dependence of the quantum efficiency of the YL band for GaN:C

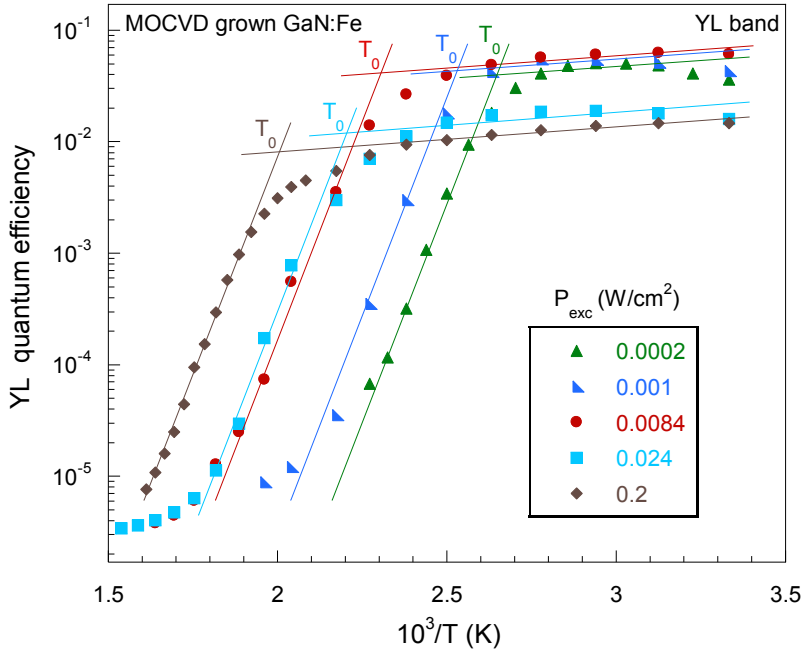

Figure 54. A zoomed-in region of temperature dependence of the quantum efficiency of the YL band for GaN:Fe

B. Dependence of the characteristic temperature on excitation intensity for YL band

In the high-resistivity samples, GaN:C and GaN:Fe, the abrupt and tunable thermal quenching for the YL band is observed; it is shown clearly in the zoomed-in region at Figures 53 and 54. To determine the ionization energy of the defect responsible for the YL band; first we need to find the characteristic temperature, T_0, at which the abrupt quenching of PL occurs. As shown in Figures 53 and 54, T_0 is the point where the extrapolated lines of the low temperature portion and the high temperature portion intersect. Next, we plot the inverse of T_0 as a function of carrier generation rate, G, Figure 55. According to equation (23), the slope of the dependence should give the ionization energy, E_A, for the acceptor contributing to YL band.

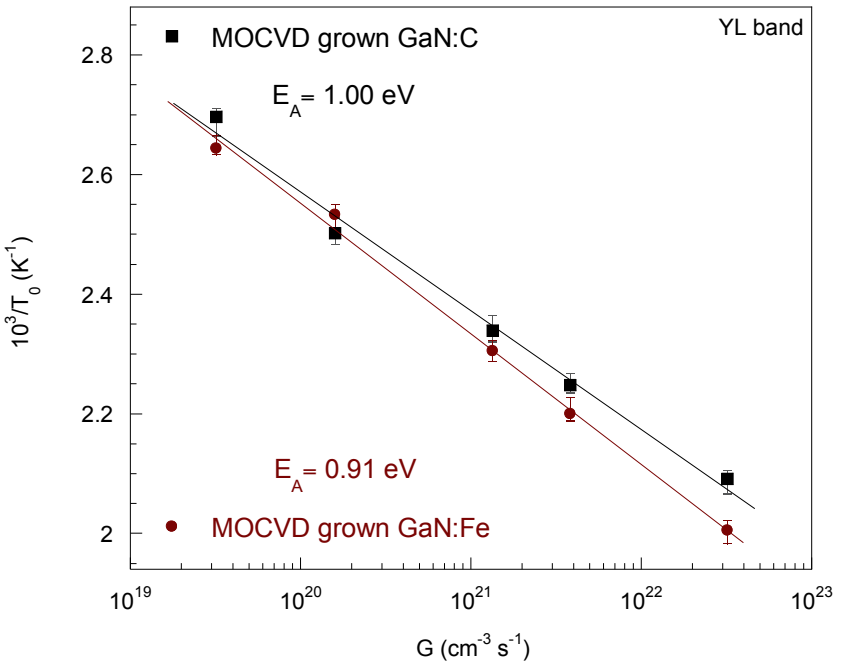

Figure 55. The dependences of the characteristic quenching temperature T_0 on the electron-hole generation rate G for the YL for GaN:C and GaN:Fe. The lines are calculated using Eq. (23).

From the fit of the dependences for the YL in Figure 55, using equation (23), the activation energy for the defect responsible for the YL band is determined, $E_A = 1.00^{+0.04}_{-0.06}\ eV$ for GaN:C and $E_A = 0.91^{+0.03}_{-0.02}\ eV$ for GaN:Fe. The activation energies found in this work are

close to those reported before and was determined from the slope of the temperature dependence of the PL intensity in the Arrhenius plot.[6, 37, 38, 46] Also, the coefficient B which is a sample-dependent constant, is determined and gives a reasonable value, B= 9.8×10^{32} $cm^{-3}s^{-1}$ for GaN:C and B= 5.3×10^{31} $cm^{-3}s^{-1}$ for GaN:Fe.

7.2 Temperature dependence of PL for HVPE-grown GaN samples

Three other high-resistivity GaN samples investigated in this work (AE3273, AE3260 and AE3276) were grown by Hydride vapor phase epitaxy (HVPE) at Kyma Technologies, Inc. All the samples are doped with iron, GaN:Fe. The PL measurements were taken for the temperature range of 13 – 320 K, and for different excitation intensity, P_{exc}, which was varied between 0.128 to 26.5 mW/cm^2 using neutral density filters. The spectral dependence of PL intensity in the temperature range of 13.5 – 200 K for three HVPE grown GaN:Fe samples are shown in Figures 56-58.

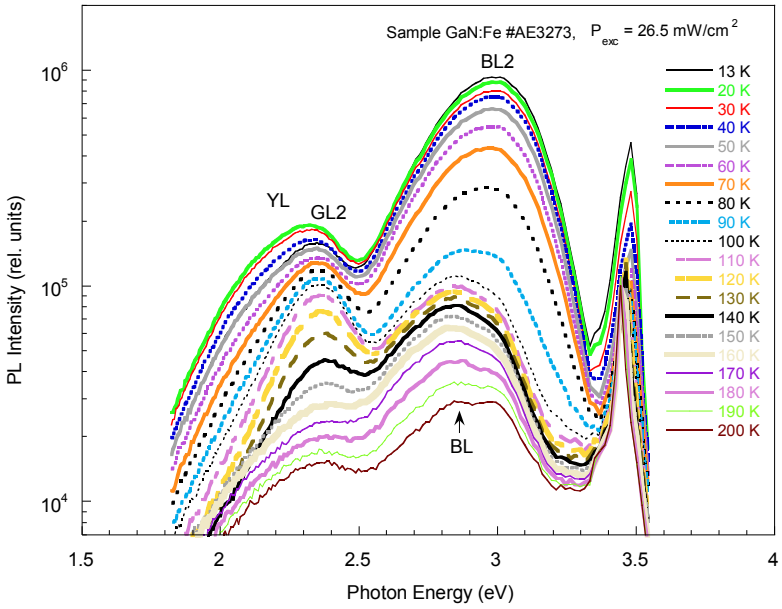

Figure 56. The PL spectra for HVPE grown GaN:Fe sample AE3273 for temperatures up to 200 K.

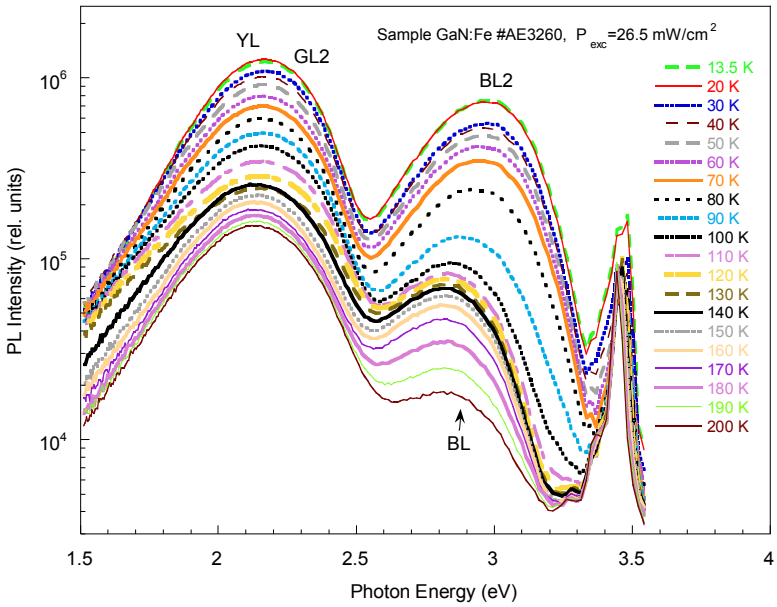

Figure 57. The PL spectra for HVPE grown GaN:Fe sample AE3260 for temperatures up to 200 K.

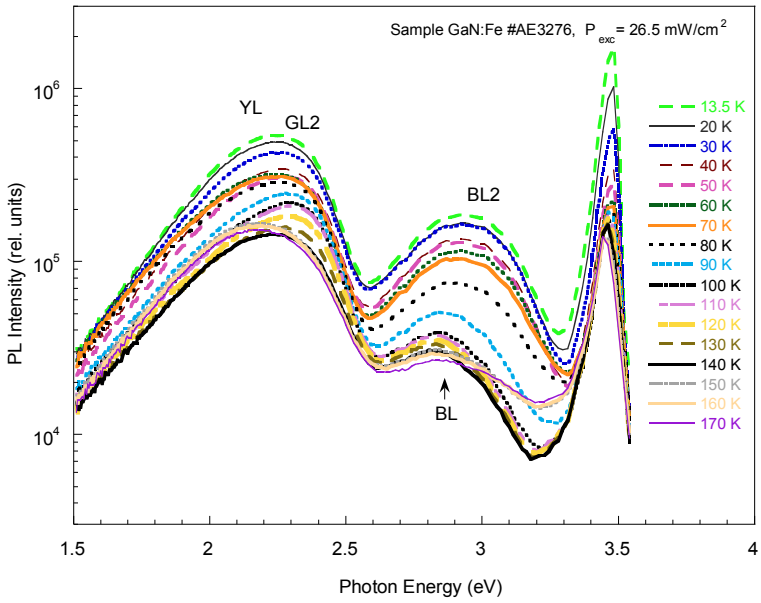

Figure 58. The PL spectra for HVPE grown GaN:Fe sample AE3276 for temperatures up to 200 K.

The PL spectra of HVPE grown GaN:Fe samples contain four bands related to defects. The BL2, BL, GL2 and YL bands in this type of samples are overlapped and obstruct each other. After resolving the overlapped bands (more details in chapter 4) and finding the contribution of

each band, the temperature dependence of the quantum efficiency of the BL2, BL, GL2 and YL bands at high excitation intensity, 26.5 mW/cm^2 for each sample are plotted and shown in Figures 59-61.

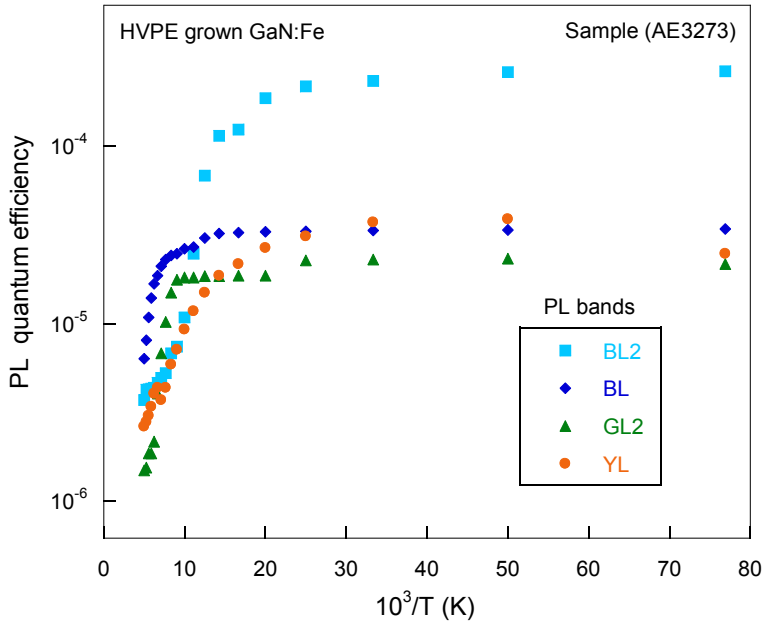

Figure 59. The temperature dependence of the BL2, BL, GL2 and YL bands at 26.5 mW/cm^2 for HVPE grown GaN:Fe sample (AE3273).

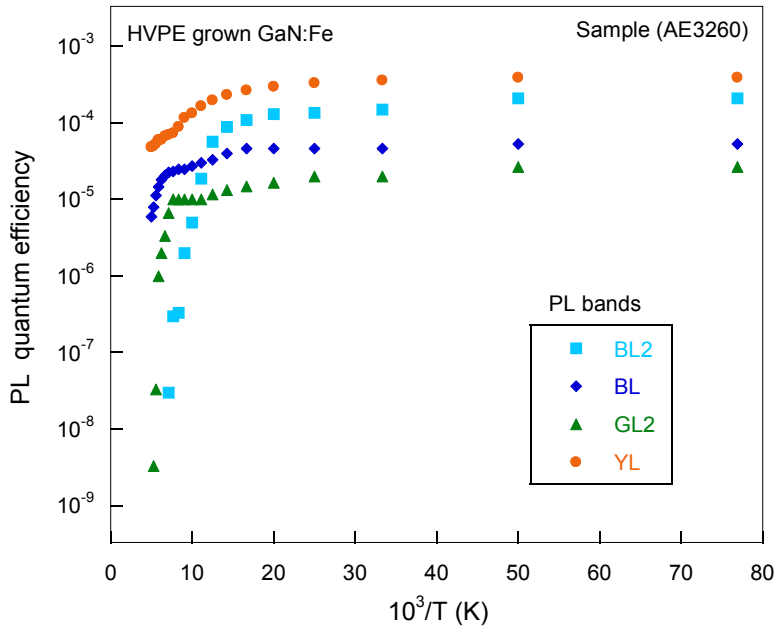

Figure 60. The temperature dependence of the BL2, BL, GL2 and YL bands at 26.5 mW/cm^2 for HVPE grown GaN:Fe sample (AE3260).

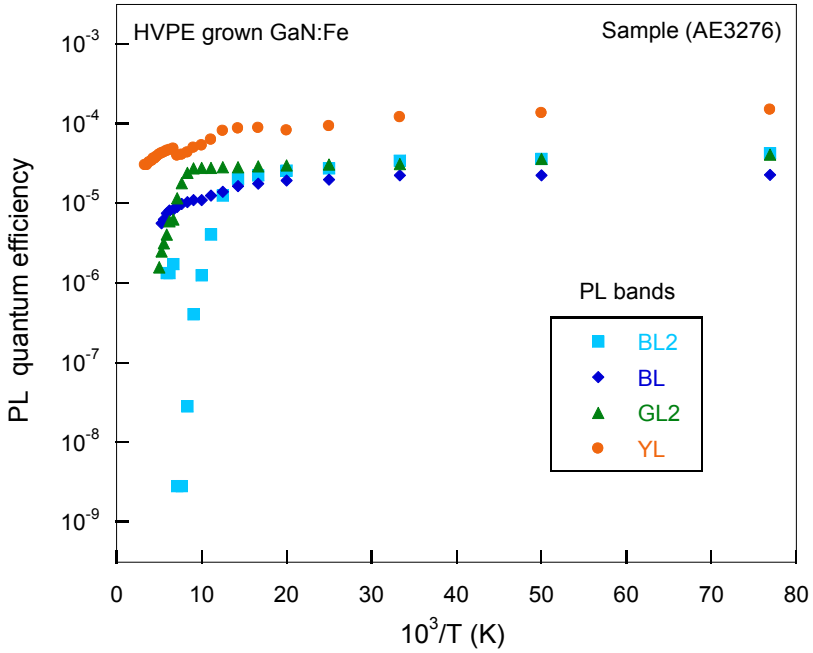

Figure 61. The temperature dependence of the BL2, BL, GL2 and YL bands at 0.2 W/cm^2 for HVPE grown GaN:Fe sample (AE3276).

7.2.1 Evolution of PL spectra under continuous UV exposure for HVPE grown GaN:Fe

The BL2 band in GaN:Fe samples grown by HVPE shows bleaching under continuous UV illumination, Figure 62. The BL2 intensity gradually decreased, while the YL intensity increased simultaneously as we can see better in the zoomed-in region in Figure 63.

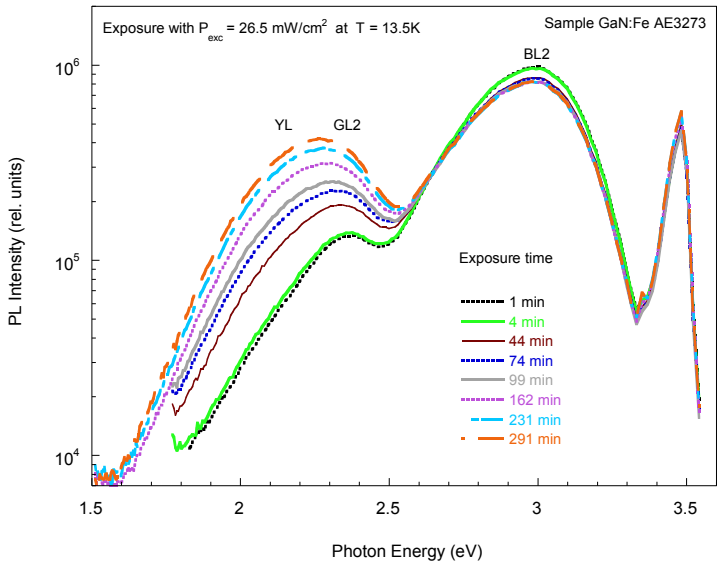

Figure 62. The bleaching of BL2 under continue UV exposure for HVPE grown GaN:Fe at T=13.5 K and P_{exc} =26.5 mW/cm^2.

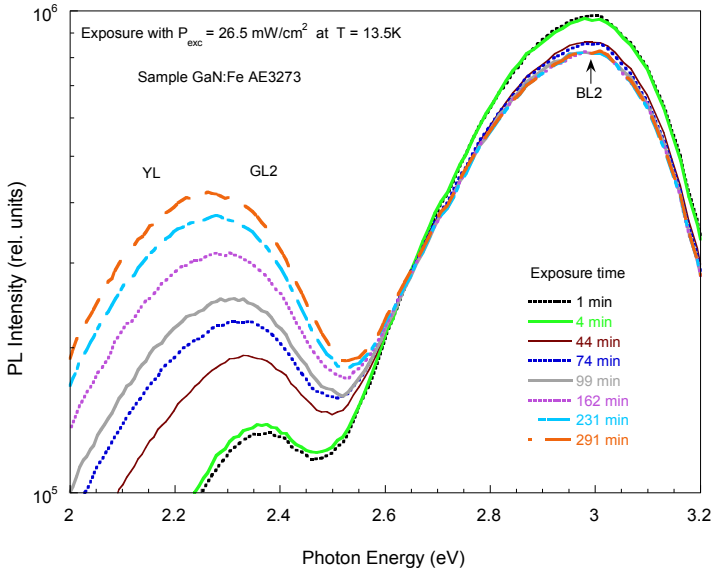

Figure 63. A zoomed- in region for the BL2 bleaching for HVPE grown GaN:Fe at T=13.5 K and P_{exc}=26.5 mW/cm^2.

By performing the deconvolution of overlapped PL bands, we obtained the dependence of quantum efficiencies for BL2, YL and exciton bands as a function of the UV exposure time, which is shown Figure 64.

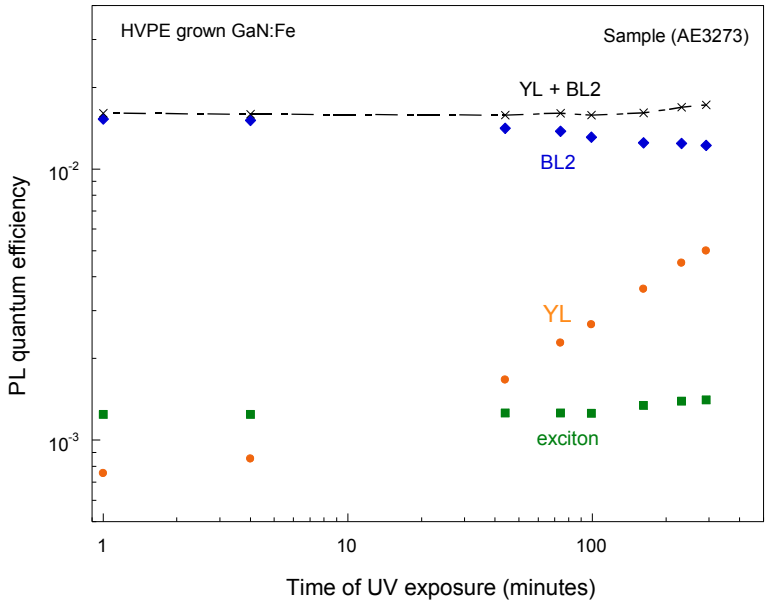

Figure 64. Evolution of PL quantum efficiency of BL2, YL and exciton for HVPE grown GaN:Fe at T=13.5 K with P_{exc} =26.5 mW/cm^2.

The absolute reduction of the BL2 quantum efficiency (about 0.3× 10^{-2}) is almost equal to the absolute increase of the YL quantum efficiency (about 0.4× 10^{-2}). As a result, the sum of the two bands, BL2 and YL, is nearly constant. This suggests that the source of BL2 bands converts into the source of YL band under continuous UV illumination.

7.2.2 Calculating the temperature dependence of quantum efficiency of the BL2 band in HVPE-grown GaN:Fe samples

The PL measurements were taken for the temperature range of 13.5 – 320 K, and for different excitation intensities, P_{exc}, which were varied between 0.128 to 26.5 mW/cm^2 using neutral density filters. The BL2 band in all three samples, AE3273, AE3260 and AE3276, overlaps with other PL bands; BL, GL2 and YL bands. Resolving overlapped bands and finding the contribution of each band are needed to calculate the PL quantum efficiency for each band. The deconvolution of the broad band into the YL, GL2, BL and BL2 bands with their known shapes helps to measure the peak intensities, see chapter 4 for more details.

From the deconvolution, the quantum efficiency of the BL2 band for HVPE grown GaN:Fe is determined and plotted versus inverse temperature at different excitation intensities. The results for three samples are shown in Figures 65-67.

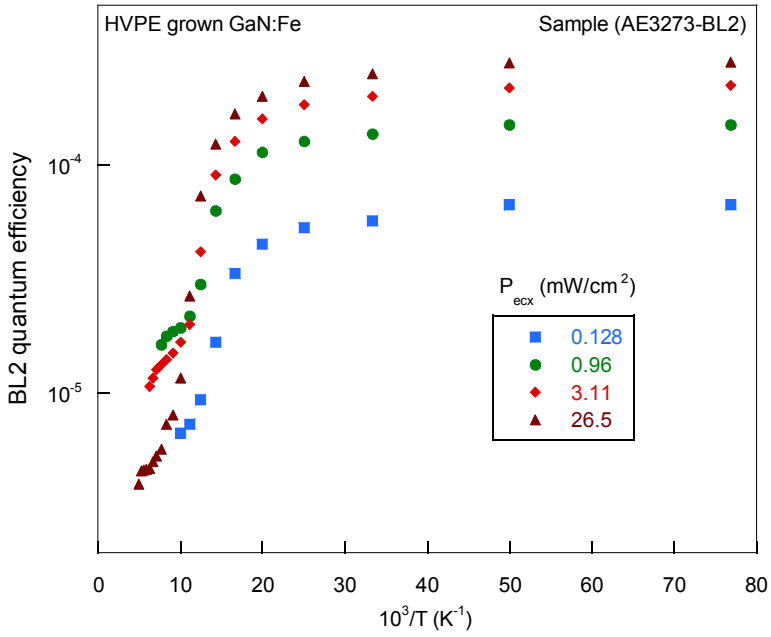

Figure 65. Temperature dependence of PL QE for the BL2 band at different excitation intensities for HVPE grown GaN:Fe Sample AE3273.

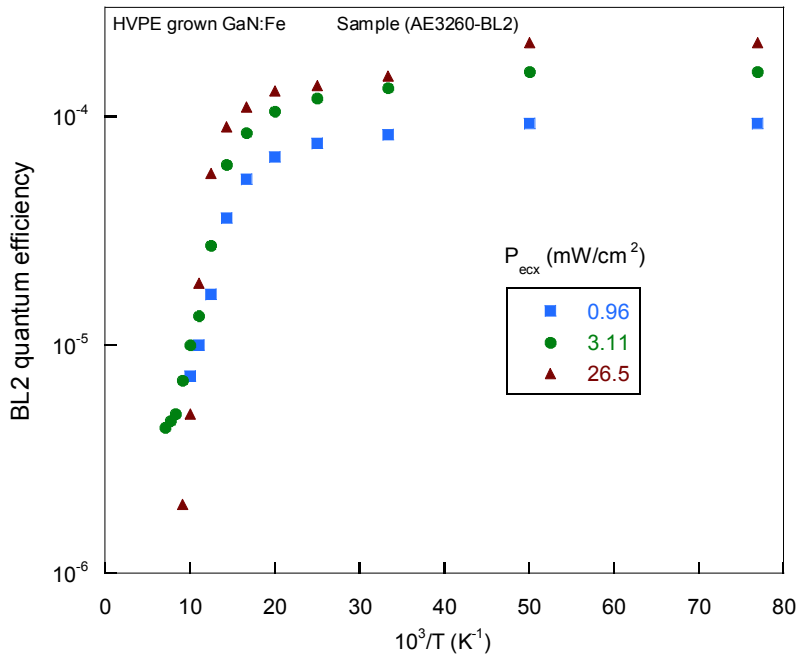

Figure 66. Temperature dependence of PL QE for the BL2 band at different excitation intensities for HVPE grown GaN:Fe Sample AE3260.

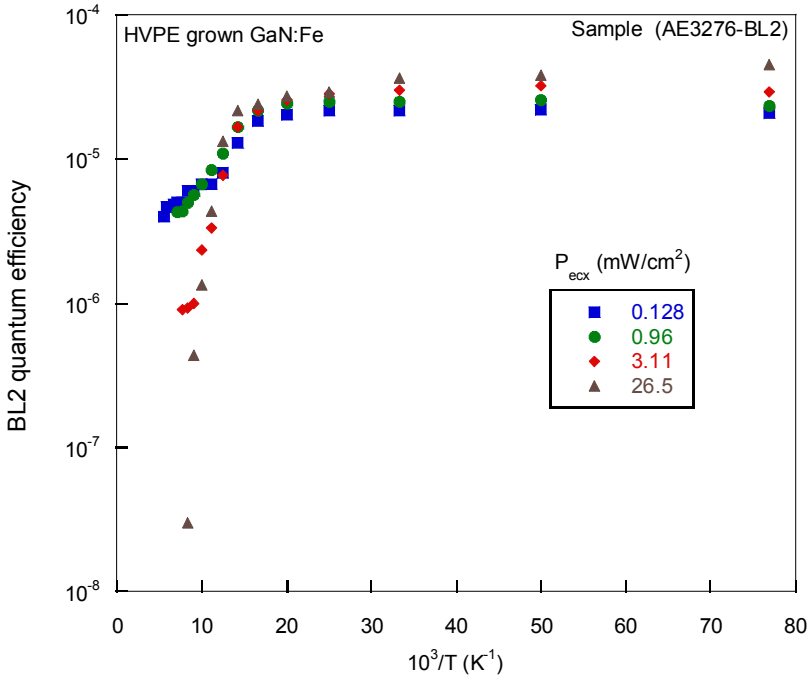

Figure 67. Temperature dependence of PL QE for the BL2 band at different excitation intensities for HVPE grown GaN:Fe Sample AE3276.

The zoomed-in regions of the temperature dependence for the three samples in Figures 68-70 show a close-up view of BL2 thermal quenching.

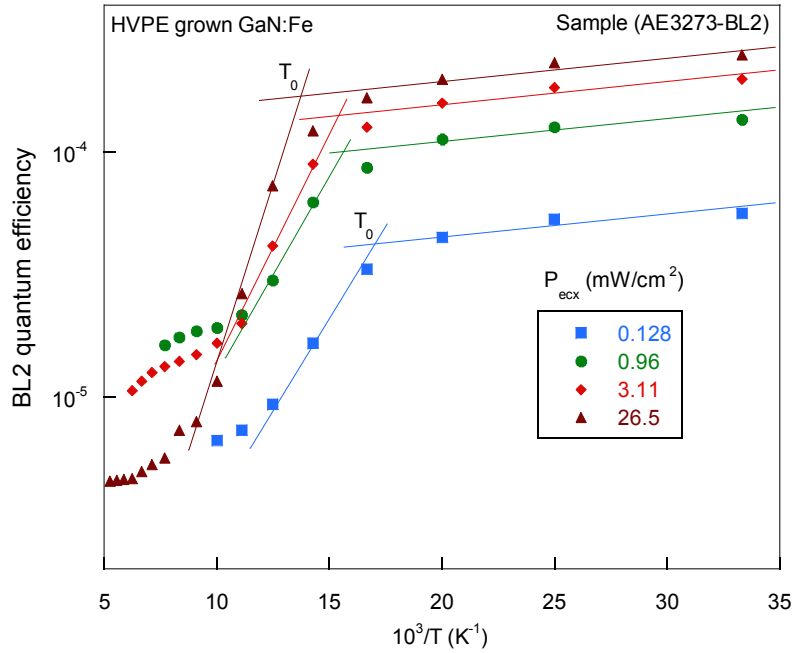

Figure 68. A zoomed-in region of temperature dependence of the BL2 band for HVPE grown GaN:Fe sample (AE3273).

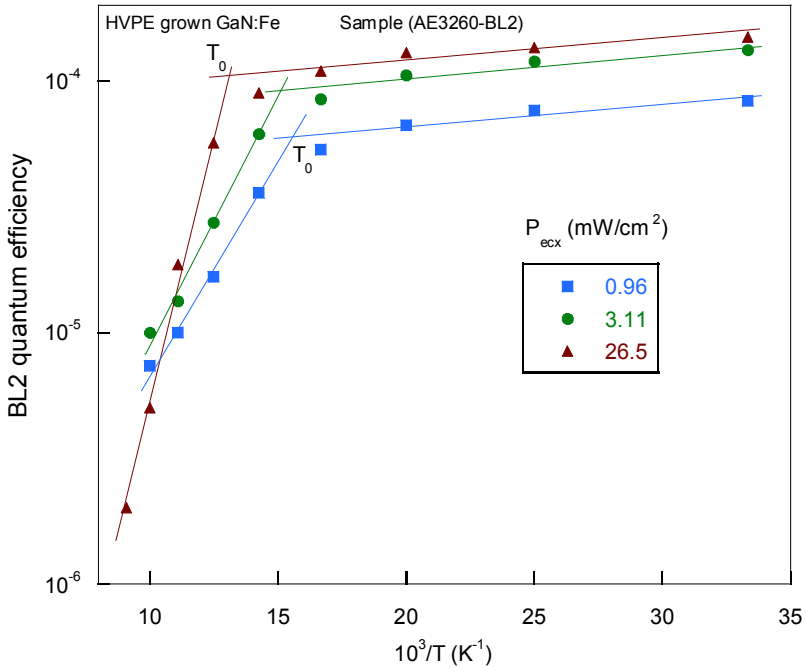

Figure 69. A zoomed-in region of temperature dependence of the BL2 band for HVPE grown GaN:Fe sample (AE3260).

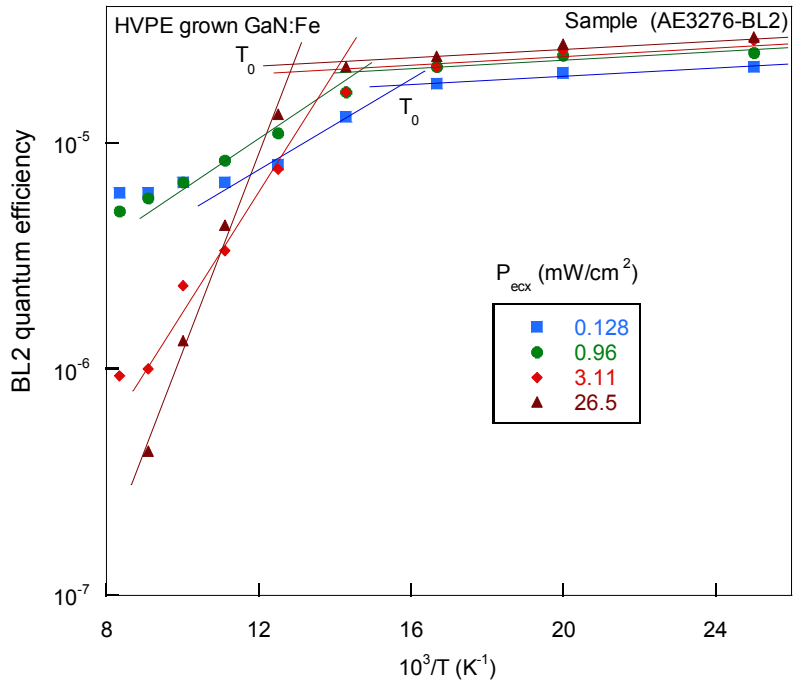

Figure 70. A zoomed-in region of temperature dependence of the BL2 band for HVPE grown GaN:Fe sample (AE3273).

7.2.2.1 Dependence of the characteristic temperature on excitation intensity of BL2 quantum efficiency for HVPE grown GaN:Fe samples

For high-resistivity samples, GaN:Fe grown by HVPE, we used the model of the abrupt and tunable thermal quenching. According to this model and based on equation (23), the inverse of characteristic temperature, T_0, was plotted as a function of carrier generation rate, G. From this plot we expected to find the ionization energy of the acceptor responsible for BL2.

The characteristic temperature, T_0, can be found by extrapolating the slopes and finding the intersection of the low and high temperature dependences in an Arrhenius plot. Usually the slope of abrupt quenching is not changing with excitation intensity [4] as we can see that in the abrupt quenching of the YL band for MOCVD samples, Figures 53 and 54. Moreover, keeping the slopes of abrupt quenching constant with changing excitation intensity is preferred to avoid the ambiguity in determining the T_0. However, for GaN:Fe samples grown by HVPE, another approach was followed to find the T_0. The big difference between the slopes of quenching is observed for these samples by changing the excitation intensity, as shown in Figures 68-70. In this case, it is reasonable to use the actual slope for each thermal quenching to reach more accurate value for T_0. Figure 71 shows the dependence of the inverse of characteristic temperature, T_0, of BL2 as a function of carrier generation rate, G, for the three samples.

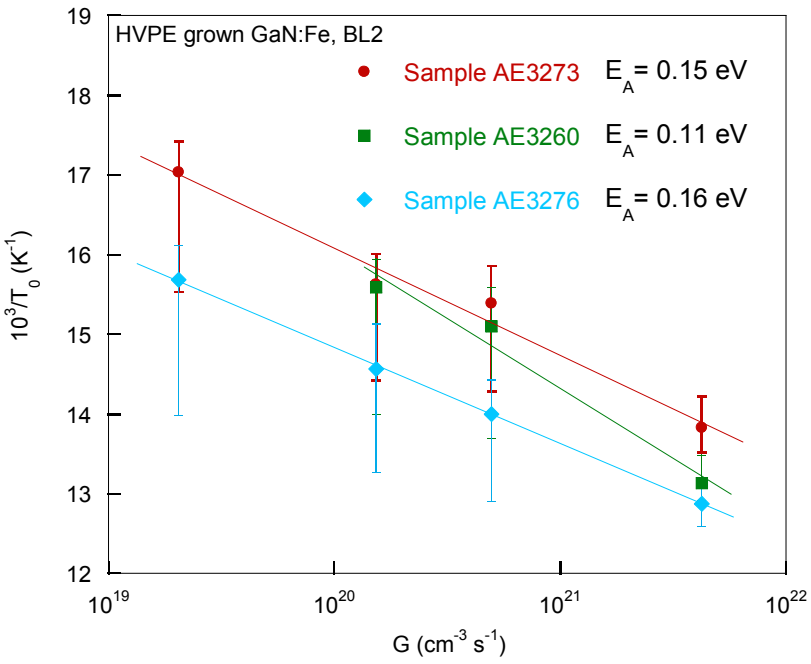

Figure 71. The dependence of the characteristic quenching temperature, T_0, of BL2 as a function of carrier generation rate, G, for the three samples: AE3273, AE3260 and AE3276.

The $T_0(G)$ dependences for the BL2 band for the three samples were fitted with Equation (23). The results are shown in Figure 71. The activation energy can be found from these plots and is given as the slope of the dependence. Thus, the calculated activation energies are E_A = 0.15 eV for sample (AE3273), E_A = 0.11 eV for sample (AE3260), and E_A = 0.16 eV for sample (AE3276). For the three samples, the values of activation energies are close the one known from literature, E_A = 0.15 eV.[20, 21] Moreover, the data fits give reasonable value of parameter B for all three samples, B= 1 $\times 10^{32}$ cm^{-3}/s for sample (AE3273), B= 1.8 $\times 10^{29}$ cm^{-3}/s for sample (AE3260), and B= 1.9 $\times 10^{32}$ cm^{-3}/s for sample (AE3276).

The errors originate from the uncertainty in finding the characteristic temperature, T_0. This type of samples needs different approaches to find other possible T_0 values. One of the approaches that cause significant spread in T_0 values is keeping the most abrupt slope as a

constant slope. However, in this particular case, we also tried to keep the slopes variable as they are to fit better the $I^{PL}(T)$ dependence. This variation of approaches ends up with large error bars as we can see that in Figure 71. Within the error bars range in Figure 71, the steepness of the slope of the dependence was changed between the largest and smallest slope to estimate the errors in the ionization energy by using Eq. (23),

$$\frac{10^3}{T_0} = \frac{10^3 k \ln\left(B / G\right)}{E_A} \tag{23}$$

In first try, the slope steepness was limited by keeping the value of fitting parameter B at the reasonable calculating range, B = 10^{26} - 10^{34} cm^{-3}/s. By using this way, the whole range of the large error bars was not covered during changing the slope steepness. The results of this try are $E_A = 0.15^{+0.05}_{-0.03}\ eV$ for sample (AE3273), $E_A = 0.11^{+0.08}_{-0.02}\ eV$ for sample (AE3260), and $E_A = 0.16^{+0.04}_{-0.03}\ eV$ for sample (AE3276). In the second try, the steepness of the slope was changed to cover the whole spread of the large error bars. This resulted in increase of the parameter B well above the reasonable values range. Namely, the value of coefficient B was in the range between 10^{40} and 10^{50} cm^{-3} s^{-1}. The results of the second try affect only the positive error bars value. The final results are as follow: $E_A = 0.15^{+0.15}_{-0.03}\ eV$ for sample (AE3273), $E_A = 0.11^{+0.22}_{-0.02}\ eV$ for sample (AE3260), and $E_A = 0.16^{+0.27}_{-0.03}\ eV$ for sample (AE3276).

Chapter 8: The Conclusions

In this study, we analyzed temperature dependences of defect-related PL and distinguished between two different types of thermal quenching: normal quenching, NQ, and abrupt and tunable thermal quenching, ATQ. The thermal quenching is normal quenching when the slope of the exponential decrease of PL intensity on inverse temperature reveals the ionization energy, E_A, of the defect involved in the thermal quenching. This type of thermal quenching is observed in conductive n-type semiconductors. In contrast, when the intensity of PL decreases by several orders of magnitude within a small range of temperature, the PL quenching is defined as abrupt quenching. The slope of this type of thermal quenching has no relation to the binding energy of the defect causing the PL band. Another unusual feature of the ATQ is that the characteristic temperature, T_0, at which the quenching occurs, strongly depends on the excitation intensity and can be tuned by changing the excitation intensity. Thus, taking the temperature dependence of PL for different excitation intensities, P_{exc}, is a new method which was developed to determine the ionization energy in high-resistivity semiconductors. This new and interesting phenomenon can be regarded as a third mechanism of PL quenching for high-resistivity materials; the other two mechanisms of thermal quenching, namely Seitz-Mott mechanism (a conversion of a defect from radiative to nonradiative) and the Schön-Klasens mechanism (normal quenching due to thermal emission of holes to the valence band).

Thermal quenching of PL from several high-resistivity ZnO and GaN samples was investigated in this work. Different PL bands in all studied samples show abrupt and tunable thermal quenching behavior. Calculating the ionization energies of the defects related to the PL bands by using the ATQ model agrees with the previously reported values obtained from

measuring the slope in the Arrhenius plot. Thus, this model helped to identify point defects in high-resistivity ZnO and GaN semiconductors. Furthermore, ATQ thermal quenching provides indirect information about unknown nonradiative defects in semiconductor center because this center plays important role in this type of quenching.

In the three ZnO samples (M6, M27 and M28) grown by hydrothermal method, the OL band with a maximum near 2.0 eV demonstrates the ATQ behavior. Moreover, the ATQ of the exciton band in the same samples verifies that the quenching of the OL band is abrupt and tunable because the concentration of electrons in the conduction band suddenly drops at $T \approx T_0$. All radiative recombination channels (OL and exciton) reveal almost the same activation energy in the T_0 (G) dependence, $E_A = 0.65 \pm 0.10$ eV, and help to determine the position of the acceptor level, Li_{Zn}.

The dominant PL bands related to defects in GaN:C and GaN:Fe samples grown by MOCVD are the yellow luminescence (YL) band and a broad band in the blue spectral region (BL2). Both PL bands show ATQ thermal quenching. However, the YL band required much higer temperatures (from 300 to 600 K) to observe a thermal quenching. The ionization energy of the acceptor causing the BL2 band is determined: $E_A = 0.17_{-0.02}\, eV$ for GaN:C and $E_A = 0.28^{+0.03}_{-0.06}\, eV$ for GaN:Fe. The calculated ionization energy for GaN:Fe is a little higher, $E_A = 0.28^{+0.03}_{-0.06}\, eV$, and this is most likely because there is no significant shift of T_0 with changing the excitation intensity. More measurements of PL intensity with different laser excitation intensities could resolve this uncertainty. Also, using ATQ model reveals the ionization energy for the defect responsible for the YL, $E_A = 1.00^{+0.04}_{-0.06}\, eV$ for GaN:C and $E_A = 0.91^{+0.03}_{-0.02}\, eV$ for GaN:Fe. These values, for BL2 and YL bands, are close to the ones

reported before and was determined from the slope of the temperature dependence of the PL intensity in the Arrhenius plot.

The PL bands in the three samples of GaN:Fe grown by HVPE are overlapped and obstruct each other. After resolving overlapped bands, the quantum efficiency of the BL2 was plotted versus inverse temperature at different excitation intensities. The dependence shows that the thermal quenching is likely to occur as abrupt and tunable quenching. Taking actual slope for each thermal quenching with changing excitation intensity was helpful to determine more accurate value for T_0. Thus, the ionization energy can be found from the T_0 (G) plot. The results are as follow: $E_A = 0.15^{+0.05}_{-0.03}\, eV$ for sample (AE3273), $E_A = 0.11^{+0.08}_{-0.02}\, eV$ for sample (AE3260), and $E_A = 0.16^{+0.04}_{-0.03}\, eV$ for sample (AE3276).

References:

1. M. A. Reshchikov, "Internal Quantum Efficiency of Photoluminescence in Wide Bandgap Semiconductors", Chapter in Photoluminescence: Applications, Types and Efficacy, Ed. M. A. Case and B. C. Stout, Nova Science Publishers, Inc., New York, pp. 53-120, 2012, ISBN: 978-1-61942-426-5.
2. M. A. Reshchikov. J. Appl. Phys. 115,012010 (2014).
3. M. A. Reshchikov and H. Morkoc. J. Appl. Phys. 97, 061301 (2005).
4. M. Leroux, N. Grandjean, B. Beaumont, G. Nataf, F. Semond, J. Appl. Phys. 86, 3721 (1999).
5. T. C. Leslie, J. W. Allen, Phy. State solid 65, 545 (1981).
6. M. A. Reshchikov, A. Kvasov, T. McMullen, M. F. Bishop, A. Usikov, V. Soukhoveev, and V. A. Dmitriev, Phys. Rev. B 84, 075212 (2011).
7. Anderson Janotti and Chris G Van de Walle. Rep. Prog. Phys. 72, 126501(2009).
8. L. Wang, "Photoluminescence Study of As-grown and Thermally Annealed Bulk ZnO Crystals", Morgantown, West Virginia (2004).
9. Y. Narukawa, et al. (2010) "White light emitting diodes with super-high luminous efficacy." Retrieved from http://phys.org.
10. V. N. Abakumov, V.I. Perel and I.N. Yassievich, "Modern Problems in Condenced Matter Sciences" Chapter in Nonradiative Recombination in Semiconductor, Types and Efficacy, A.F. Ioffe Physics-Technical Ins., Volume 33. A. M. Stoneham, Theory of Defects in Solids (Clarendon Press, Oxford, 2001).
11. ISBN 0 19 850780 1.
12. H. A. Klasens. J. Phys. Chem. Solids. 7, 175(1958)
13. J. I. Pankove, Optical Properties in Semiconductors (Dover Publ. Inc., New York, 1971), pp. 165–167.
14. M. A. Reshchikov and R. Y. Korotkov. Phys. Rev. B 64, 115205 (2001)
15. H. A. Klasens, Nature 158, 306 (1946).
16. G. F. Garlick and A. F. Gibson. J. Opt. Soc. Am. B 39(11), 935 (1949).
17. H. A. Klasens. J. Phys. Chem. Solids. 9, 185(1959).
18. K. Maeda, J. Phys. Chem. Solids 26, 595 (1965).

19. M. A. Reshchikov, J. D. McNamara, S. Fernández-Garrido, and R. Calarco, Phys. Rev. B 87,115205 (2013).
20. M. A. Reshchikov, J. D. McNamara, F. Shahedipour-Sandvik, Phys. Stat. Sol. (c)11, 389 (2014).
21. M. A. Reshchikov, "Point defects in GaN", in "Semiconductors and Semimetals", Chapter nine, Volume 91, Elsevier Inc. ISSN 0080-8784 (2015)
22. D. Lang, J. Appl. Phys. 45(7), 3023 (1974).
23. C. Sah and J. Walker, Appl. Phys. Lett. 22, 384 (1973).
24. D.L. Losee, J. Appl. Phys. 21, 54 (1972).
25. D.L. Losee, J. Appl. Phys. 46, 2204 (1975)
26. C. T. Sah, W.W. Chan H.S Fu and J.W. Walker. Appl. Phys. Lett. 20, 193 (1972).
27. A. Polyakov, I. Lee, N. Smirnov, A. Govorkov, E. Kozhukhova, S. Pearton, J. Appl. Phys. 109, 123701 (2011).
28. W. Gotz, N.M. Johnson, H. Amano and I. Akasaki, J. Appl. Phys. 68, 3144 (1996).
29. A. Polyakov, N. Smirnov, A. Govorkov, M. Shin, M. Skowronski and D. Greeve, J. Appl. Phys. 84(2) (1998).
30. A. Hierro, D. Kwon, S. Ringel, E. Pelucchi and A. Franciosi, J. Appl. Phys. 87(2),730 (2000).
31. Z. Zhang, C.A. Hurni, C.A., A.R. Arehart, J. Yang, R.C. Myers, J.S. Speck, J. Appl. Phys. 100, 052114 (2012).
32. A. Mitonneau, A. Mircea, G. M. Martin, & D. Pons, Revue de Physique Appliquee 14, 853-861 (1979).
33. A. Y.Polyakov & I. H. Lee, Mater. Sci. Engineer. R 94, 1-56 (2015).
34. Lee, I.-H. et al. J. Appl. Phys. 115, 223702 (2014).
35. M. A. Reshchikov, M. Foussekis, J. D. McNamara, A. Behrends, A. Bakin, and A. Waag, J. Appl. Phys. 111, 073106 (2012).
36. M. A. Reshchikov, J. D. McNamara, A. Behrends, M.S. Mohajerani, A. Bakin, and A. Waag, Phys. Stat. Sol. (c) 10, 507 (2013).
37. M. A. Reshchikov, D. O. Demchenko, A. Usikov, H. Helava, and Yu. Makarov, Phys. Rev. B, 90, 235203 (2014).

38. D. O. Demchenko, I. C. Diallo, and M. A. Reshchikov. J. Appl. Phys.119, 035702 (2016)
39. M. A. Reshchikov, D. O. Demchenko, J. D. McNamara, S. Fernández-Garrido, and R. Calarco, Phys. Rev. B 90, 035207 (2014)
40. M. A. Reshchikov, A. J. Olsen, M. F. Bishop and T. McMullen. Phys. Rev. B 88, 075204 (2013).
41. M. A. Reshchikov, D. O. Demchenko, A. Usikov, H. Helava, and Yu. Makarov, Phys. Rev. B, 90, 235203 (2014)
42. M. A. Reshchikov, Y. T. Moon, X. Gu, B. Nemeth, J. Nause, and H. Morkoç, Physica B, 376-377, 715 (2006).
43. M. A. Reshchikov and H. Morkoç, Physica B, 376-377, 428 (2006).
44. J.D. McNamara, N.M. Albarakati, M.A. Reshchikov. J. Lumin. 178, 301 (2016)
45. M.A. Reshchikov, H. Morkoc, B. Nemethc, J. Nause, J. Xie, B. Hertog, A. Osinsky, Sci. Dir. Phys. B 401-402, 358 (2007).
46. D. O. Demchenko, I. C. Diallo, and M. A. Reshchikov. Phys. Rev. B 110, 087404 (2013)
47. M. A. Reshchikov, Y. T. Moon, and H. Morkoç, Phys. Stat. Sol. (c) 2, 2716 (2005).